Geology and geochemistry of the Raglan Hills metagabbro

by

Seamus Johannes Magnus

A thesis submitted to the Faculty of Graduate and Postdoctoral
Affairs in partial fulfillment of the requirements
for the degree of

Master

in

Earth Sciences

Carleton University
Ottawa, Ontario

Abstract

Recent bedrock mapping and academic endeavors have helped gain a better understanding of the geological processes which formed the Central Metasedimentary Belt (CMB), which has set the stage for the production of exploration models for the various prospective commodities present within this part of the Grenville orogen. With respect to Ni-Cu sulphide mineralization, this requires a detailed examination of the mafic igneous rocks present within the CMB with emphasis on the tectonic setting and conditions of their genesis, as well as the metamorphic and structural processes which have since affected these rocks in order to assess their potential for significant Ni-Cu sulphide mineralization.

The Raglan Hills metagabbro, located northeast of Bancroft, Ontario, has been explored sporadically over the past century, and currently contains five documented Ni-Cu sulphide occurrences. By examining these occurrences in conjunction with geological, geochemical and structural data collected from the intrusion and publicly available aeromagnetic data, a preliminary model for the igneous, metamorphic and structural history of the Raglan Hills metagabbro has been produced which has implications for Ni-Cu sulphide mineralization potential in this intrusion and others of the Central Metasedimentary Belt.

The Raglan Hills metagabbro, which crystallized at roughly 1229 Ma (Pehrsson et al. 1996) is composed of four distinct rock types: regular metagabbro, calcic metagabbro, Fe-tholeiitic amphibolite and alkalic metagabbro. The regular and calcic metagabbro comprise the majority of the intrusion, and likely crystallized simultaneously, the regular metagabbro representing an un-assimilated primary magma, whereas the calcic metagabbro likely crystallized as a result of regular gabbroic magma which assimilated calcitic carbonate country rocks. The Fe-tholeiitic amphibolite occurs as dikes which cross-cut the regular and calcic metagabbro, and the alkalic metagabbro occurs in close proximity to the Fe-tholeiitic amphibolite dikes, cross-cutting each of the previous rock types.

Trace element and isotope geochemical analyses indicate that the parent magmas which crystallized the regular, calcic and alkalic metagabbroic rocks were derived from a metasomatized asthenospheric mantle consistent with a back-arc tectonic setting, whereas the geochemical signatures of the Fe-tholeiitic rocks suggest the presence of an unaltered depleted mantle component in the melt source for these rocks, and that they may have been generated due to an increase in temperature within the mantle wedge in order to melt this less metasomatized, and therefore likely less hydrous component of the mantle wedge.

Northwest-vergent thrusting and thrust-folding during the Shawinigan (1190-1170 Ma) and Ottawan (1080-1020 Ma) orogenies caused extensive mylonitic deformation and highly varied metasomatism along the northwest edge (structurally the bottom) of the intrusion, herein named the basal thrust sheet, and intense ductile shearing along the southern margin of the intrusion (McArthurs Mills Shear Zone) during the Ottawan Orogeny caused similar but much more spatially constricted mylonitic deformation and metasomatism.

The metastable mineral assemblages present throughout the intrusion indicate that the rocks experienced amphibolite-facies metamorphism with peak conditions between 600 and 700°C and between 3 and 8 kilobars, with local retrograde metamorphism to upper greenschist/lower amphibolite facies conditions proximal to northeast-trending sinistral shear zones conjugate to the dextral shearing associated with the McArthurs Mills Shear Zone.

Although the mafic to ultramafic rocks within the intrusion (currently present as coronitic-textured olivine gabbro) contain up to 500 ppm nickel, the parent magmas were undersaturated in sulphur, and were therefore incapable of crystallizing magmatic Ni-Cu sulphide minerals without an external sulphur source. Therefore the known Ni-Cu sulphide mineral

occurrences within the Raglan Hills metagabbro have been attributed to interaction between primary (regular gabbroic) magma with sulphur-rich siliceous metasedimentary rocks which are sparsely intercalated with the metacarbonate rocks which host the intrusion. Late hydrothermal remobilization of the chalcophile elements caused local upgrading of Ni and especially Cu concentrations, likely related to ductile shearing associated with the McArthurs Mills Shear Zone.

It is recommended to use aeromagnetic data, in combination with detailed mapping to identify mafic to ultramafic portions of this and other metagabbroic rocks in the CMB, and to perform detailed whole rock and soil geochemical surveys to help identify areas where these metal-bearing melts may have interacted with sulphur rich country rocks in order to crystallize magmatic Ni-Cu sulphides.

Acknowledgements

The author would like to thank doctors Brian Cousens and Michael Easton for their guidance and assistance throughout this study. More specifically, Brian for helping the author to learn and comprehend the complex life cycle of a magma and how to analyse geochemical data in order to piece together a magmatic history, and Michael for his bottomless well of knowledge pertaining to Grenvillian tectonics, geochronology and igneous geochemical affinities. Brian and Mike comprised a solid supervisory team that helped make execution of this thesis smooth and stress-free, as both are very understanding, laid-back and become personally invested in their associated research.

The multidisciplinary nature of this study (with respect to geological fields of study at least) caused the author to seek a better understanding of metamorphic and structural processes, with which Travis McCarron (MSc) and Dr. Fred Gaidies (the metamorphic super-team) and Dr. Manuel Duguet (géologue structural extraordinaire) voluntarily provided endless knowledge of these subjects, for which the author is ever thankful.

Numerous technical staff provided critical support for this thesis as well, including Mike ???? in the rock lab at Carleton University, who was patient and helpful while the author wore out several blades cutting over 200 samples for this project, and especially Dr. Lizzy Ann Spencer and Rhea Mitchell (MSc), who put up with the many inventive ways the author found to muck up the isotope analytical process. The author would also like to thank Peter Jones, an invaluable member of the earth sciences team at Carleton for teaching the author the ways of the (ancient) electron microprobe.

For access to their core library, visits in the field and insightful conversations about the Raglan Hills metagabbro and Ni-Cu mineralization potential in general, the author would like to thank Scott Halliday and Paul Davis of First Nickel Inc. Without their support, this project would never have been possible, and by allowing the authors access to their information, a model for Ni-Cu mineralization in the Central Metasedimentary Belt is one step closer to completion. Likewise, the author is indebted to the management at the Ontario Geological Survey, for funding the field exercises and geochemical analyses required for this project and for producing the Preliminary Map and Data Release provided in the back pocket of this thesis. The author highly recommends the OGS mapping school program to anyone interested in learning how to properly make a map and hone their observational skills in the field, the experience is truly one of a kind.

For their help in the field, the author would like to give special thanks to Brigid Prouse, Vincent Dubé Bourgeois, Kelsey Campbell and Laura Ratcliffe, each of whom lent extraordinary assistance and displayed extreme patience while the author struggled to see the gabbro through the trees. The author would also like to thank Mike and Wanda Wood, the energetic purveyors of fun, relaxation and fishing at the Silgrey Rustic Resort in Boulter, Ontario for their hospitality throughout August 2011.

Finally, the author would like to thank his family and friends for all of their encouragement and support throughout the duration of this project and beyond, without which the author would certainly lack motivation to undertake such a project.

Table of Contents

List of Figures

List of Tables

1 - Introduction

Despite containing a great diversity of rock-types and tectonic features with potential for a wide variety of economic mineral deposits, the Grenville Province has suffered a lack of interest from the mineral exploration industry. Until the mid nineties, the geological processes which formed and affected the Grenville Province were poorly understood. This likely deterred early mineral exploration, consequently stunting the acquisition of geological data. More recently, geoscientists have been utilizing a more advanced understanding of geologic processes to piece together the complex history of the Grenville Province.

Each academic leap forward has been slowly pulling the attention of the mineral exploration industry toward the Grenville Province, bringing with it more funding to fuel further studies, an upward trend which may lead to a more prolific metallic mining and mineral exploration economy in south-eastern Ontario and the Grenville Province as a whole.

Of the potential commodities present in the Grenville Province, mafic intrusive-hosted nickel-copper ± platinum group element (Ni-Cu PGE) deposits such as those of the past-producing Renzy and Lac Mitaine mines in Québec have proven to be at least somewhat productive. In Ontario, abundant mafic intrusive rocks are present within the Central Metasedimentary Belt (figure 1.1) which has attracted the attention of mineral exploration companies.

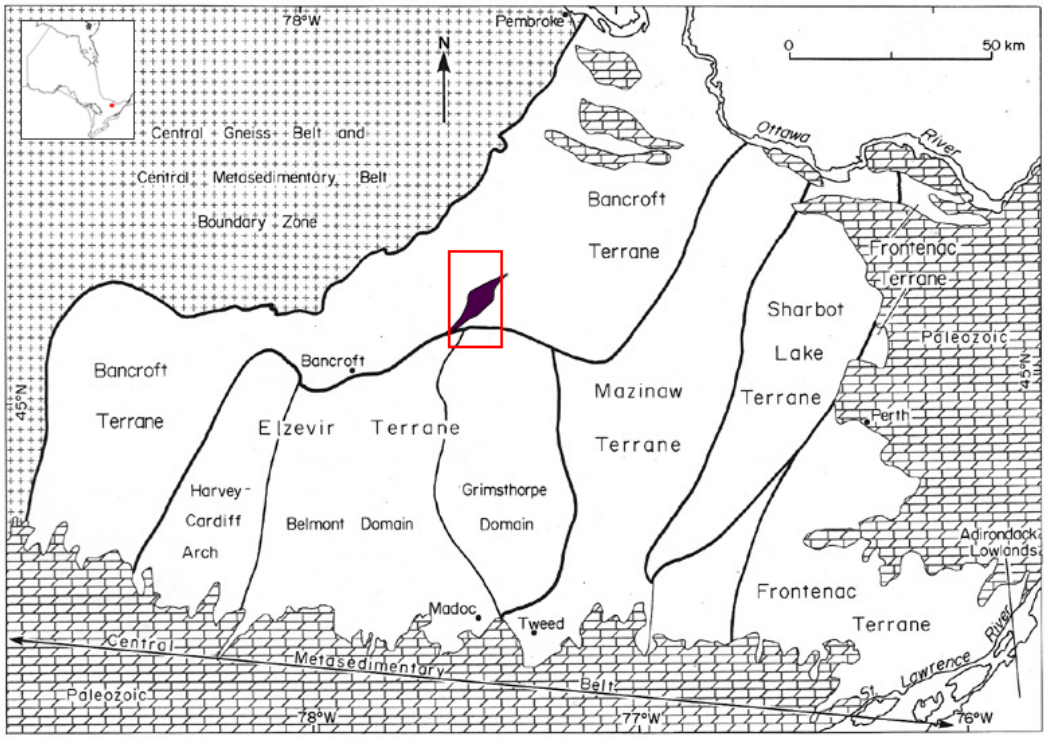

Figure 1.1 – The Central Metasedimentary Belt of the Grenville Province in Ontario, with the map area covered by this study and Ontario Geological Survey project PU11-05 (Magnus, 2012 and Easton, Duguet and Magnus, 2011) outlined in red, which contains the Raglan Hills metagabbro (purple). Modified from Easton (1992).

First Nickel Inc. has been actively exploring mafic intrusive rocks within the Elzevir and Bancroft terranes since 2009, with particular interest in the Raglan Hills metagabbro, located along the tectonic boundary between the Bancroft and Elzevir terranes. In 2010, First Nickel Inc. sold high-resolution aeromagnetic data covering the Raglan Hills metagabbro and surrounding rocks to the Ontario Geological Survey, spurring the project presented herein. First Nickel also graciously allowed the author to inspect and study diamond drill-core collected in 2009 and 2010 to aid with this project.

The primary purpose of this project is to use First Nickel Inc.'s data combined with data collected by the author during the 2011 and 2012 field seasons in order to determine and historically reconstruct the processes which formed and affected the Raglan Hills metagabbro, and how those processes may have affected its potential for Ni-Cu PGE mineralization. As outlined herein, this was achieved by combining studies of the morphology, igneous and metamorphic petrology, whole-rock, isotope and mineral geochemistry, geochronology and ore-mineralogy of the metagabbro.

The data from Raglan Hills metagabbro is also compared to that obtained from previous studies on other metagabbroic rocks of the Central Metasedimentary Belt in order to gauge the potential for Ni-Cu PGE mineralization in the Grenville Province in Ontario.

1.1 - Geological Setting

Located within the Central Metasedimentary Belt of the Grenville Province of Ontario, the Raglan Hills metagabbro lies within the Bancroft Terrane along its southeastern margin, adjacent to the Elzevir Terrane (figure 1.1).

The Central Metasedimentary Belt has been divided into a number of lithotectonic terranes and domains (cf. Easton 1992, figure 1.1). A tectonic based subdivision for the Grenville Province (broadly synonymous with the Grenville Orogeny) is proposed in Carr et al. (2000), with the Grenville divided into 3 main tectonic elements: the Laurentian Margin (most of former Central Gneiss Belt), the Composite Arc Belt (all of Central Metasedimentary Belt except Frontenac terrane), and the Frontenac-Adirondack Belt. Detailed summaries of the geologic and tectonic history of the Grenville Province in Ontario can be found in Easton (1992) and Carr et al. (2000).

Metamorphosed supracrustal rocks of the Bancroft Terrane are composed primarily of calcitic marble intercalated with minor siliciclastic sedimentary rocks and minor mafic to felsic calc-alkaline volcaniclastic rocks. Abundant mafic to felsic intrusive rocks are present within the Bancroft Terrane, ranging in age from 1340 to 1030 Ma, with representative intrusions from each of the major intrusive suites present in the Central Metasedimentary Belt as described by Easton (1992).

The supracrustal rocks, locally younger than 1301 Ma (Magnus 2013a) and pre-1190 Ma intrusive rocks of the Bancroft Terrane contain geochemical signatures which suggest the terrane in a former back-arc volcanic environment with a mature shallow-water carbonate platform (Easton 1992).

The Central Metasedimentary Belt Boundary Thrust Zone (CMBBTZ) is located roughly 12 km northeast of the Raglan Hills metagabbro, which contains a well-developed northeast-striking mylonitic fabric with a strong southeast-dipping stretching lineation (Easton 1992). This same fabric is present in the rocks between the CMBBTZ and the Raglan Hills metagabbro, along with northwest-vergent folding, such as that which folds the metasedimentary and metaigneous rocks near Moccasin Lake, located roughly 2 kilometres north of the Raglan Hills metagabbro. However, this fabric is non-existent to the south of the intrusion, where it is interrupted by the strong, steeply-dipping mylonitic foliation with shallowly-plunging stretching lineations which belong to the McArthurs Mills Shear Zone (Magnus 2013a).

Several orogenic events have been recognized within the Central Metasedimentary Belt of the Grenville Province (cf. Easton 1992; Rivers 1997; Carr et al. 2000) following arc amalgamation within the Composite Arc Belt, which culminated at approximately 1245 Ma. These are:

- Elzevirian Orogeny (circa 1250-1190 Ma)
- Shawinigan Orogeny (circa 1190-1170 Ma)
- Ottawan Orogeny (1080-1020 Ma)

The nature and character of the Elzevirian orogeny is currently poorly constrained. The long-lived character (approximately 60 million years) of the Ottawan orogeny is real, and not an artefact of limited geochronological data.

1.2 - Previous Work

The Raglan Hills area has been mapped regionally by the Ontario Geological Survey at various scales in the past, by Hewitt in late 1940s at a scale of 1:63,360 (1 inch = 1 mile) (Hewitt 1954), by Lumbers in the late 1970s at a scale of 1:100,000 (Lumbers 1982, Lumbers and Vertolli 2001), and most recently by Magnus between 2011 and 2012 at a scale of 1:20,000 (Magnus 2013a). The previous maps provided significant information with respect to the mineralogy and rock units surrounding the Raglan Hills metagabbro, with minor focus on geochemical trends and less focus on the structural context of the arrangement of these rocks. With the aid of these previous maps, Magnus (2013a) re-mapped the Raglan Hills area at a much smaller scale with more focus on the geochemistry of the rocks and the structural geology of the area, with particular focus on the Raglan Hills metagabbro.

Previous academic works on gabbroic rocks of the Central Metasedimentary Belt include Jessett, (2010) on the alkalic Glamorgan nepheline gabbro located in the western Bancroft Terrane and Gemmell (2009) on the Fe-tholeiitic Lavant metagabbro located in the Sharbot Lake Terrane. Both studies were conducted as undergraduate theses at Carleton University in conjunction with the Ontario Geological Survey. Nd-Sm isotopic analyses of these intrusions suggests that they were derived from an arc-metasomatized depleted mantle and emplaced with minimal crustal interaction, with εNd values of around +5.1 at around 1250 Ma (depleted mantle $\varepsilon Nd_{1250} = +5.14$).

Other research projects on gabbroic rocks of the Central Metasedimentary Belt include Smith et al. (2001) on the Lavant intrusive complex in the Sharbot Lake Terrane, and Pehrsson et al. (1996) on the "Raglan Gabbro Belt", which includes the Raglan Hills, Trooper Lake (Glamorgan), Faraday, Mallard Lake and Chenaux intrusions, all located in a roughly linear northwest-trending arrangement proximal to the Bancroft-Elzevir Terrane boundary.

The geochronological study by Pehrsson et al. concluded that the intrusions, except the Faraday gabbro, were contemporaneously emplaced (circa 1227-1246 Ma) and that they likely share a genetic history as part of an ensialic back-arc basin marginal to the Laurentian margin, in part due to several grains of zircon with ages of 1301-1440 Ma interpreted as crystals inherited from a rifted cratonic basement.

The geochemical study by Smith et al. (2001) resulted in a similar conclusion: that since the chemistry of the tholeiitic Lavant gabbro in the Sharbot Lake Terrane is similar to that of volcanic rocks of the Belmont and Grimsthorpe Domains within the Elzevir Terrane, the terranes of the Central Metasedimentary Belt may have collectively developed as a multiply rifted and attenuated ensialic basin between the Laurentian margin and the Frontenac volcanic arc.

Carr et al (2000), took a different view than Smith et al. (2001), and divided the Central Metasedimentary Belt into 2 main tectonic elements, the Composite Arc Belt, consisting of the Elzevir, Sharbot Lake, Mazinaw, Belmont, Grimsthorpe and parts of the Bancroft terranes and domains, and the Frontenac-Adirondack Belt, consisting of Frontenac Terrane and the Adirondack Highlands and Lowlands. They viewed the Composite Arc Belt as a number of dominantly ensimatic arc and back-arc fragments that were amalgamated at circa 1230 Ma during the Elzevirian Orogeny. The Composite Arc Belt was then stitched to the Frontenac-Adirondack Belt at circa 1170 Ma during an orogeny. Both the Composite Arc Belt and Frontenac-Adirondack belts were subsequently affected by the more significant and longer-lived Ottawan orogeny (1080-1020 Ma).

The Killer Creek gabbro suite has been studied to a lesser extent by Easton (1992). Tonalitic rocks of the Elzevir suite have been observed cross-cutting rocks of the Killer Creek suite, placing a lower limit on their age of roughly 1270 Ma, considerably older than the rocks of the Lavant suite intrusions. Elevated concentrations of TiO_2, P_2O_5 and Cu have led to the interpretation that the intrusions of the Killer Creek suite were emplaced in an island arc setting.

1.3 - Ni-Cu Exploration

The Raglan Hills metagabbro and surrounding mafic to ultramafic rocks are currently being explored for Ni-Cu mineralization by First Nickel Inc., who have been working on the property since 2009 (www.fnimining.com). Their work has included stripping and outcrop mapping, drilling and cross-section construction, and an airborne geophysical survey which was purchased by the Ontario Geological Survey in 2010 for public release (Ontario Geological Survey 2010a, b). Their efforts have also been focussed on the Moccasin Lake occurrence, located just north of the Raglan Hills metagabbro. Examination of this occurrence was not a primary focus of this thesis.

Five significant catalogued Mineral Deposit Inventory points are present within the Raglan Hills metagabbro, which are indicated on the map in the back pocket (Magnus 2013a), which have been recognized since at least 1953 (Carter et al. 1980). Various companies (cf. Carter et al. 1980) have explored sporadically the intrusion for nickel and copper, and some rock has reportedly been mined using artisanal methods from several of the occurrences.

Mineral exploration within the Central Metasedimentary Belt for all commodities has been limited, perhaps due to intimidation by the complexity of the rocks in the Grenville Province, or perhaps because the processes which formed and affected the Grenville Province were not conducive to ore mineralization. A better understanding of the rocks through academic endeavours such as this one will hopefully entice and promote a greater interest in mineral exploration in the Grenville Province.

2 - Methods of Investigation

All of the raw data collected in the field, along with petrographic analyses, detailed outcrop descriptions, whole rock, isotope and electron microprobe analyses are available in Ontario Geological Survey Miscellaneous Release—Data (MRD) 309, entitled "Geological, geochemical, geophysical and petrographic data from the Raglan Hills area, Central Metasedimentary Belt, Grenville Province, Ontario", (Magnus 2013b) included as a compact disc in the back pocket of this thesis, along with a copy of Ontario Geological Survey preliminary map P3774 "Raglan Hills metagabbro and environs, Grenville Province" (Magnus 2013a). Both products were produced solely by the author.

2.1 - Sampling

- 128 outcrops were visited and described within the Raglan Hills metagabbro
- Outcrop descriptions, including notes on lithology, structure, metamorphism, alteration, mineralization and photograph descriptions were collected using a Trimble handheld computer running a customized ArcPad application, in combination with notebooks for special notes and sketches.
- Of the visited outcrops, 79 hand samples were collected from the Raglan Hills metagabbro in the field and 11 samples were collected from diamond drill core from the First Nickel Inc. core shack. Care was taken to collect samples which were homogenous and appropriately representative of their suspected affinity.
- Outcrop and sample locations were measured using handheld GPS systems using UTM coordinates in North American Datum 1983 (NAD83), zone 18.
- Magnetic susceptibility data was acquired using an Exploranium® KT-9 or KT-10 magnetic susceptibility meter, collecting ten measurements for each rock type to ensure representative values were collected.
- Structural measurements were collected using a Brunton transit compass.

2.2 - Petrographic Analysis

- Covered thin sections were prepared for each sample, including several oversized thin sections for rocks with particularly large grain-sizes or interesting features.
- Polished thin sections were prepared for all samples containing significant sulphide mineralization, and for those which were meant for analysis using electron microprobe.
- Modal analyses for each covered and polished thin section were performed using basic transmitted and reflected light petrographic methods, available in MRD-309 (Magnus 2013b).

2.3 - Geochemical Analysis

Each of the 79 samples collected were processed for whole rock geochemical analysis. Altered and weathered portions of the samples were trimmed off by the author, and then sent to the OGS Geoscience Laboratory in Sudbury, Ontario for crushing and major and trace element analysis.

- The samples were pulverized in a 99.8% pure Al_2O_3 planetary ball mill
- Powdered samples were dissolved using a closed-vessel multi-acid digest (hydrofluoric, hydrochloric, nitric and perchloric acid, sequentially) in preparation for analysis by Inductively Coupled Plasma Mass-Spectrometry (ICP-MS) and Inductively Coupled Plasma Atomic Emission Spectrometry (ICP-AES)
- ICP-MS and ICP-AES were employed to measure the trace element concentrations, with several overlapping elements for the added benefit of quality assurance
- Powdered samples were run for Loss on Ignition (LOI) at 100°C under nitrogen atmosphere, then at 1000°C under oxygen atmosphere, then fused with a borate flux to produce a glass bead for analysis by X-Ray Fluorescence (XRF)
- XRF was used to measure major oxide concentrations, as well as numerous trace elements including arsenic, which was not analysed by the ICP methods
- Carbon and sulphur concentrations (as CO_2 and S by weight percent) were measured by combusting samples in an oxygen rich environment to be analysed by infrared absorption
- For ferrous iron (Fe^{2+} as FeO) powdered samples were dissolved in non-oxidizing acid and measured using potentiometric titration with standardized permanganate.
- The lead fire-assay method was applied for analysis of Au and platinum group elements, which were analysed by ICP-MS
- Silver was measured using the atomic absorption method

- Laboratory blanks and standards were used thoroughly, and any dubious results were returned to the author. No major discrepancies concerning pertinent elements occurred.

2.4 - Electron Microprobe Analysis

Quantitative analyses were made on an automated 4 spectrometer Camebax MBX electron probe by the wavelength dispersive x-ray analysis method (WDX) housed at the Department of Earth Sciences at Carleton University. Operating conditions were: 20kv accelerating potential and a beam current of 20 nano-amperes (nA) for silicate and oxide minerals, and 20 kv and 30 nA for sulphide minerals. Beam sensitive material such as feldspar, micas and scapolite using a rastered electron beam 5 x 5 to 10 x 10 microns in size. Peak counting times for analysed elements were: 15-40 seconds or 40,000 accumulated counts. Background positions were chosen carefully to avoid interferences from adjacent peaks. Background measurements were made at 50% peak counting time on each side of the analyzed peak. Raw x-ray data were converted to elemental weight % by the Cameca PAP matrix correction program. A suite of well characterized natural and synthetic minerals and compounds were used as calibration standards. Analyses are accurate to 1-2 % relative for major elements (>10 wt. %); 3-10 % relative for minor elements (<10 wt. %> 0.5 wt. %). As detection limit is approached (<0.1 wt. %), relative errors approach 100 %.

Digital back-scattered electron (BSE) images were collected with an Electron Optic Services digital imaging system at 512 x 512 pixel resolution with a Lamont 4 element solid state BSE detector and BSE Quad Summing Amplifier interfaced to: a 4Pi Analysis Inc. digital imaging and EDX x-ray system and Power Macintosh computer running NIH image and NIST desktop spectrum analyzer programs.

Cameca Camebax Electron probe equipped with:

- 4 WDX spectrometers, Henderson automation system (Henderson XXX Services, C. Henderson, U. of Michigan),
- Macintosh Power PC computer
- Kevex EDX X-Ray detector
- Aptec model FP6300B spectroscopy amplifier, high voltage power supply and Liquid nitrogen sensor

Silicate Mineral Standards

Element	Line	Standard.
Si	KA	olivine
Al	KA	spinel synthetic (syn.)
Mg	KA	olivine
Na	KA	albite
K	KA	microcline USNM
Ca	KA	wollastonite
Ti	KA	$MnTiO_3$ syn.
Cr	KA	Cr_2O_3 syn.
Fe	KA	fayalite syn.
Ni	KA	NiO syn.
Ba	LA	barite
S	KA	barite
Cl	KA	tugtupite
F	KA	Lithium fluoride syn.

Sulphide Mineral Standards

Elem	Line	Standard
As	LA	NiAs
S	KA	FeS_2
Ni	KA	NiAs
Fe	KA	FeS_2
Cu	KA	chalcopyrite
Co	KA	CO

2.5 - Isotopic Analysis

Between 100 and 300 mg of sample powder are weighed into a screw-cap Teflon vial, to which a mixed ^{148}Nd - ^{149}Sm spike is added. The powder-spike mixture is dissolved in HNO_3-HF, and then further attacked with HNO_3 and HCl until no residue is visible. The bulk REEs are separated using cation chromatography (Dowex 50-X8). The REE-bearing residue is dissolved in 0.26N HCl and loaded into an Eichrom chromatographic column containing Teflon powder coated with HDEHP [di(2-ethylhexyl) orthophosphoric acid, *Richard et al.,* 1976]. Nd is eluted using 0.26N HCl, followed by Sm in 0.5N HCl.

Total procedural blanks for Nd are <100 picograms. $^{147}Sm/^{144}Nd$ ratios are reproducible to 0.5%. Samples are loaded with 0.3N H_3PO_4 on one side of a Re double filament assembly, and run at temperatures of 1750-1800°C in a 9-cup ThermoFinnigan TRITON T1 multicollector mass spectrometer housed in the Department of Earth Sciences at Carleton University. Isotope ratios are normalized to $^{146}Nd/^{144}Nd = 0.72190$. Analyses of the USGS standard BCR-1 yield Nd = 29.02 ppm, Sm = 6.68 ppm, and $^{143}Nd/^{144}Nd = 0.512668 \pm 20$ (n=4). Over 30 runs of the La Jolla standard average $^{143}Nd/^{144}Nd = 0.511848 \pm 10$ (April. 2004-Dec 2012). Epsilon values at time T are calculated using the following relation:

$$\varepsilon Nd_T = [(^{143}Nd/^{144}Nd_{sample}{}^{T} / {}^{143}Nd/^{144}Nd_{CHUR}{}^{T}) - 1] * 10000$$

Where CHUR is the Chondrite Uniform Reservoir and T is generally the time the rock was formed. Depleted mantle model ages are calculated assuming a modern upper mantle with $^{147}Sm/^{144}Nd = 0.214$ and $^{143}Nd/^{144}Nd = 0.513115$.

Rb/Sr: The sample, dissolved in 2.5N HCl, is pipetted into a 14-ml Bio-Rad borosilicate glass chromatography column containing 3.0 ml of Dowex AG50-X8 cation resin. Rb and Sr are eluted in succession using 2.5 N HCl. The rare earth elements are then eluted using 6N HCl. The REE solution is dried and the residue dissolved in 0.26N HCl.

Total procedural blanks for Sr are < 450 picograms. Sr is loaded onto a single Ta filament with H_3PO_4 and are run at filament temperatures of 1480-1520ºC. Isotope ratios are normalized to $^{86}Sr/^{88}Sr = 0.11940$ to correct for fractionation. Two standards are run at Carleton, NIST SRM987 ($^{87}Sr/^{86}Sr = 0.710251 \pm 18$, n=50, Sept. 1992 - May 2003) and the Eimer and Amend (E&A) $SrCO_3$ ($^{87}Sr/^{86}Sr = 0.708032 \pm 24$, n=20, Sept. 1994-Feb. 2004). Rb is loaded with HCl onto one side of a double Re filament assembly and run at temperatures of 1250-1300°C. No correction for fractionation is made.

2.6 - Data Analysis

Whole rock and isotope geochemical data were analysed using Microsoft Excel, and Igpet2010 (TerraSoft 2000) was used specifically for the purposes of plotting rare-earth and trace element diagrams. Chondritic and primitive mantle normalization values of Sun and McDonough (1989) were applied where required.

Structural data was analysed using Stereonet, an appropriately named open source program used for plotting planes and poles onto digital stereonets, performing spherical trigonometric functions, calculating fold axes, and calculating point contours (Allmendinger et al. 2013, Cardozo et al. 2013).

3 - Rock Type Descriptions

Due to textural similarities in the field, differentiation between the various rock types in the Raglan Hills metagabbro is based on a combination of petrography and whole rock geochemistry. Each of the rock types contains similar mineralogy, dominated by hornblende and plagioclase. Slight differences in mineral composition, modal mineral abundance and texture may be used to assign rocks observed in the field to the rock types described herein, however the distinct major and trace element concentrations in each rock type allows for definite distinction between rock types (tables 3.1 and 3.2). Therefore the rock types will be described based on both petrographic and geochemical observations. Map unit numbers correspond to the map units shown on P3774 (Magnus, 2013a, back pocket). Details on individual stations referred to in chapters 3 to 6 can be found in Magnus (2013b).

3.1 - Regular Metagabbro – map unit 9

3.1.1 - Petrography

The regular metagabbroic rocks in the Raglan Hills metagabbro were named as such due to their relatively simple mineralogy (generally hornblende, plagioclase and biotite), their abundance throughout the intrusion (by far the dominant rock type) and due to their major element concentrations being close to those of the "average" basaltic composition (Le Maitre 1976).

9a-9c – leucocratic to melanocratic metagabbro

The metagabbroic rocks in this unit are composed of varied amounts of plagioclase and amphibole with minor biotite, trace chlorite, trace calc-silicate minerals (epidote and scapolite), and trace titanite and Fe-Ti oxides. The large (centimetre scale) crystal size and high colour contrast between the feldspars and amphiboles give these rocks an easily recognizable texture in the field (figure 3.1a-d).

Plagioclase (~40% anorthite content, "andesine") is present in the mesocratic and melanocratic metagabbroic rocks as subhedral to euhedral laths up to 4 cm long, whereas in the leucocratic rocks the crystals appear more blocky and irregular. These crystals often display simple and Carlsbad twinning characteristic of plagioclase. In hand sample, plagioclase appears dark grey to purple due to a high concentration of fluid inclusions visible in thin section (figure 3.2a-c). White, inclusion-free plagioclase is present in samples with protomylonitic fabrics.

Amphibole ($(K_{0.07}Na_{0.27})(Ca_{1.84}Na_{0.04}Fe_{0.12})(Mg_{2.98}Fe_{1.44}Al_{0.48})(Si_{7.08}Al_{0.92})O_{22}(OH)_2$, "magnesiohornblende") displays brown to green pleochroism and rare twinning. In melanocratic samples, massive aggregates of amphibole host plagioclase laths, whereas in leucocratic samples, massive aggregates of plagioclase host minor aggregates of amphibole. Crystals are often observed with Fe-Ti oxides ($Fe_{0.97}Ti_{1.98}O_3$, "ilmenite") and/or titanite in their cores, commonly as elongate crystals parallel to the two hornblende cleavage directions.

Chlorite (optically length fast, magnesium-rich) is present in several samples as fine radiating acicular aggregates in contact with (and likely replacing) biotite and hornblende, and rarely pseudomorphing epidote. These occurrences of chlorite have been interpreted as indications of localized retrograde metamorphism.

Biotite ($((K_{0.74}Na_{0.01})(Fe_{0.78}Mg_{1.40})[(Si_{2.55}Al_{1.26}Fe_{0.19})O_{10}](OH))$ is present mostly along the interface between plagioclase and hornblende, and within crystals of plagioclase which have been recrystallized (figure 3.1c).

These rocks are generally massive to weakly foliated, with foliations defined by an alignment of strained plagioclase laths caused by weak mylonitic deformation. The mineral assemblage hornblende-plagioclase-biotite has been interpreted as a stable metamorphic mineral assemblage consistent with the amphibolite facies of metamorphism.

Sample#	**11SJM166A**	**12SJM012A**	**12SJM167A**	**12SJM035A**	**12SJM033A**	**11SJM120B**
Petrographic Rock Name	biotite amphibolite	scapolite leuco-amphibolite	biotite amphibolite	olivine gabbro	diopside scapolite amphibolite	epidote amphibolite
Map Code	9a	9b	9c	9d	10a	10b
Al_2O_3 wt.%	16.15	24.69	8.75	7.05	16.12	22.96
CaO wt.%	10.13	10.38	10.48	11.02	12.99	13.21
Fe_2O_3t wt.%	8.89	2.34	14.82	16.01	6.36	6.81
FeO wt.%	6.43	1.66	10.95	13.40	4.68	3.54
Fe_2O_3 wt.%	2.46	0.68	3.87	2.61	1.68	3.27
K_2O wt.%	0.95	0.38	0.53	0.23	0.40	0.45
LOI wt.%	1.20	0.64	0.75	-0.34	0.67	1.08
MgO wt.%	9.01	2.36	14.31	16.29	8.44	4.10
MnO wt.%	0.13	0.05	0.25	0.26	0.12	0.07
Na_2O wt.%	2.73	4.76	1.52	1.41	2.71	2.55
P_2O_5 wt.%	0.030	0.019	0.069	0.026	0.015	0.020
SiO_2 wt.%	50.11	53.67	47.90	47.73	51.24	47.77
TiO_2 wt.%	0.47	0.19	0.79	0.63	0.39	0.62
Total wt.%	99.81	99.47	100.17	100.32	99.46	99.65
ΣREEs ppm	50.55	19.55	67.34	48.33	33.24	23.41

Sample#	**11SJM179A**	**11SJM6002**	**12SJM159B**	**12SJM044A**	**Le Maitre (1976)**
Petrographic Rock Name	scapolite diopside amphibolite	clino-pyroxenite	biotite amphibolite	diopside epidote amphibolite	average basalt
Map Code	10c	10d	11a	12a	
Al_2O_3 wt.%	10.66	5.12	18.97	13.49	15.7
CaO wt.%	16.18	22.18	7.60	12.26	9.47
Fe_2O_3t wt.%	8.43	13.42	9.07	14.46	10.92
FeO wt.%	5.84	8.48	6.59	10.01	7.13
Fe_2O_3 wt.%	2.59	4.94	2.48	4.45	3.79
K_2O wt.%	0.22	0.15	1.46	0.21	1.10
LOI wt.%	0.67	0.89	0.99	0.65	0.95
MgO wt.%	11.68	10.23	3.10	7.27	6.73
MnO wt.%	0.15	0.17	0.12	0.22	0.20
Na_2O wt.%	1.65	0.68	4.77	2.46	2.91
P_2O_5 wt.%	0.010	1.340	0.272	0.132	-
SiO_2 wt.%	49.32	44.71	52.22	47.00	49.2
TiO_2 wt.%	0.64	1.36	1.89	1.67	1.84
Total wt.%	99.61	100.24	100.46	99.83	99.02
ΣREEs ppm	40.60	117.86	126.09	53.94	-

Table 3.1 – representative whole-rock geochemistry for each of the unmetasomatized metagabbroic rock types in the Raglan Hills metagabbro. Abbreviation: wt. % = weight percent, ppm = parts per million (or wt. % x 10,000), ΣREEs = total concentration of rare earth elements (lanthanide series, excluding yttrium), LOI = loss on ignition.

Rock Type	regular metagabbro	regular leucogabbro	regular melanogabbro	olivine metagabbro	alkalic metagabbro
Map Code	9a	9b	9c	9d	11a
plagioclase	XX	XXX	X	X	XXX
hornblende	XXX	X	XXX	trace	XX
clinopyroxene				XX	trace
biotite	XX	X	XXX	trace	X
chlorite	trace	trace			
epidote					
scapolite	trace	X	trace		
titanite	X		X		X
orthopyroxene				XX	
olivine				X	

Rock Type	calcic metagabbro	calcic leucogabbro	calcic melanogabbro	clino-pyroxenite	Fe-tholeiitic amphibolite
Map Code	10a	10b	10c	10d	12a
plagioclase	XXX	XXX	X		XX
hornblende	XX	X	XXX	XX	XXX
clinopyroxene	X		XX	XXX	X
biotite	trace	trace		trace	X
chlorite	trace	trace		trace	
epidote	X	X	X	X	trace
scapolite	X	X	X	X	trace
titanite	trace			trace	trace
orthopyroxene					
olivine					

Table 3.2 – simplified mineralogy for all unaltered metagabbroic rock types within the Raglan Hills metagabbro. Abundances: trace = < 1%, X = 1-10%, XX = 10-49%, XXX = > 50%, values taken from average modal % for each rock type from petrographic descriptions in Magnus (2013b).

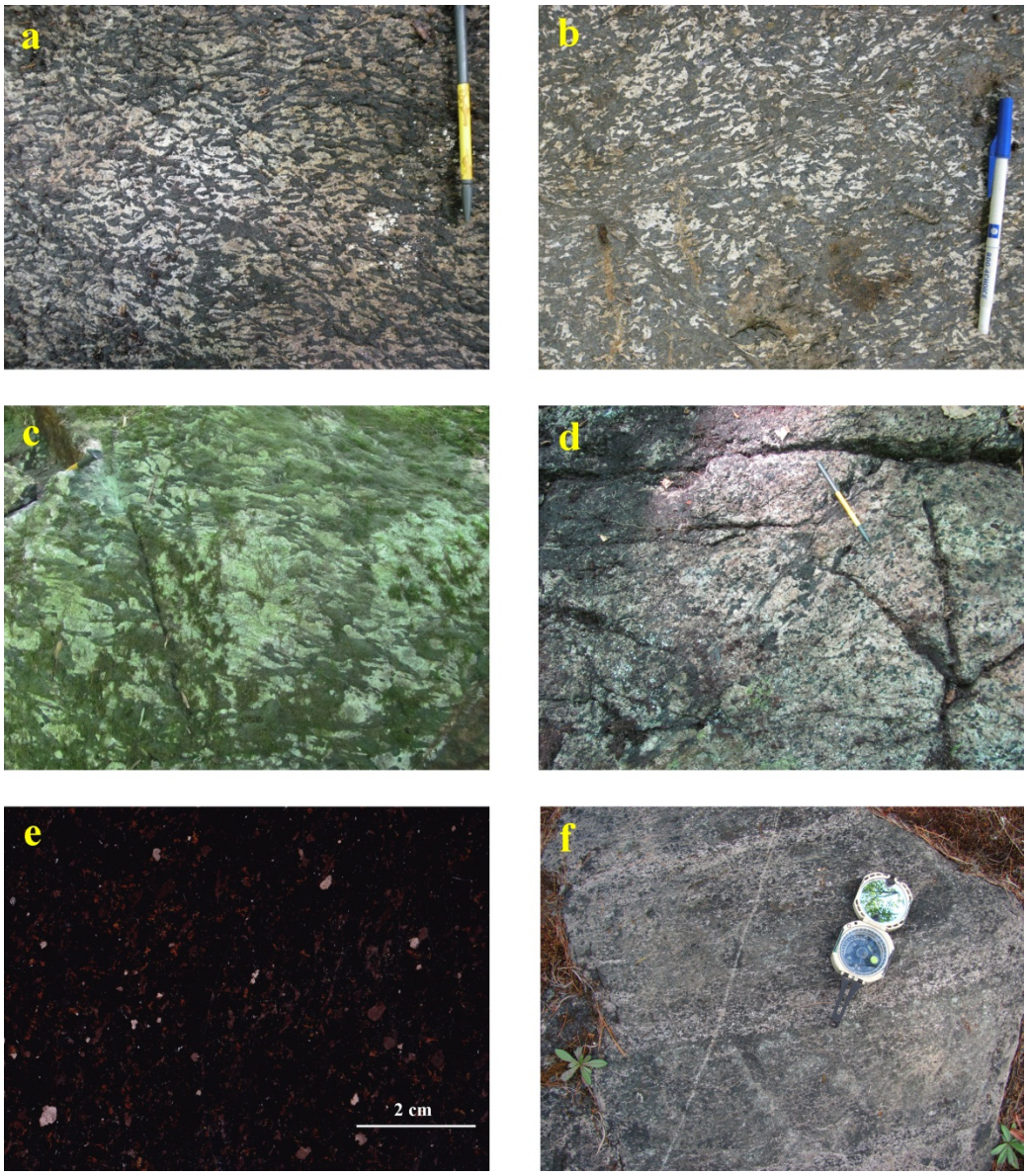

Figure 3.1 – a) Regular metagabbro (station 11SJM177), b) melanocratic metagabbro (11SJM163), c) very coarse-grained regular metagabbro (12SJM024) and d) leucocratic metagabbro (d 12SJM012), all of which contain grey to white plagioclase and dark green amphibole. e) A scanned image of a polished sample of olivine metagabbro (from station 12SJM035) displays orange olivine, purple plagioclase, and dark (reflects white, vitreous) brown pyroxene. Compositional layering between olivine metagabbro and mesocratic metagabbro is visible in station 12SJM167 (f).

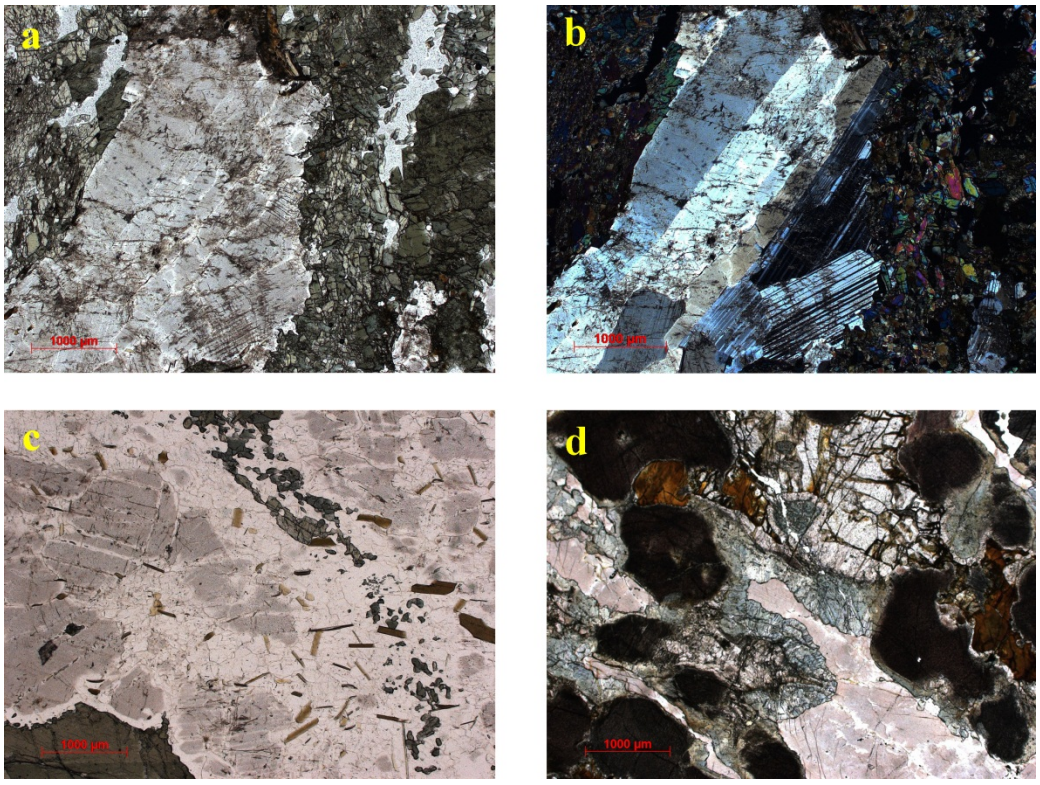

Figure 3.2 – a) Sample 11SJM166A in plane-polarized light (PPL) and b) the same field of view in cross-polarized light (XPL) (b). Biotite is present near the contact between green amphibole and a twinned, inclusion-rich plagioclase lath. Sample 12SJM033B (c) contains similar minerals, with biotite closely associated with inclusion-free plagioclase (PPL). Sample 12SJM035A contains inclusion-rich plagioclase separated from olivine and pyroxene with coronae of green amphibole and minor biotite (PPL). Epidote and scapolite are present mostly within the leucocratic samples (11SJM6005, 12SJM012A, 12SJM033B) closely associated with plagioclase.

9d – coronitic olivine metagabbro

These rocks are composed of primary magmatic pyroxene, olivine and plagioclase that have reacted to form coronitic textures including orthopyroxene, amphibole and biotite. These rocks are entirely melanocratic, medium-grained and equigranular (~3-7mm), giving them a texture in hand sample that is clearly distinct from the other rock-types in the Raglan Hills metagabbro (figure 3.1e).

Plagioclase (~40% anorthite content, "andesine") is present as anhedral crystals interstitial to pyroxene and olivine (figure 3.2d). Crystals display both simple and Carlsbad twinning, and are rich in fluid inclusions, causing them to appear dark purple in hand sample (colourless in PPL).

Olivine (54-60% forsterite content) is colourless in PPL, and displays typical high relief, irregular fracture patterns and alteration to iddingsite, which gives it an orange appearance in hand-sample.

3.1.2 - Geochemistry

As mentioned above, the regular metagabbro rock type has major element concentrations fairly close to those of the average basalt as defined by Le Maitre (1976), with the exception of higher magnesium (9.01 wt. % vs. 6.73 wt. % MgO in the average basalt) and lower titanium (0.47 wt. % vs. 1.84 wt. % TiO_2 in the average basalt).

The composition of the regular metagabbroic rocks varies between melanocratic and leucocratic end members, following a typical trend of increasing silica, aluminum and alkali metals with a relative decrease in iron and magnesium (Table 3.1). More pertinent is the fact that the relative concentration of calcium is consistent throughout all of the samples (roughly 10.4 wt. % CaO).

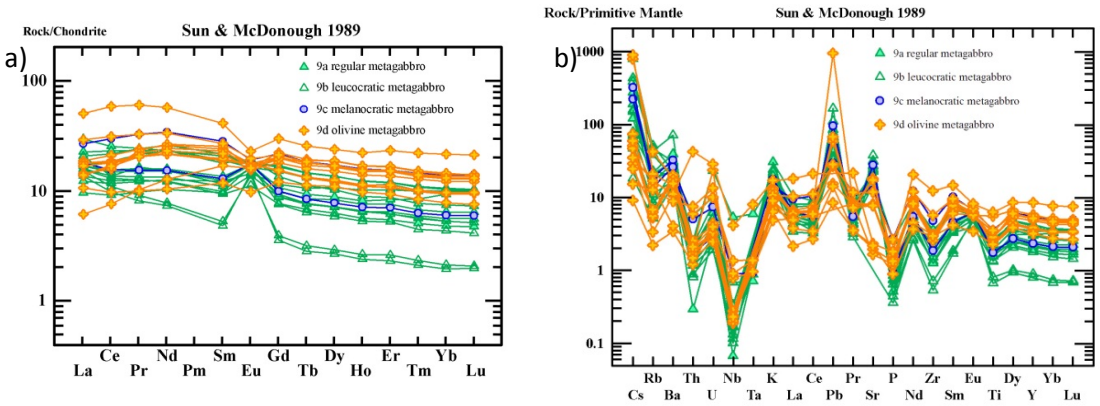

Figure 3.3 – a) REE plot normalized to chondritic values and b) trace element plot normalized to primitive mantle values, all normalization according to Sun and McDonough (1989). Note the generally shallow negative slope towards the more incompatible elements in both diagrams, and the general increase in total rare earth element concentration from leucocratic samples (green) to melanocratic samples (blue to orange).

Rare earth element (REE) concentrations are generally highest in the more melanocratic samples (figure 3.3a). Relative REE concentrations display a generally shallow negative slope from lanthanum to the more incompatible lutetium, with a concave downward shape developing in the light REEs of the melanocratic samples. The overall slope varies between melanocratic and leucocratic samples, from nearly horizontal in the melanocratic sample patterns, to a moderate shallow slope in the leucocratic sample patterns (slope taken as difference between lanthanum and lutetium), a slight clockwise rotation from melanocratic to leucocratic patterns.

The leucocratic samples display positive europium (Eu) anomalies, whereas the melanocratic samples display negative Eu anomalies, causing their relative Eu concentrations to converge at roughly 20 times chondritic values.

When plotted on a rock vs. primitive mantle trace element plot (figure 3.3b), several patterns are apparent. These samples all display depletion of the high field strength elements (HFSEs) such as niobium (Nb), tantalum (Ta), zirconium (Zr), and titanium (Ti), consistent with the prior observation that the rocks have generally low TiO_2 concentrations relative to the average basalt, and depletion of phosphorous (P). These samples also display enrichment in the large ion lithophile elements (LILs), such as cesium (Cs), rubidium (Rb), barium (Ba), potassium (K) and strontium (Sr), along with a strong enrichment of lead (Pb).

3.2 - Calcic Metagabbro – map unit 10

3.2.1 - Petrography

10a-10c – leucocratic to melanocratic calcic metagabbro

The metagabbroic rocks in this unit are normally massive to weakly foliated (similar to the regular metagabbro), composed of varied amounts of plagioclase and clinopyroxene (always partially replaced by amphibole), epidote and scapolite, with minor titanite, trace opaque minerals and trace biotite. The coarse grain size and high contrast in colour between the felsic and mafic minerals give these rocks a similar texture to the "regular" metagabbroic rocks, although the presence of clinopyroxene phenocrysts may be observable in hand-sample, allowing for proper classification in the field (figure 3.4a).

Figure 3.4 – a) Outcrop picture of calcic metagabbro (station 12SJM033A) and b) leucocratic calcic metagabbro (12SJM033B), both of which are composed of green clinopyroxene (with rims of amphibole) and grey to white plagioclase. Station 12SJM028 contains (c) clinopyroxene megacrysts up to 8cm across. Primary igneous layering defined by bands of green clinopyroxene and white plagioclase is visible in station 12SJM172 (d).

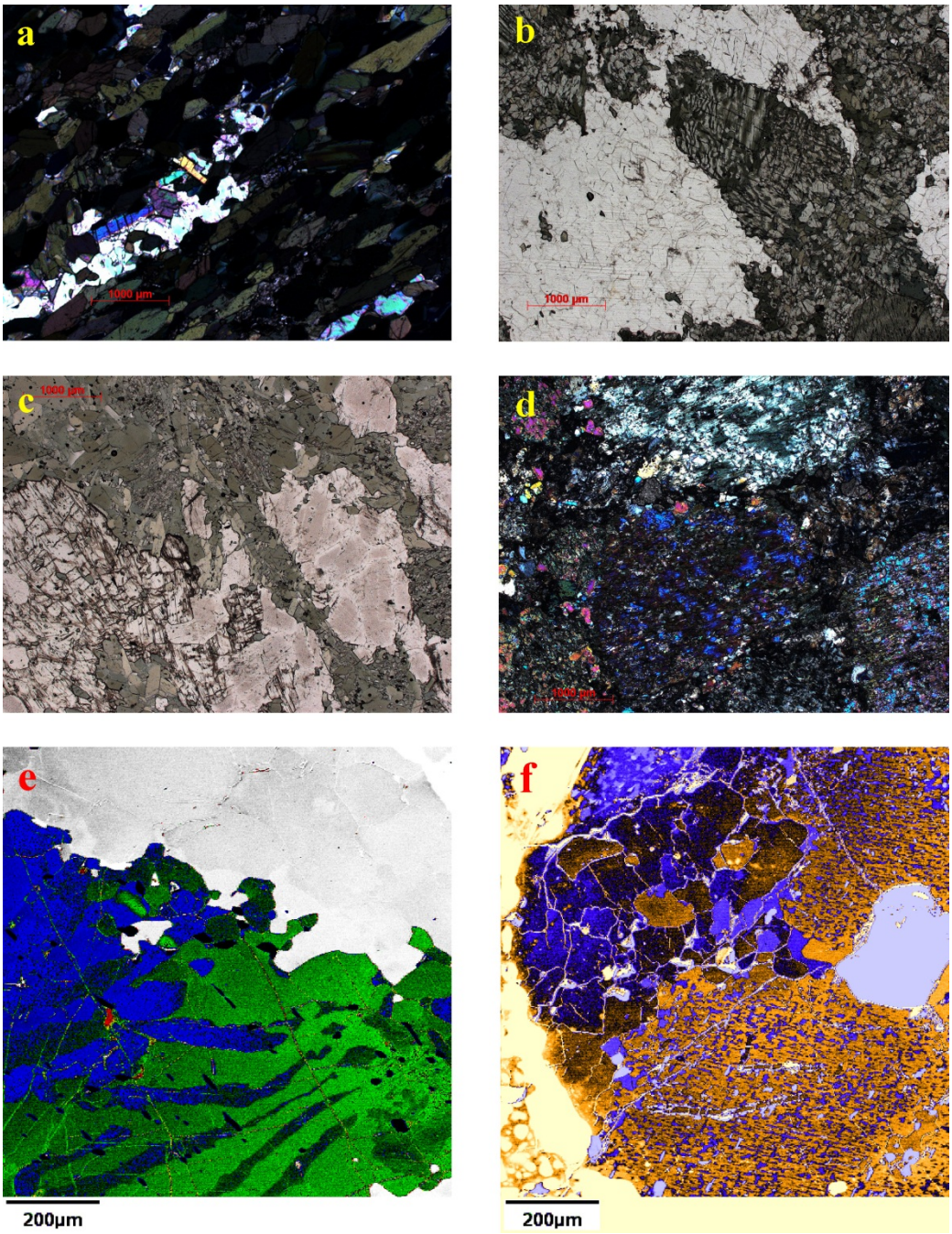

Figure 3.5 – a) A melanocratic sample (11SJM102A) containing green amphibole with minor epidote and scapolite (XPL). b) Phenocrysts of colourless diopside partially replaced by green amphibole in a matrix of colourless, inclusion-free plagioclase (11SJM169A, PPL). c) A mesocratic sample (12SJM033A) comprised of green amphibole, inclusion-rich plagioclase and colourless scapolite (high relief) (PPL). d) A sample of clinopyroxenite (12SJM021A) comprised of clinopyroxene partially replaced by green amphibole with interstitial epidote (XPL). e) A false colour back-scattered electron (BSE) image of a diopside phenocryst (green) partially replaced by magnesiohornblende (blue) and Fe-Ti oxides (black), with plagioclase (white) from a sample of calcic metagabbro (11SJM169A). f) A false colour BSE image of diopside (orange) partially replaced by tschermakite (blue) with Fe-Ti oxides and sulphide minerals (grey) and epidote (black) from a sample of clinopyroxenite (11SJM6006). Beige is ink used to mark the polished section. A crystal of apatite was identified just out of the field of view.

Plagioclase in these rocks does not occur as euhedral laths as they do in the "regular metagabbro" rock type. Instead, the feldspars occur as equant, blocky crystals. Primary (not recrystallized) crystals often display simple and Carlsbad twinning and contain a high concentration of fluid inclusions, giving them a purple colour in hand sample. Recrystallized plagioclase crystals in these rocks contain very few fluid inclusions and appear white in hand sample. Scapolite and epidote are often associated with plagioclase in these rocks. Plagioclase composition ranges from roughly 40% anorthite content in the mesocratic samples, to roughly 69% anorthite content in leucocratic samples, as measured by electron microprobe.

Clinopyroxene ($(Ca_{0.95}Na_{0.03})(Mg_{0.74}Fe_{0.22}Al_{0.04})(Si_{1.97}Al_{0.03})O_6$, "diopside") occurs as phenocrysts and aggregates, and in all cases is partially replaced by green amphibole(figure 3.5b, e and f). The presence of these phenocrysts produces a "spotted" texture in mesocratic samples, making them distinguishable from "regular metagabbro"; however melanocratic and leucocratic calcic metagabbroic rocks are more difficult to distinguish from their "regular" counterparts (figure 3.4b). Diopside (light green in PPL) is also present as fine-grained secondary metamorphic growths accompanying green amphibole.

Amphibole ($(K_{0.15}Na_{0.38})(Ca_{1.94}Fe_{0.07})(Mg_{2.59}Fe_{1.68}Al_{0.59})(Si_{6.67}Al_{1.33})O_{22}(OH)_2$, "magnesiohornblende") is present in these rocks as partial replacements (and entire pseudomorphs) of diopside, often accompanied by titanite.

Epidote and scapolite occur along the contacts between plagioclase and amphibole, and as patchy or vein-like alteration products after plagioclase where the dark purple inclusion-rich plagioclase has been recrystallized to granoblastic, colourless inclusion-free plagioclase (figure 3.5b and c).

10d – clinopyroxenite

Several samples from outcrop and diamond-drill core contain cumulate-textured diopside (approximate composition $(Ca_{0.95}Mg_{0.01}Na_{0.04})(Mg_{0.63}Fe_{0.31}Al_{0.06})(Si_{1.96}Al_{0.04})O_6$, similar to diopside in the calcic metagabbro (map unit 10a)) with trace interstitial epidote and apatite (figure 3.5d). The diopside crystals are sheathed by and in places entirely pseudomorphed by green amphibole (tschermakite), giving them a textural appearance in hand sample similar to a hornblendite (metamorphosed regular melanogabbro to olivine gabbro, map units 9c and 9d). To distinguish between these rock types in the field, a regular hornblendite will likely be magnetic, may be softer (due to the absence of pyroxene and the presence of biotite) and should contain no epidote or scapolite.

The consistent euhedral shape of the diopside in the calcic metagabbroic rocks, and their localized layered arrangement (observed at several stations proximal to the core of the Raglan Hills metagabbro and along the southeast margin of the intrusion (station 12SJM172) (figure 3.4d)) suggest that these rocks display primary igneous texures.

3.2.2 - Geochemistry

The major element concentrations of these rocks are similar to those of the regular metagabbro, with the exception of calcium (Table 3.1). The calcic metagabbroic rocks contain at

least 2 wt. % more CaO than their regular metagabbroic counterparts, ranging from 12.99 wt. % CaO in the mesocratic samples to 16.18 wt. % CaO in the melanocratic samples and up to 22.18 wt. % CaO in samples of clinopyroxenite. This enrichment in CaO likely caused the dilution of Fe, Mg, Na and K with respect to the concentration of those elements in the regular metagabbro. Also, the samples of clinopyroxenite tend to be rich in phosphorous, with up to 1.34 wt. % P_2O_5 in sample 11SJM6002.

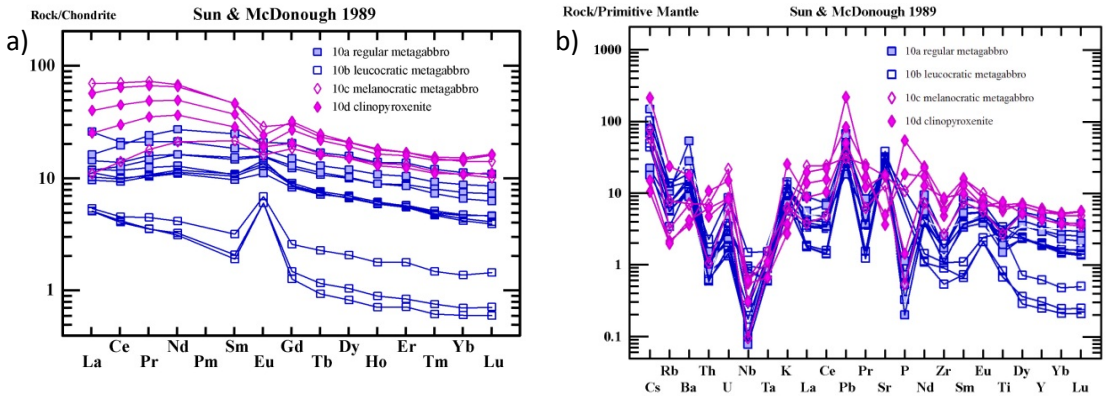

Figure 3.6 – a) REE plot normalized to chondritic values and b) trace element plot normalized to primitive mantle values, all normalization according to Sun and McDonough (1989). Note the generally shallow negative slope towards the more incompatible elements in both diagrams, and the general increase in total rare earth element concentration from leucocratic samples (blue) to melanocratic samples (pink).

REE pattern topology for calcic metagabbroic samples is similar to that of the regular metagabbroic rocks: melanocratic samples contain higher concentrations of total REEs, and generally display shallow slope (little difference between La and Lu), whereas the leucocratic samples contain the lowest concentrations of total REEs and display a steeper slope overall (figure 3.6a). These patterns also display similar Eu anomalies, which converge at 10-20x chondritic concentrations. The calcic metagabbroic samples (apart from the clinopyroxenite samples) display what appears to be a slightly negative cerium anomaly not observed in the samples of regular metagabbro.

Likewise, the trace element patterns for calcic metagabbro are roughly parallel to those of the regular metagabbro, with slightly lower concentrations of the LILs, likely due to dilution through calcium enrichment (figure 3.6b).

The samples of clinopyroxenite display slightly different REE patterns than the other calcic metagabbroic samples. They contain the highest total REE concentrations amongst this group of rocks, and also (as seen in the major oxide concentrations) contain higher than normal phosphorous concentrations (figures 3.6b and 3.7). Their patterns show a concave downward pattern in the light REEs, and a very slight concave upward pattern in the heavy REEs, as opposed to the negative to horizontal slope as observed in the remainder of the regular and calcic metagabbroic rocks.

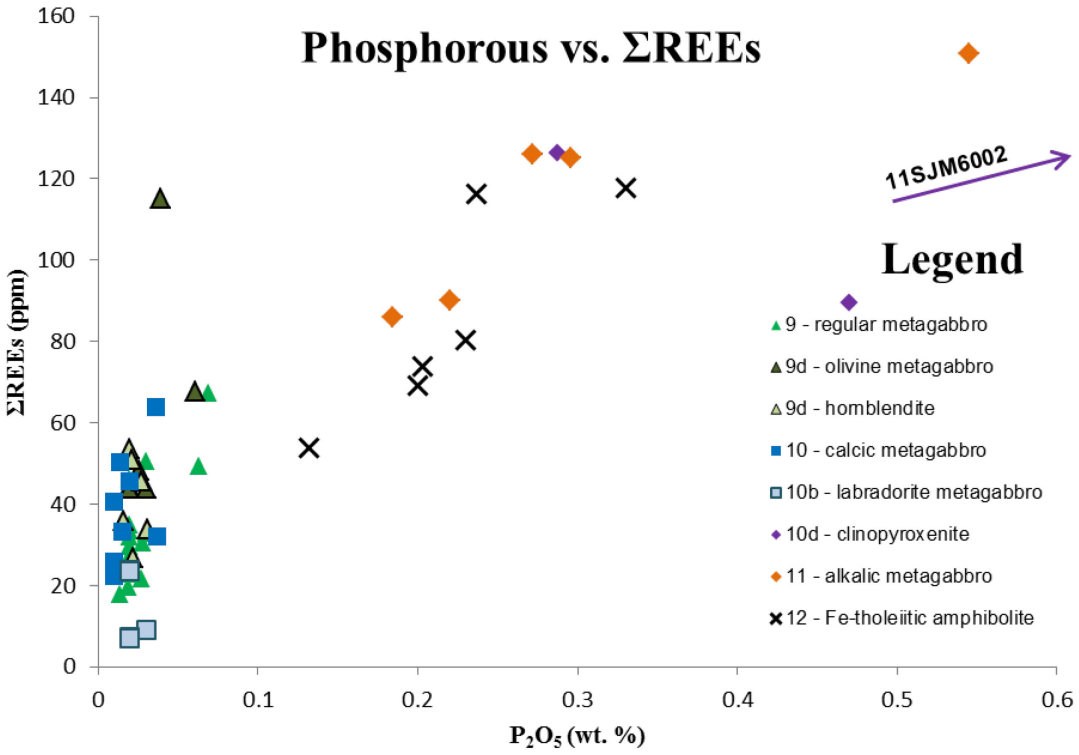

Figure 3.7 – plot of phosphorous vs. total REE concentrations. Samples of alkalic metagabbro and Fe-tholeiitic amphibolite appear to follow a positive trend, whereas the regular and calcic metagabbroic rocks appear to become enriched in REEs (in the melanocratic rocks) with very little enrichment of P. However, samples of clinopyroxenite have both high P and high REE concentrations.

3.3 - Alkalic Metagabbro, map unit 11

3.3.1 - Petrography

Several samples of metagabbro collected from the Raglan Hills metagabbro contain geochemical concentrations with alkalic affinity (described below), which are difficult to distinguish from other metagabbroic rocks texturally. These rocks occur both as fine- to coarse-grained gabbroic rocks (11a) and as fine-grained granoblastic rocks (11b).

These alkalic metagabbroic rocks occur in close proximity to rocks of map unit 12, the iron-tholeiitic amphibolitic rocks, and dikes of alkalic metagabbro have been observed cross-cutting both unit 12 (at stations 12SJM146 and 12SJM147) and unit 9 (at station 12SJM038).

11a – coarse-grained alkalic metagabbro

The fine- to coarse-grained gabbro-textured alkalic metagabbroic rocks (figure 3.8a) are composed mainly of euhedral dark grey plagioclase laths up to 3cm long with straight, sharp crystal boundaries with interstitial green hornblende poikiloblasts with inclusions of colourless plagioclase, minor biotite concentrated along the boundaries of the plagioclase laths, and abundant disseminated Fe-Ti oxides (up to 4mm) with titanite coronae (figure 3.9c).

The poikiloblastic hornblende-plagioclase intergrowths are unique to this rock-type, and likely represent pseudomorphic replacement of magmatic crystals of pyroxene or amphibole (figure 3.9a and b). The poikiloblastic hornblende has been broken down into subgrains by mylonitic deformation.

Station 12SJM159 contains alkalic metagabbro with both well-developed mylonitic fabrics and massive non-deformed fabrics. As seen in figure 3.8b, c and d, there is a sharp boundary between these fabrics, rather than a smooth transition between massive and mylonitic rocks. In some areas of the outcrop, the shape of this boundary is irregular, which causes the deformed and massive rocks to appear intercalated. In places where the boundary is straight, there appears to be a preferred alignment of plagioclase laths perpendicular to the boundary, whereas farther away from the boundary, plagioclase laths appear randomly oriented and in places oriented parallel to the boundary.

11b – fine-grained dike of unit 12a cutting other metagabbroic rocks

Fine-grained dikes of alkalic metagabbro have been observed cutting both Fe-tholeiitic amphibolite (unit 12a) and regular metagabbro (unit 9a). In both cases, the rocks are composed of the same mineralogy as their coarse-grained counterparts (unit 11a), though the plagioclase phenocrysts have an equant, subhedral form rather than euhedral laths.

The dikes of alkalic metagabbro in station 12SJM146 (figure 3.8e) have a massive, non-deformed fabric, whereas the amphibolitic rocks which host them have well-developed foliations which have themselves been folded.

The dike of alkalic metagabbro in station 12SJM038 (figure 3.8f) displays straight, sharp contacts with the host regular metagabbro (unit 9a) which contains a well-developed protomylonitic foliation. The dike contains an internal foliation defined by hornblende-rich and plagioclase-rich banding visible in thin section which is parallel to the mylonitic foliation in the host metagabbro.

3.3.2 - Geochemistry

As their name implies, the samples of alkalic metagabbro contain higher concentrations of alkali metals (sodium and potassium) than the remainder of the metagabbroic rocks in the Raglan Hills metagabbro. Figure 3.10 shows that these samples even plot within the alkaline field (as proposed by Irvine and Baragar, 1971) whereas the remainder of the samples plot mostly within the subalkaline field.

Unlike the regular and calcic metagabbroic rocks, the alkalic metagabbroic rocks contain higher concentrations of titanium, with up to 1.89 wt. % TiO_2, roughly equivalent to the average basaltic composition, and as seen in Figure 3.7, contain higher concentrations of phosphorous (higher than the average basaltic composition) and REEs than the other metagabbroic rocks, which show a positive correlation. This titanium enrichment is consistent with the observed abundance of Fe-Ti oxides and titanite within these rocks. On a Jensen (1976) diagram, they plot in the tholeiitic field, making them distinct from younger alkalic metagabbroic rocks of the Woermke suite, which plot within the calc-alkalic field (circa 1073 Ma, Easton 2012).

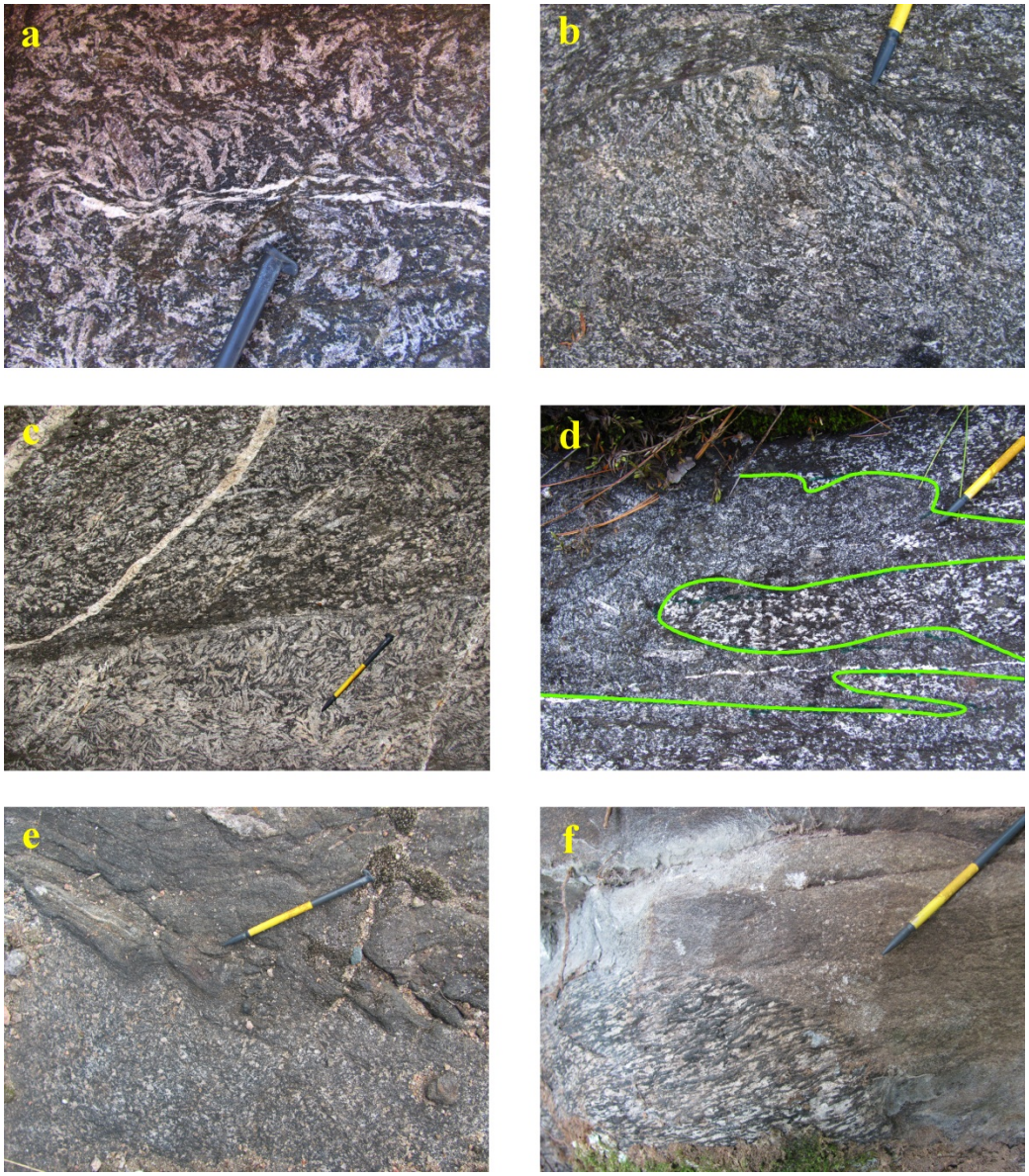

Figure 3.8 – a) Alkalic metagabbro containing grey to beige euhedral plagioclase laths with interstitial dark green amphibole and Fe-Ti oxides (station 12SJM159). A small ductile shear zone with unknown displacement cuts the massive fabric of the metagabbro. b) Plagioclase crystals in alkalic metagabbro display a preferred alignment perpendicular to shear bands within deformed alkalic metagabbro (b and c). d) outlined boundary between mylonitized alkalic metagabbro (beneath stylus) and non-deformed (magmatic) alkalic metagabbro (inside). e) A small dike of fine to medium-grained alkalic metagabbro in contact with highly deformed Fe-tholeiitic amphibolite at station 12SJM146. f) A small dike of fine-grained alkalic metagabbro cutting protomylonitic regular metagabbro. The dike has an internal foliation parallel to that in the protomylonitic metagabbro host rock, indicating they were both deformed simultaneously.

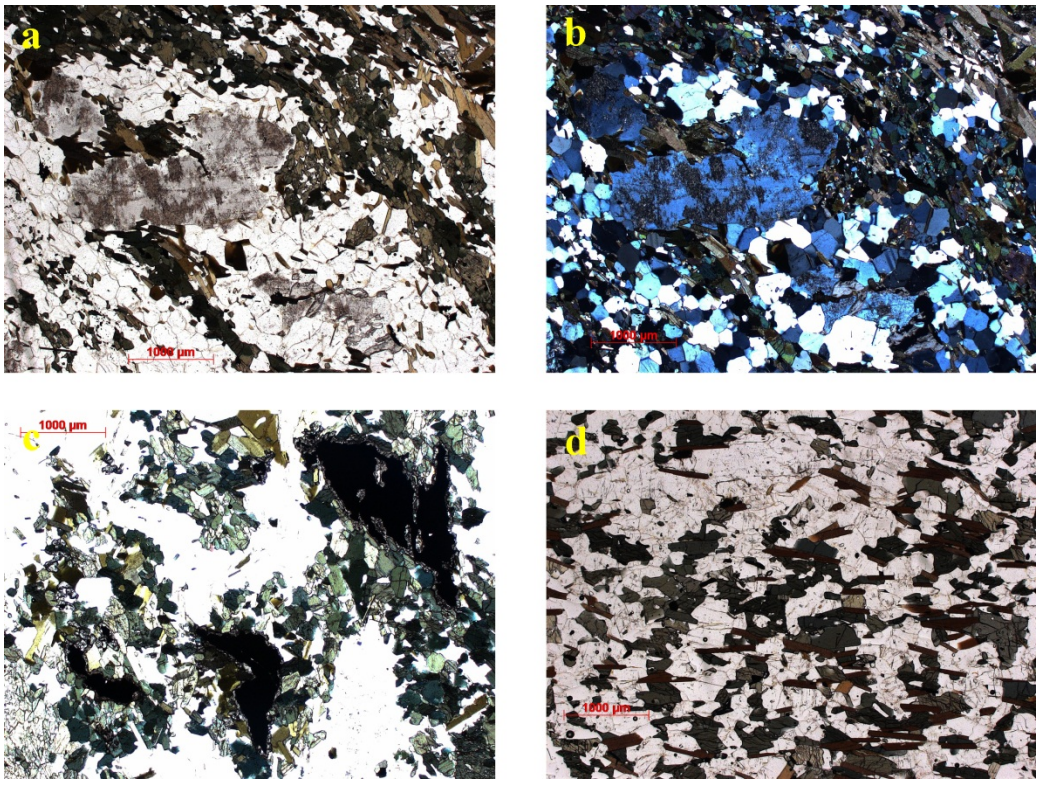

Figure 3.9 – a) Sample 12SJM159 is composed mainly of green amphibole, brown biotite, and inclusion-rich plagioclase, as displayed in PPL and XPL (b). All samples of alkalic metagabbro contain abundant Fe-Ti oxides, often sheathed with titanite, such as in sample 11SJM122A (c, PPL). Dikes of fine-grained granoblastic rocks with similar geochemistry and mineralogy are located throughout the Raglan Hills intrusion, such as sample 12SJM030A (d, PPL).

Rocks of unit 11 – alkalic metagabbro are generally enriched in ΣREEs compared to the regular and calcic metagabbroic rocks, and display distinct negative sloping REE patterns, from 80x chondritic lanthanum down to 20x chondritic lutetium, without the concavity displayed by the REEs in regular and calcic metagabbroic rocks (figure 3.11a). Only slightly positive and negative Eu anomalies are present in these samples.

Trace element patterns for alkalic metagabbroic rocks display a negative niobium-tantalum anomaly, though the other HFSEs (zirconium, hafnium, titanium) do not appear to be enriched or depleted relative to their neighboring elements (figure 3.11b). These patterns also display positive Pb anomalies (much less pronounced than those of the regular and calcic metagabbroic rocks), and high concentrations of LILs compared to regular and calcic metagabbroic rocks.

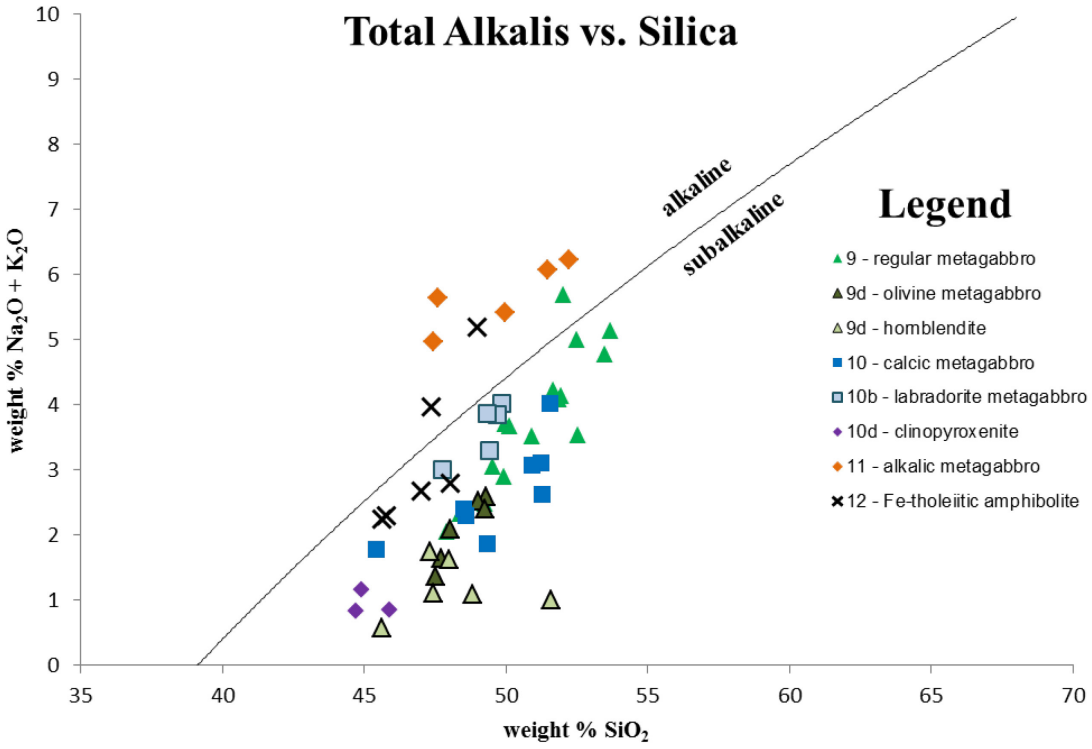

Figure 3.10 – Total alkalis vs. silica diagram including the alkaline-subalkaline division of Irvine and Baragar (1971). Note that the two samples of Fe-tholeiitic amphibolite which plot within the alkaline field are located near the boundary of the metagabbro and have likely been altered. All of the samples of unit 11 plot above the division, allowing for their classification as "alkalic metagabbro". Note that two samples of Fe-tholeiitic amphibolite and one sample of leucocratic regular metagabbro also plot within the alkaline field, possibly due to alteration and/or the geochemical effects of crystal fractionation.

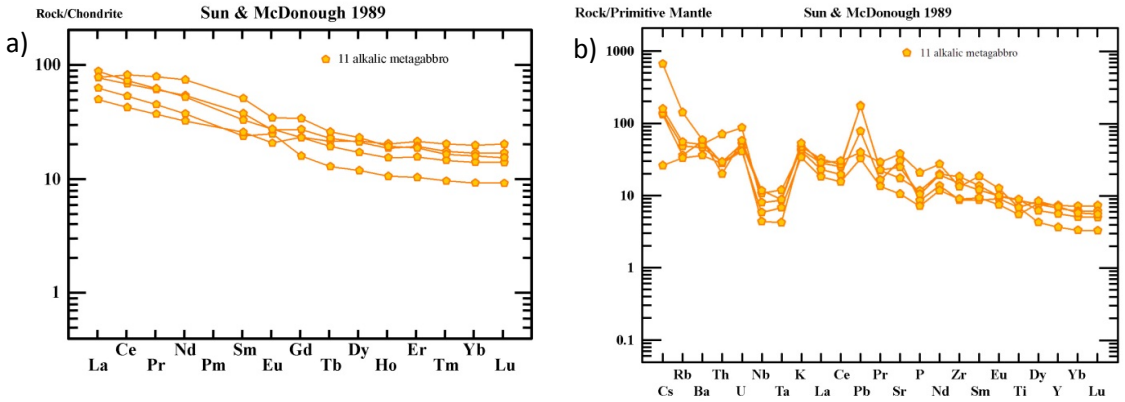

Figure 3.11 – a) REE plot and b) trace element plot for samples of unit 11 – alkalic metagabbro, normalized to chondritic and primitive mantle values (respectively) according to Sun and McDonough (1989).

3.4 - Fe-Tholeiitic Amphibolite – map unit 12

3.4.1 - Petrography

The samples which belong to the Fe-tholeiitic amphibolite rock type are so named due to their unique geochemical properties with respect to the other rocks in the Raglan Hills metagabbro (described below). These rocks also have unique textures observable in outcrop and hand sample: typically fine-grained and granoblastic with no phenocrysts or porphyroblasts, with mineralogy dominated by hornblende and plagioclase, hence the rock name amphibolite (figure 3.12).

12a – Fe-tholeiitic amphibolite

The rocks within this unit are composed of fine-grained (<1mm) equigranular granoblastic hornblende, plagioclase, and biotite, with minor titanite and Fe-Ti oxides, locally with diopside. These rocks commonly contain a well-developed foliation defined by hornblende-rich and plagioclase-rich bands of varied sub-centimetre scale thickness. These rocks display no identifiable primary igneous textures. Abundant tonalitic veins are commonly parallel to and/or offset by the well-developed foliation.

12b – dike of unit 12a cross-cutting other metagabbroic rocks

Several Fe-tholeiitic dykes have been observed cross-cutting other metagabbroic rocks, and have been interpreted as dikes. These dikes are up to 20 cm in width and commonly contain an internal foliation parallel to the foliations present in the host metagabbroic rocks.

3.4.2 - Geochemistry

As seen in figure 3.10, the samples of Fe-tholeiitic amphibolite plot within the subalkaline field. Plotting these samples on a ternary plot as developed by Jensen (1976) serves to further differentiate these rocks from the rest of the metagabbroic rocks in the Raglan Hills metagabbro (figure 3.13). These samples plot in a distinct group within the tholeiitic field, with the more mafic samples plotting in the high iron basalt field, whereas the regular and calcic metagabbroic rocks plot more towards the Al_2O_3-MgO edge of the diagram, passing from the basaltic komatiite field through to the calc-alkaline field.

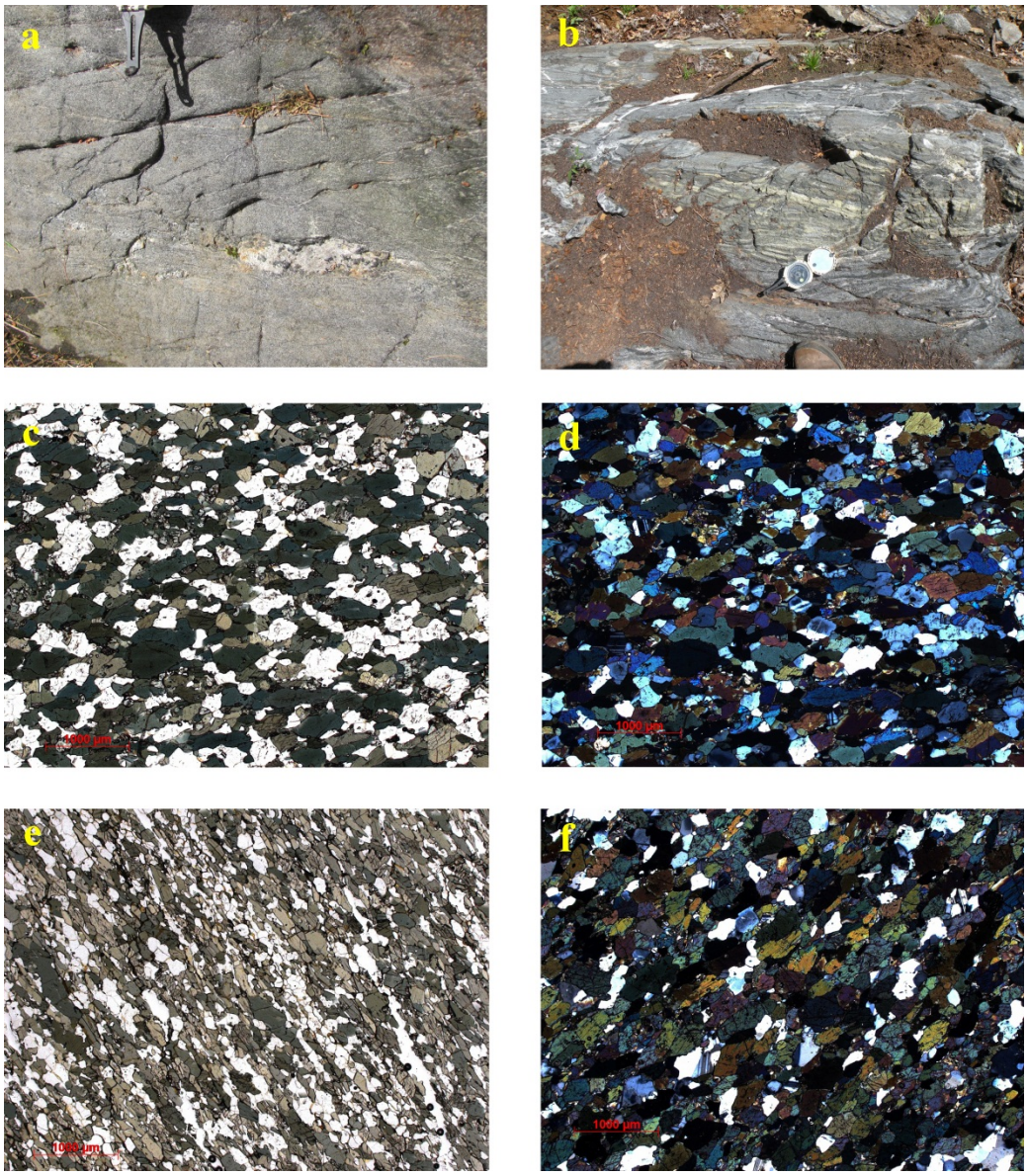

Figure 3.12 – a) fine-grained granoblastic amphibolite with a pod of tonalitic material which has been dextrally sheared through penetrative mylonitic deformation (station 12SJM045). Multiple deformed veins cross the mylonitic foliation trending northeast. b) Intensely deformed fine-grained amphibolite with abundant deformed tonalitic dikes. Most outcrops of Fe-tholeiitic amphibolite display strong foliations related to mylonitic deformation and shearing with intrafolial folds. c) Sample 12SJM044A is composed of fine-grained granoblastic green amphibole, colourless inclusion-free plagioclase, and light green clinopyroxene (PPL, see d) for XPL). e) Bands of plagioclase and amphibole in sample 12SJM160A describe a well-developed foliation visible in outcrop and hand-sample (PPL). d) Similar to 12SJM044A, sample 11SJM028 contains fine-grained granoblastic green amphibole and colourless plagioclase, with minor titanite and scapolite (XPL).

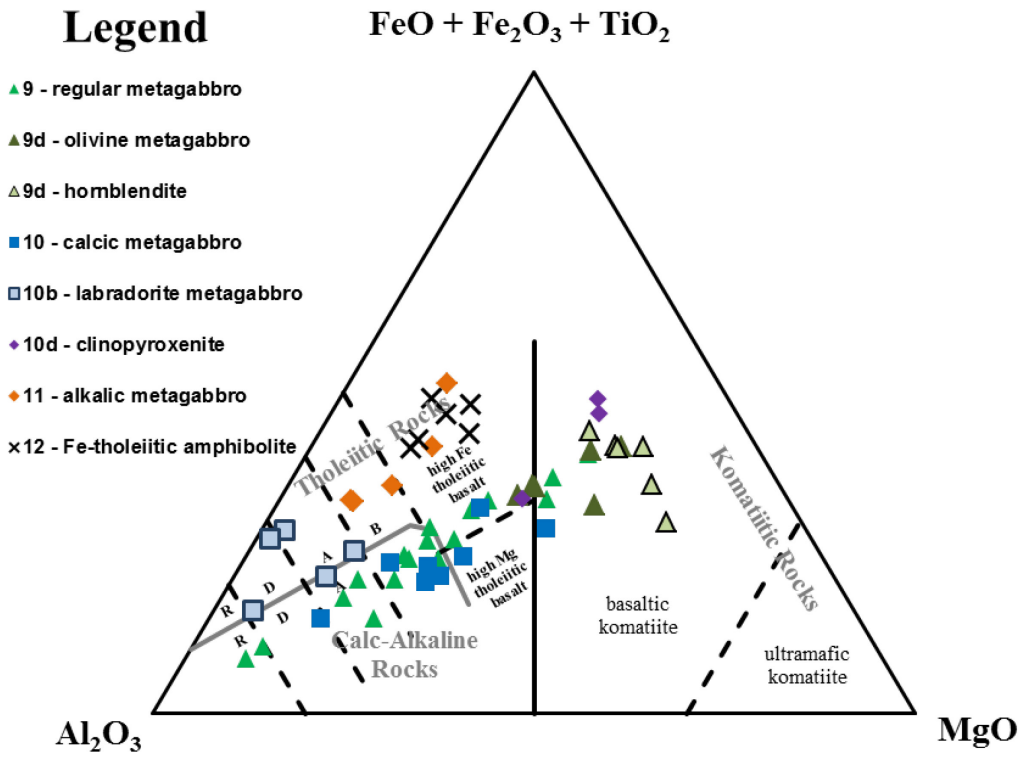

Figure 3.13 – Jensen (1976) plot including all unaltered metagabbroic rocks. Regular metagabbroic rocks are coloured green and calcic metagabbroic rocks are coloured blue to purple. Note the distinct separation between the amphibolitic rocks and alkalic rocks from the regular and calcic metagabbroic rocks. Samples of labradorite metagabbro plot in the tholeiitic field due to high iron contents (sulphide mineralization).

When plotted on REE diagrams, the samples of Fe-tholeiitic amphibolite display distinct topology with fairly flat HREE patterns and both positively and negatively sloping LREE patterns (figure 3.14a). Only very slight negative europium anomalies are visible for these samples.

The samples which display enrichment in LREEs (blue squares in figure 3.14) also happen to be variably enriched in large ion lithophile elements compared to the LREE depleted samples (black crosses in figure 3.14b). The LREE-enriched samples also have generally more pronounced depletions in the HFSEs (zirconium, hafnium and titanium).

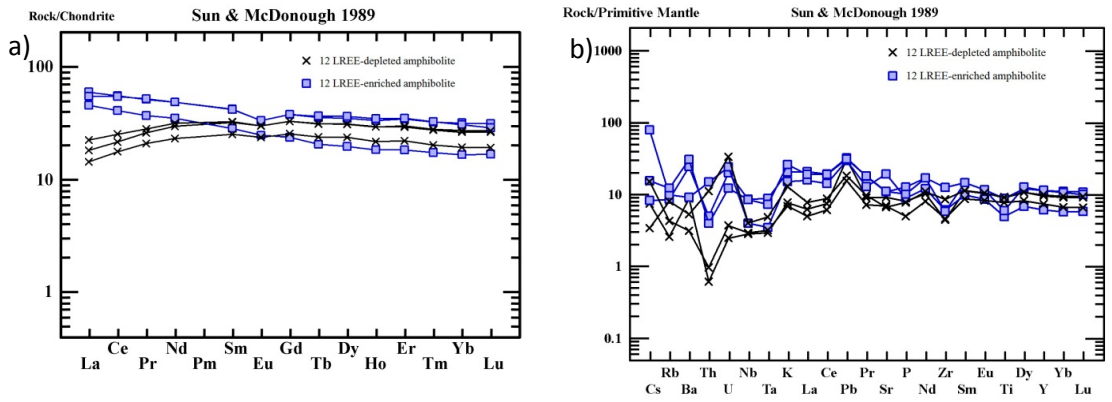

Figure 3.14 – a) REE plot and b) trace element plot for samples of unit 12 – Fe-tholeiitic amphibolite, normalized to chondritic and primitive mantle values (respectively) according to Sun and McDonough (1989). Black crosses represent LREE depleted amphibolite, and blue squares represent LREE enriched amphibolite.

3.5 - Altered Metagabbro – map unit 13

The distinction between the different types of altered metagabbro in the Raglan Hills metagabbro is largely based on whole rock geochemical analyses discussed below. However, there are several distinct mineralogical and textural differences between these altered metagabbroic rock types.

One distinct feature of the altered metagabbroic rocks to help differentiate them from regular metagabbroic rocks in the field is that felsic minerals in the altered metagabbroic rocks located within the basal thrust sheet tend to have a reddish-brown hue on their weathered surfaces (figure 3.15), unlike those in the core of the Raglan Hills metagabbro and along the southeast margin, where the felsic minerals tend to weather white.

The altered metagabbroic samples are located within two distinct zones in the Raglan Hills metagabbro: the basal thrust sheet and the southern edge of the intrusion as described in chapter 5.

3.5.1 - 13a – altered regular or calcic metagabbroic rock

Rocks of this unit located along the southern edge of the Raglan Hills metagabbro that were affected by deformation along the McArthurs Mills shear zone have undergone extensive mylonitic deformation, which overprinted what could have been medium- to coarse-grained gabbroic textures. These rocks are texturally distinguishable from the Fe-tholeiitic amphibolites through a mineralogical heterogeneity in these rocks likely caused by the mylonitic deformation of coarse magmatic grains, as opposed to the rather homogeneous mineralogy of the amphibolitic rocks. These altered rocks are composed of bands of plagioclase and hornblende with minor calc-silicate bands.

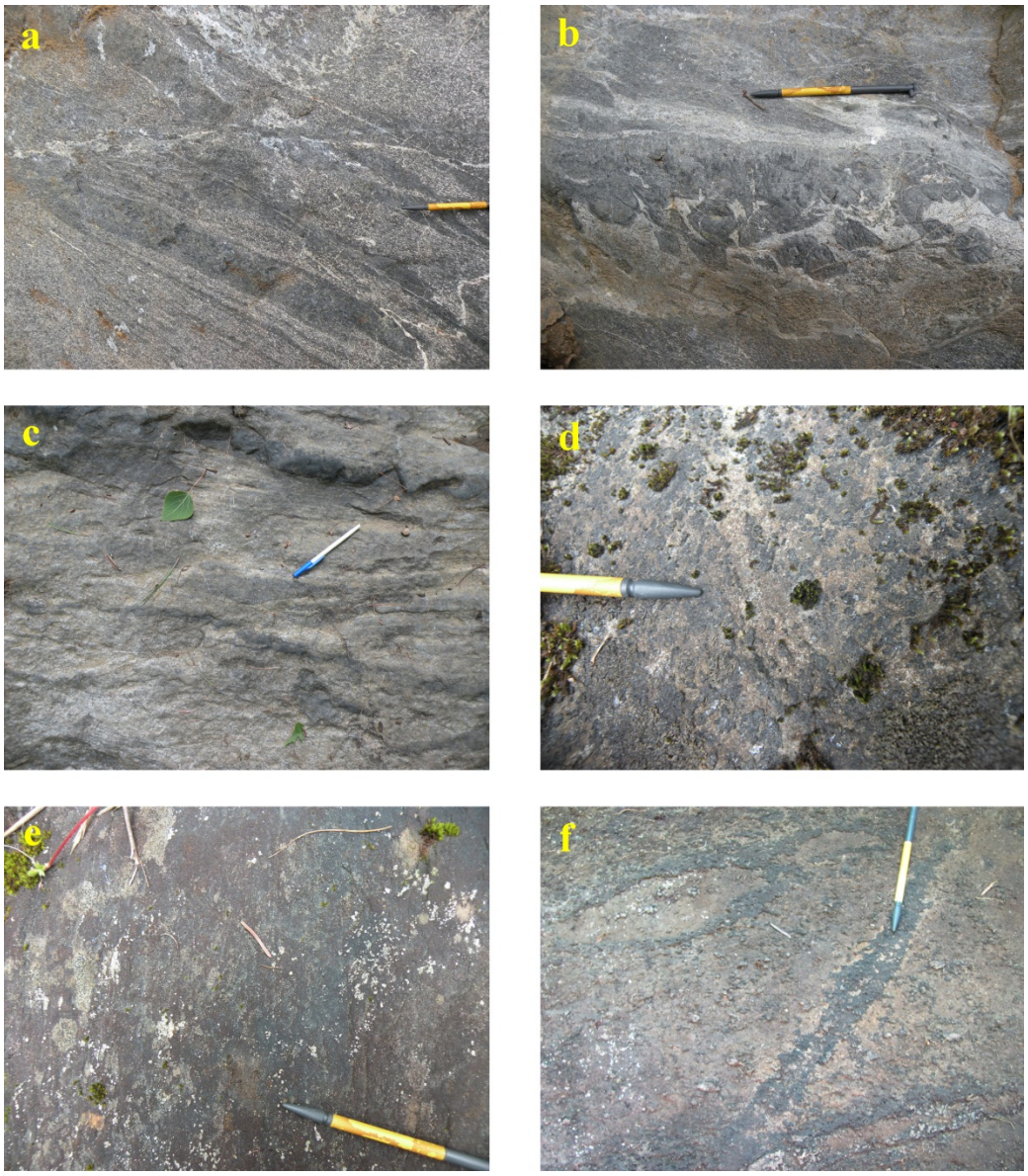

Figure 3.15 – a) Metagabbro from station 11SJM099, displaying heterogeneous textures likely related to both primary magmatic layering and ductile shearing, cut by a 15 cm vein of calcic metagabbroic composition with clinopyroxene megacrysts up to 4 cm across. Outcrops at stations 11SJM182 (c), 11SJM097 (d) and 11SJM094 (e) display a washed-out texture with a mottled-brownish colour similar to the rocks at 11SJM099. Station 12SJM005 (f) contains melanocratic and leucocratic zones with an irregular arrangement.

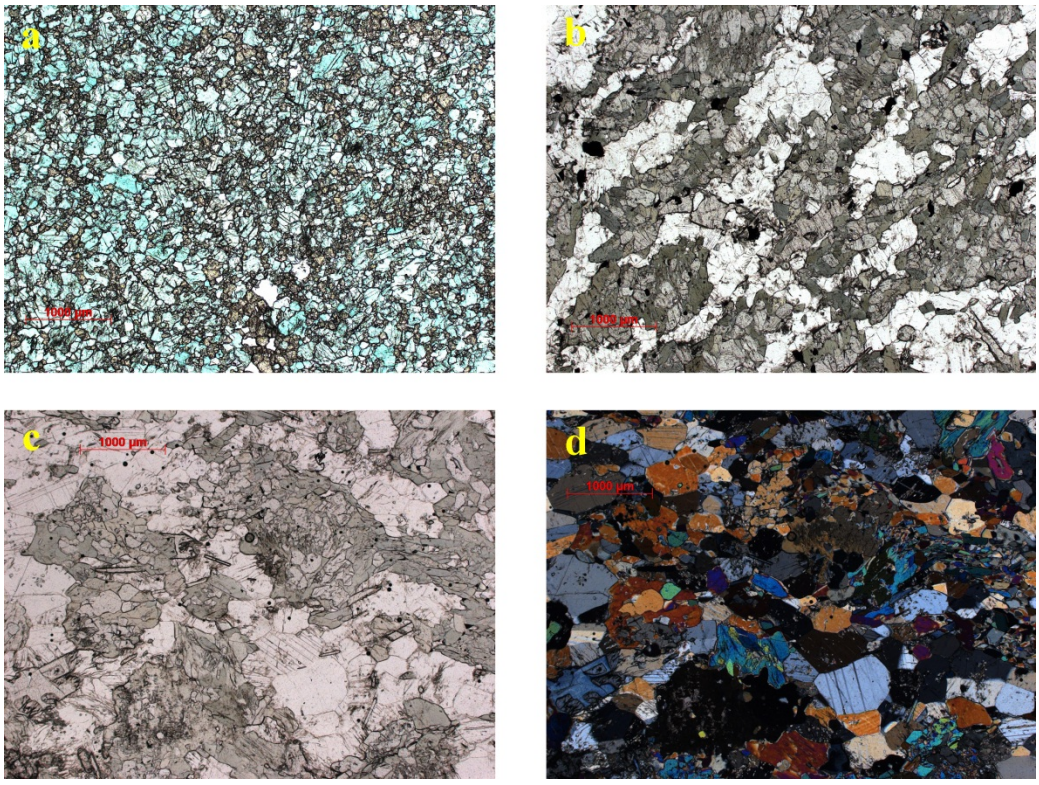

Figure 3.16 – Sample 11SJM100A (a) is composed almost entirely of fine-grained green amphibole and pink garnet (PPL). b) sample 11SJM095A is composed of colourless plagioclase, epidote, green amphibole and light green clinopyroxene which appears to have grown during prograde metamorphism, as opposed to the colourless clinopyroxene phenocrysts contained in samples of "calcic metagabbro" (PPL). c) Sample 12SJM006A (PPL) has similar mineralogy to sample 11SJM095A, except that the crystals of plagioclase display higher birefringence, up to 1st order brown/orange, as seen in XPL (d, same field of view as c).

Rocks in this unit located within the basal thrust sheet display recognizable metagabbroic textures, and are generally composed of colourless, inclusion-free plagioclase crystals (no inclusion-rich, twinned plagioclase crystals are observed), and massive aggregates of green hornblende which display no textural evidence for the primary magmatic minerals (there are no pseudomorphs) with minor granoblastic diopside, scapolite and/or epidote (figure 3.16). Due to the abnormal trace element concentrations in these rocks which suggest that they have been metasomatized, the presence or absence of calc-silicate minerals can not be used to distinguish between regular metagabbroic, calicic metagabbroic or other possible protoliths.

A variety of calc-silicate and tonalitic veins with diffuse, irregular contacts are common in rocks of this unit, locally accompanied by calc-silicate rich equigranular granoblastic rocks ("washed out" texture), likely indicative of metasomatism during metamorphism.

3.5.2 - 13b – altered metagabbroic rock with low Si and/or REE concentration

Rocks in this unit are generally located along the southern margin of the basal thrust sheet, and proximal to areas affected by significant sinistral displacement within the basal thrust sheet. These rocks generally display recognizable metagabbroic textures; however in thin section

it is apparent that these rocks have experienced extensive recrystallization, and in places hydrothermal alteration (sericitization, chlorite development).

The outcrop at station 12SJM005 displays textures unique within the Raglan Hills metagabbro. In this outcrop, pods of tonalite (fine-grained granoblastic plagioclase and quartz) are sheathed by melanocratic zones of orthoamphibole, which grade (compositionally) to a generally leucocratic to mesocratic metagabbro composed of fine-grained equigranular granoblastic plagioclase, needles of epidote and poikiloblastic orthoamphibole, with minor sericite alteration of plagioclase. The melanocratic material is also present in vein-like structures, as seen in figure 3.15f.

3.5.3 - 13c – altered metagabbroic rock with high iron concentration

Two elongate positive magnetic anomalies are present within the basal thrust sheet which trend parallel to the edge of the metagabbro (see PMap 3774, back pocket, geophysically delineated unit G13c). Rocks located within these magnetic anomalies are composed of fine-grained equigranular granoblastic hornblende, diopside, epidote and plagioclase with minor Fe-Ti oxides. In hand sample these rocks may appear similar to hornblendites or clinopyroxenites, since all three of these rocks are almost uniformly dark green. However, the hornblendites should not contain diopside and epidote, whereas clinopyroxenites are normally medium- to coarse-grained and not magnetic.

3.5.4 - Geochemistry

As mentioned above, classification of the altered metagabbroic rocks in the Raglan Hills metagabbro is largely based on major and trace element geochemistry. Three major trends of alteration were observed in these samples.

Map unit 13a consists of samples which have major and trace element compositions similar to those of regular or calcic metagabbroic rocks, however the rocks have been metamorphosed and recrystallized such that primary magmatic mineralogy cannot be determined, making the distinction between a regular or calcic metagabbroic protolith difficult. These rocks tend to have higher CaO and SiO_2 and lower concentrations of light REEs with respect to the regular and calcic metagabbroic rocks, which causes these samples to display horizontal to positively sloping light REE patterns (figure 3.17a). Otherwise, these samples display all of the same anomalies as their unaltered counterparts (figure 3.17b).

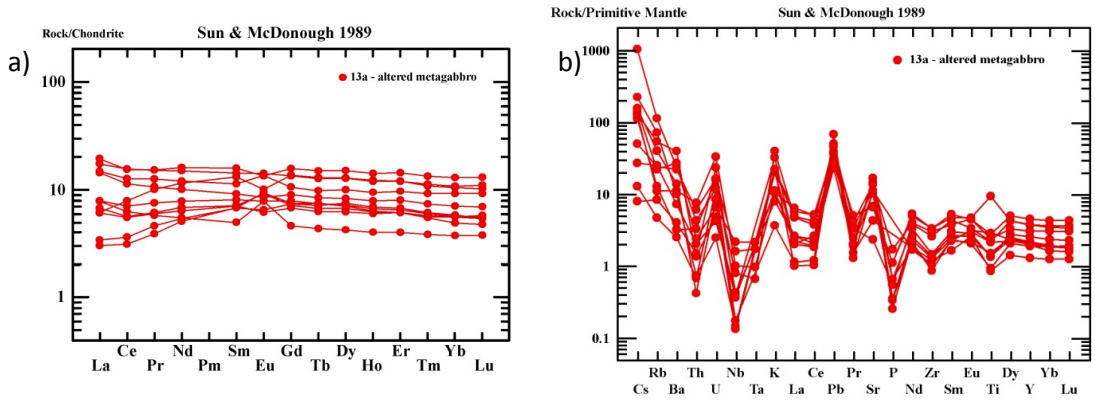

Figure 3.17 – a) REE plot and b) trace element plot for samples of unit 13a – altered metagabbroic rocks, normalized to chondritic and primitive mantle values (respectively) according to Sun and McDonough (1989).

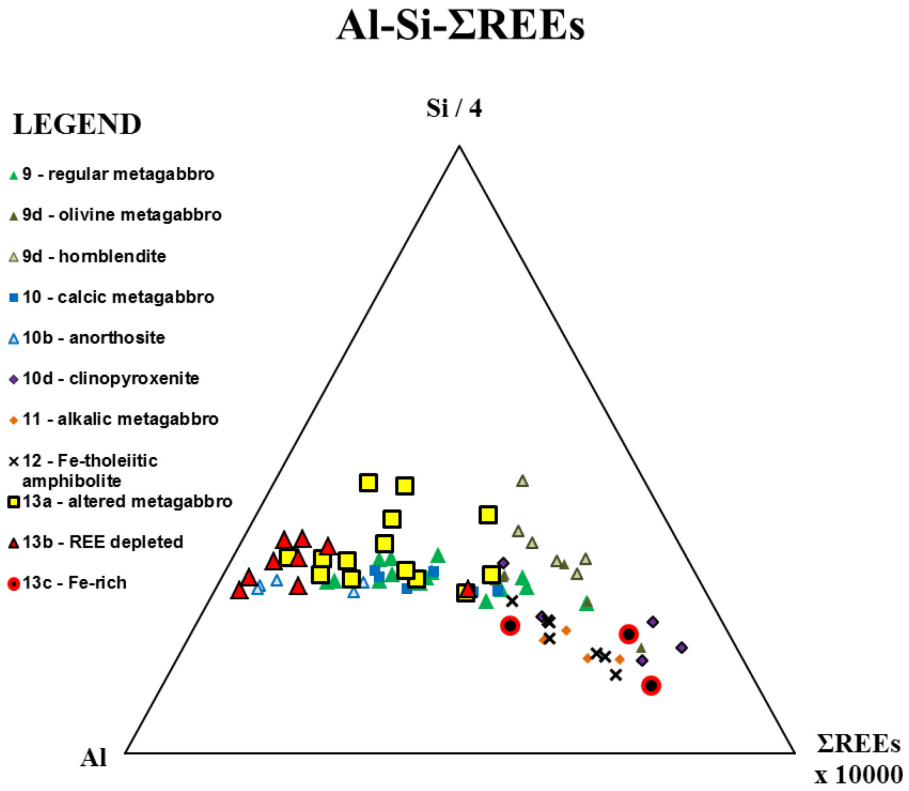

Figure 3.18 – Ternary plot of molar ionic proportions for all metagabbroic rocks sampled from the Raglan Hills metagabbro, with emphasis on the three major types of altered metagabbroic rocks. Note that the samples of hornblendite plot near the samples of olivine gabbro and trend away from the ΣREEs corner and towards the Si/4 corner. Ionic proportions were multiplied and divided in order to expand the area within which the samples plot, for ease of viewing.

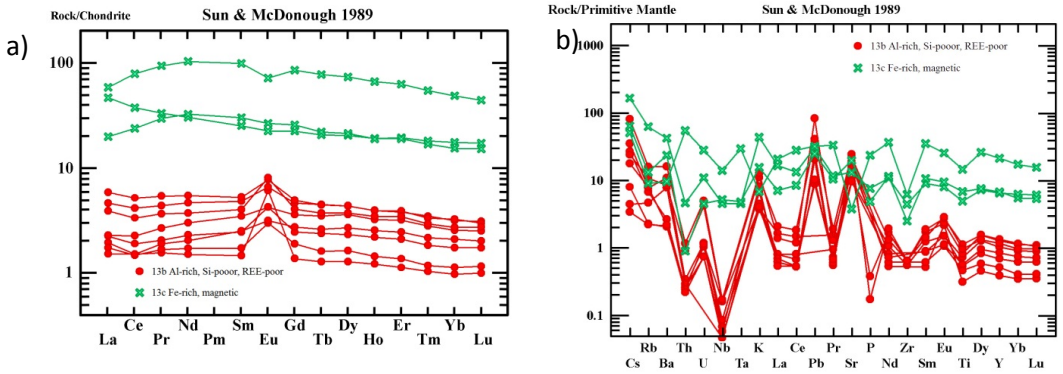

Figure 3.19 – a) REE plot and b) trace element plot for samples of unit 13 – altered metagabbroic rocks, normalized to chondritic and primitive mantle values (respectively) according to Sun and McDonough (1989). Green crosses represent altered metagabbroic rocks with high iron content (13c) and red circles represent altered metagabbroic rocks with low REE and SiO_2 concentrations. Samples of unit 13a are not plotted on here,

Map unit 13b consists of altered regular or calcic metagabbroic rocks (indeterminable) with particularly low ΣREE and SiO_2 concentrations with respect to regular and calcic metagabbro, as opposed to the samples of map unit 13a which tend to have higher SiO_2 concentrations and only depleted light REEs (figures 3.19a and b).

Map unit 13c consists of altered metagabbroic rocks with particularly high concentrations of iron and/or magnesium and highly variable SiO_2 concentrations (37 to 50 wt. % SiO_2). These samples tend to display REE patterns similar to those of olivine gabbro (map unit 9d) or clinopyroxenite (map unit 10d) and highly erratic trace element patterns. These samples lie within positive aeromagnetic anomalies which are elongate and oriented parallel to the northern edge of the Raglan Hills metagabbro.

3.6 - Metagranitoid Rocks, map units 15 and 19

3.6.1 - Petrography

Several outcrops of metagranitoid rocks are located within the Raglan Hills metagabbro, concentrated within the basal thrust sheet (figure 3.20). These rocks display a variety of metamorphic fabrics according to the amount of deformation they have experienced, indicating that they likely were not emplaced simultaneously, but throughout the magmatic and metamorphic history of the Raglan Hills metagabbro.

Tonalite dikes up to 10 cm wide are common throughout the Raglan Hills metagabbro in each structural domain, which cut through the metagabbroic host with sharp, straight intrusive contacts.

15a – granodiorite to monzogranite

A band of granitoid rocks roughly 3 kilometres in length is located within the eastern end of the basal thrust sheet of the Raglan Hills metagabbro. These rocks range from granodiorite (fine-grained equigranular plagioclase and quartz, minor biotite, and minor potassium feldspar

present both in foliation-parallel veins and within the host rock) to monzogranite (medium-grained equigranular plagioclase and potassium feldspar with mylonitic quartz bands).

These rocks all contain a well-developed mylonitic foliation that dips moderately to the southeast, striking west by southwest. The contact between this intrusion and the host metagabbro is visible in a roadside outcrop along County Road 514 (Schutt Road) (station 11SJM059) (figure 3.20a). Granitoid dikes sprout from the main intrusion and cross-cut the host metagabbro, indicating that the intrusion is younger than the metagabbroic host. This dike contains an internal foliation parallel to the strong, pervasive foliation present within the host metagabbro.

19a – white pegmatitic tourmaline monzogranite

At station 12SJM032 there is an outcrop of white pegmatitic granitoid rock composed of coarse-grained massive quartz, plagioclase and potassium feldspar with trace fine-grained black-green tourmaline (figure 3.21b). There is no textural evidence for deformation in this outcrop. This rock is unique within the Raglan Hills metagabbro.

Several other outcrops within the Raglan Hills metagabbro contain pink pegmatitic biotite granite dikes with little to no internal fabric which cut metagabbroic rocks.

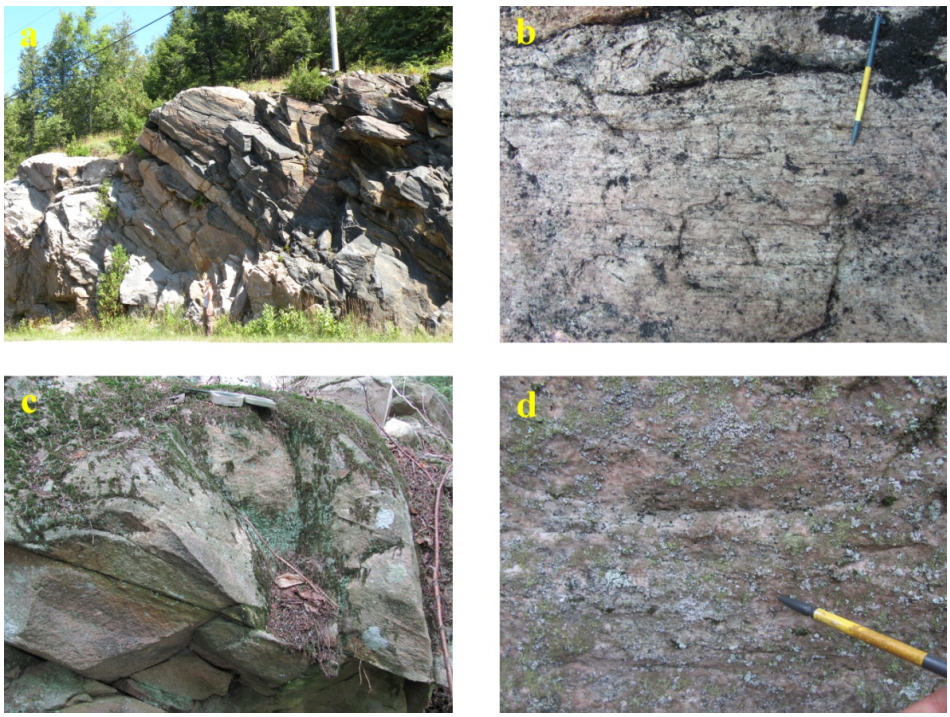

Figure 3.20 – a) station 11SJM059 along Schutt Road, which contains grey monzogranite (left) which is observed cutting metagabbroic rocks (right). Both rocks display parallel foliations dipping moderately towards the southeast. The station was also a U-Pb geochronology site for the monzogranite. b) Station 12SJM031 contains mylonitic syenogranite with trace potassium feldspar porphyroclasts. c) Stations 12SJM155 and d) 12SJM156 are composed of pink monzogranite with pervasive mylonitic fabrics.

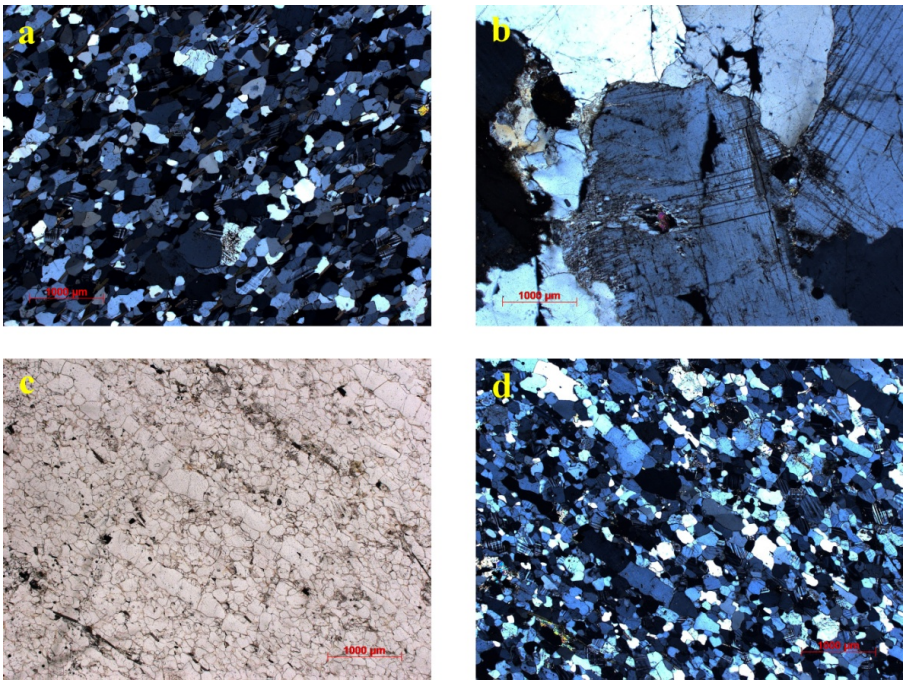

Figure 3.21 – a) Sample 11SJM059B is composed of fine-grained granoblastic alkali feldspar, plagioclase and quartz with minor biotite and trace zircon (XPL). b) A coarse-grained white granite that displays almost no textural evidence of deformation. c) Sample 12SJM031A, a mylonitic syenogranite, is composed of fine-grained alkali feldspar and plagioclase with quartz "stringers" (in PPL; d, in XPL).

3.6.2 - Geochemistry and Classification

The classification scheme proposed by Frost et al. (2001) has been used to classify the samples of granitoid rocks in the Raglan Hills metagabbro. Major oxide concentrations for granitoid samples are presented in Table 3.3.

Based on the first tier of classification (figure 3.22a), all of the granitoids are ferroan. This indicates that the crystallizing magma likely experienced iron enrichment during fractional crystallization.

Based on the second tier of classification (figure 3.22b), the samples from the elongate felsic intrusive (11SJM059B, 12SJM031A, 12SJM155A and 12SJM156A) all plot near the alkali-calcic – calc-alkalic boundary, whereas the sample of white monzogranite (12SJM032A) plots within the calcic field.

The third tier of classification, the "Aluminum Saturation Index" (ASI) is based on a simple value calculated by the following equation:

$$equation\ 1: \qquad ASI = Al_2O_3/(CaO - 1.67 * P_2O_5 + Na_2O + K_2O)$$

The results (Table 3.3) show that all of the granitoid samples are peraluminous; they contain more aluminum than may be accounted for solely by aluminum in feldspar, and thus they must have contained other aluminous phases in its magmatic mineral assemblage, such as mica.

Sample	11SJM059B	12SJM031A	12SJM032A	12SJM155A	12SJM156A
Petrographic Rock Name	granodiorite	pink monzogranite	white monzogranite	pink monzogranite	pink monzogranite
Map Code	15a	15a	19a	15a	15a
Al_2O_3	15.59	14.65	14.61	14.58	15.06
CaO	1.595	0.942	1.318	0.728	0.949
Fe_2O_3t	1.79	0.54	0.44	0.76	0.85
FeO	1.28	0.23	0.19	0.42	0.44
Fe_2O_3	0.51	0.31	0.25	0.34	0.41
K_2O	3.38	4.43	1.59	4.94	4.28
LOI	0.36	0.47	0.42	0.47	0.39
MgO	0.34	0.06	0.03	0.08	0.08
MnO	0.026	0.012	0.01	0.009	0.01
Na_2O	4.47	4.2	5.6	3.85	4.54
P_2O_5	0.061	0.012	0.004	0.019	0.016
SiO_2	71	75.22	76.51	74.9	74.5
TiO_2	0.25	0.03	0.02	0.05	0.04
Total	98.86	100.57	100.55	100.39	100.72
Fe^{number}	0.79	0.79	0.86	0.84	0.85
MALI	6.26	7.69	5.87	8.06	7.87
ASI	1.67	1.53	1.72	1.54	1.55

Table 3.3 – Major oxide concentrations (reported in weight %) for granitoid samples collected from within the Raglan Hills metagabbro. Values for Fe^{number}, MALI (Modified Alkali Lime Index) and ASI (Aluminum Saturation Index) are unitless. Equations for Fe^{number} and MALI may be found in their respective graphs (figure 3.22).

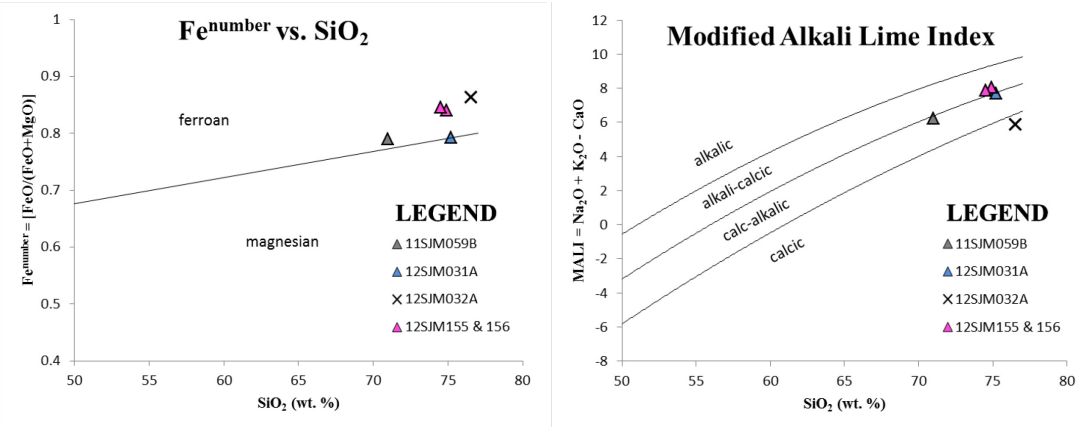

Figure 3.22 – Fe* and MALI discrimination diagrams for granitoid rocks, from Frost (2001). Note that sample 11SJM059B plots separately from the other granitoid samples collected from this intrusion. Sample 12SJM032A, the white monzogranite also plots separately, and is likely not at all related to the other felsic intrusive rocks present in the Raglan Hills metagabbro.

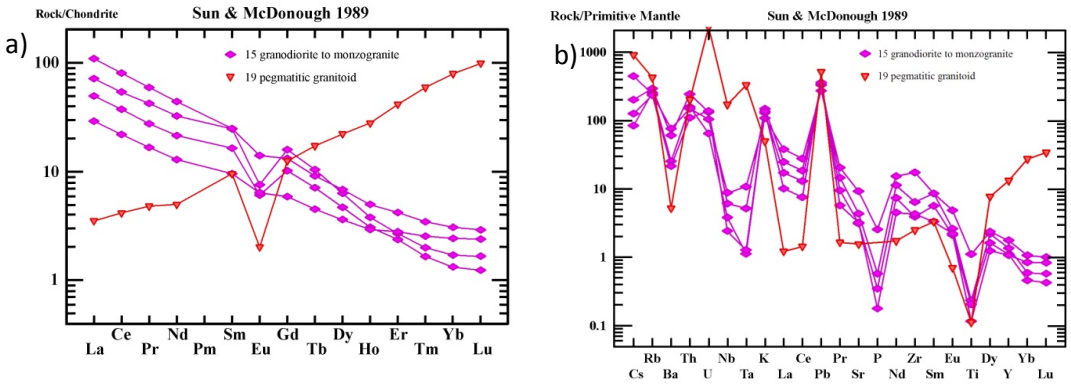

Figure 3.23 – a) REE plot and b) trace element plot for samples of granitoid rocks collected from within the Raglan Hills metagabbro. Note that the two samples of rock type 15 which display more pronounced negative Eu anomalies and lower concentrations of heavy REEs are samples 12SJM155A and 12SJM156A, mylonitic pink monzogranite.

The samples of rock type 15a display strong negative slopes which are shaped slightly concave upward. This pattern is typical or arc-derived felsic rocks (FI type of Lesher et al. 1986). Samples 11SJM059B and 12SJM031A display slightly negative Eu anomalies, whereas samples 12SJM155A and 12SJM156A display much more pronounced negative Eu anomalies and contain lower concentrations of heavy REEs (figure 3.23a).

These samples produce a similar negatively sloping pattern on a trace element diagram (figure 3.23b), and display negative anomalies of niobium, tantalum, phosphorous and titanium, variably enriched and depleted zirconium, and positive Pb and K anomalies.

The sample of non-deformed white monzogranite displays REE and trace element patterns unique from the samples of tonalite described above. This sample is strongly enriched in heavy rare earth elements, Th, U, Nb, Ta, and Pb, with strong negative Eu, Ba and Ti anomalies (figure 3.23). This suggests that there was likely a refractory LREE-bearing mineral in the melt source for this rock, and the negative Eu anomaly suggests that either plagioclase was fractionated out of the magma, or the magma was produced under reducing conditions in the presence of a refractory Ca-bearing phase.

Plotting these samples on trace element discrimination diagrams for the tectonic setting of granitic rocks (Pearce et al. 1984) places the samples of 15a within the volcanic arc granite field when the HFSEs (Nb, Ta) and REEs (Y, Yb) are plotted against each other (figure 3.24a and b), and places them along the boundary between the volcanic arc granite field and the syn-collisional granite field when the HFSEs and REEs are plotted against Rb (a large ion lithophile element)(figure 3.24c and d).

The sample of white monzogranite (station 12SJM032A) plots within the “within plate granite” field on all of these diagrams.

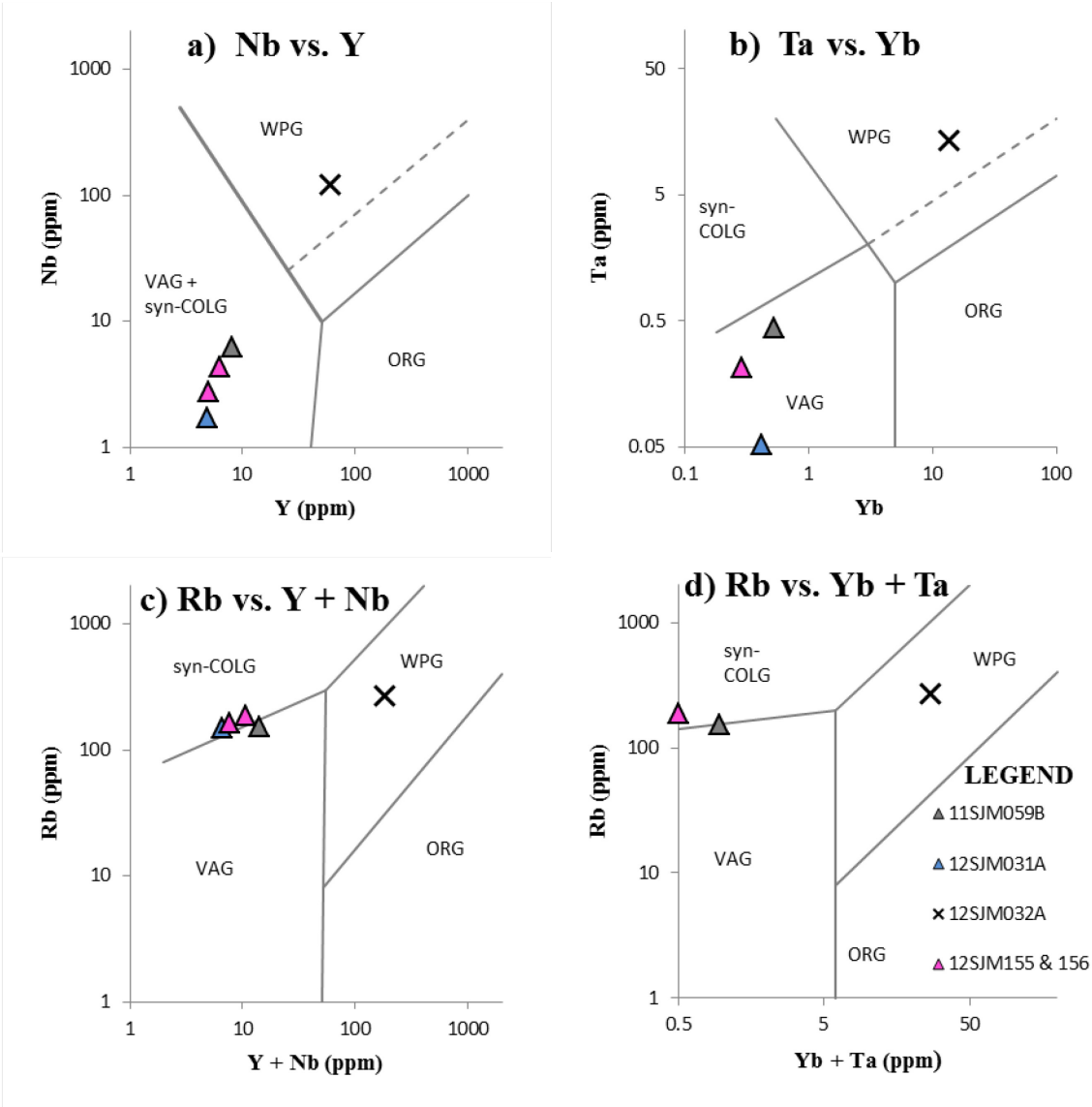

Figure 3.24 – trace element tectonic discrimination diagrams for granitic rocks, as developed by Pearce et al. (1984). Abbreviations: WPG = within-plate granite, ORG = ocean ridge granite, VAG = volcanic arc granite, and syn-COLG = syn-collisional granite. Note that the samples of rock type 15a plot within the VAG and syn-COLG fields, whereas the sample of white monzogranite plots consistently within the WPG field. The legend in d) applies to all four diagrams.

4 – Geochemistry

4.1 – Major and Trace Element Geochemistry

The descriptions above show that a clear distinction may be made between the different unaltered metagabbroic rocks found within the Raglan Hills metagabbro based on major and trace element geochemistry. Geochemical diversity within each rock type is also present, and may be significant for determining the petrogenetic and metamorphic history of the Raglan Hills metagabbro.

For instance, when plotting Al_2O_3 against Eu* (figure 4.1), several samples of olivine gabbro (map unit 1d) lie close to Eu* = 0, which means that the europium concentration in these samples is not anomalous. The more felsic samples (higher Al_2O_3) of regular and calcic metagabbro tend to plot with positive Eu* values and the more mafic samples (lower Al_2O_3) tend to plot with negative Eu* values. The samples with Eu* close to zero will be used as a reference point for the remainder of this chapter.

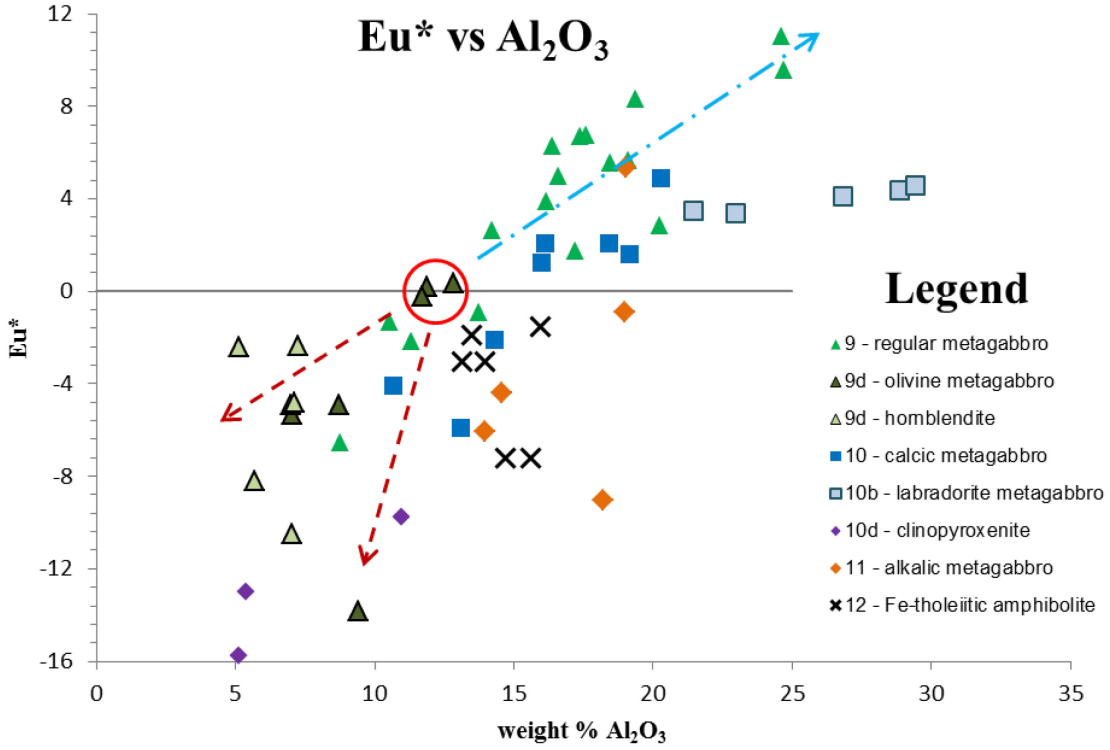

Figure 4.1 – plot of Al_2O_3 vs. Eu*, where Eu* = - [(Sm_{chon} + Gd_{chon})/2] + Eu_{chon}. These trace elements (with subscript "chon") have been normalized to chondritic concentrations using the values determined by McDonough and Sun (1995). Note that there are not enough samples of map units 11 and 12 to properly evaluate any trends involving Eu*. The blue line traces a general trend

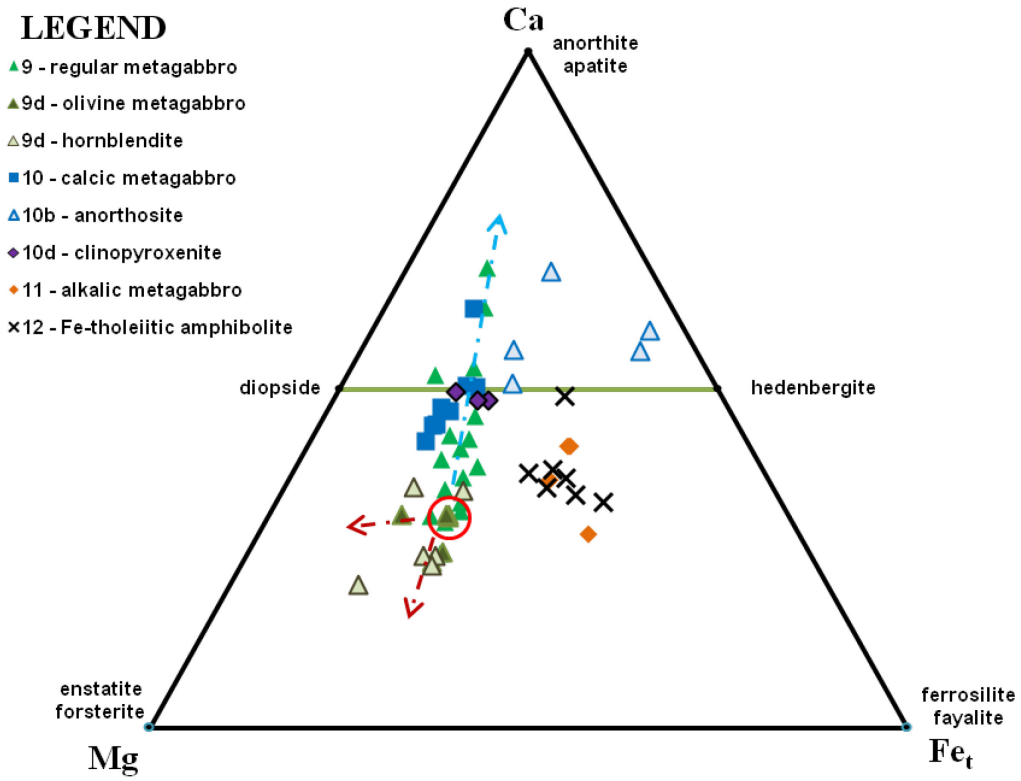

Figure 4.2 – Ternary plot of molar ionic proportions for all unaltered metagabbroic rocks sampled from the Raglan Hills metagabbro. The red circle includes the samples with Eu* close to 0. The blue line traces a trend towards the Ca corner of the diagram, whereas the brown lines show the variable deviation of ultramafic samples from the red circle. Pyroxene end member compositions, olivine end member compositions, anorthite and apatite compositions plotted for reference.

As seen in figure 4.2, the samples with Eu* close to zero plot well within the pyroxene compositional field (in Mg-Ca-FE space), slightly on the Mg-rich side. From this point, the more felsic samples of regular and calcic metagabbro plot along a straight line that trends towards the Ca corner of the diagram, whereas the samples of olivine gabbro and hornblendite (map unit 1d) deviate variably throughout the pyroxene compositional field, and the samples of clinopyroxenite (map unit 2d) cluster along the diopside-hedenbergite compositional tie line.

Adding aluminum to the ternary diagram (figure 4.3) produces a similar effect, which shows that the more felsic regular and calcic metagabbro plot along lines which converge towards the plagioclase compositional tie line (labradorite in composition), whereas the more mafic samples diverge from the red circle towards variable pyroxene compositions.

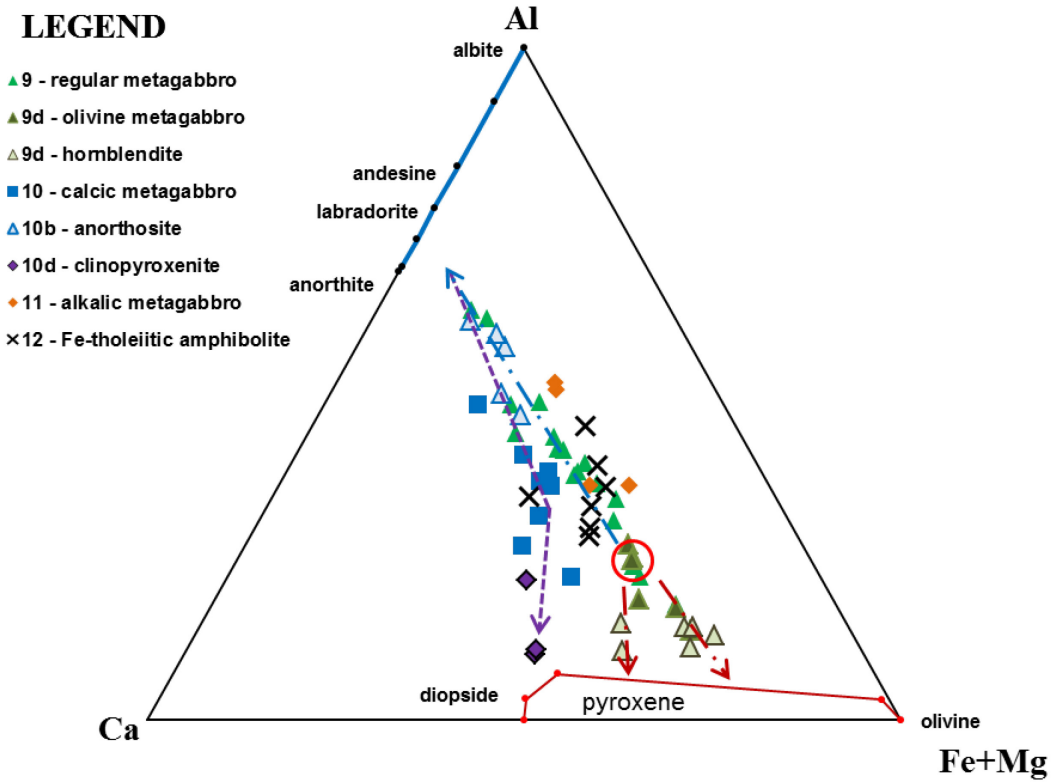

Figure 4.3 – Ternary plot of molar ionic proportions for all unaltered metagabbroic rocks sampled from the Raglan Hills metagabbro. The red circle includes the samples with Eu* close to 0. The blue line traces a trend towards the Ca-Al edge of the diagram (labradorite plagioclase) whereas the brown lines show the variable deviation of ultramafic samples towards different pyroxene compositions. Pyroxene end member, plagioclase end member and olivine compositions plotted for reference.

4.2 - Isotope Geochemistry

Nineteen samples of metagabbroic rocks were collected from the Raglan Hills metagabbro for isotopic analysis, including samples from each of the unaltered metagabbroic rock types (table 4.1). In general, care was taken to choose samples that have geochemical signatures typical of their rock types, with the exception of sample 11SJM120A, a sulphide-mineralized sample of labradorite metagabbro collected from the Raglan Hills showing.

In a parent/daughter isotope trace element ratio plot (figure 4.4), which is used to determine the geochemical signature of the melt source relative to bulk earth, some distinctions may be made between the rock types. The majority of the regular and calcic metagabbroic rocks cluster together within the light REE-enriched field, consistent with the REE-patterns described earlier (chapter 3), and several samples with increased Rb/Sr ratios plot within the Rb and LREE-enriched field, including a sample of hornblendite (11SJM173A) which has a Rb/Sr value of 0.160. The single sample of alkalic metagabbro plots within the Rb and LREE-enriched field, with a similar Sm/Nd value to the regular and calcic metagabbroic rocks. The samples of Fe-tholeiitic amphibolite consistently plot above the LREE-enriched fields, closer to the MORB field.

These patterns are conserved when all of the metagabbroic samples within the Raglan Hills metagabbro are included in this plot (figure 4.5). The samples of regular and calcic metagabbro cluster together in the LREE-enriched field, and the samples of alkalic metagabbro plot within the Rb and LREE-enriched field. The three remaining samples of Fe-tholeiitic amphibolite plot within the LREE-enriched field, consistent with their horizontal to negatively sloping LREE patterns (figure 3.14), and have similar Rb/Sr ratios to their LREE-depleted counterparts. This plot also includes the samples of altered metagabbroic rocks (map unit 13), which spread across all fields, and tend to plot more towards and within the Rb-enriched, LREE-depleted field, except for the samples of REE-depleted altered metagabbro (map unit 13b) that are wholly confined within the LREE-depleted/ low Rb/Sr field.

On a $^{143}Nd/^{144}Nd$ vs. $^{87}Sr/^{86}Sr$ isotopic plot (figure 4.6), all of the samples plot within the depleted quadrant, with $^{143}Nd/^{144}Nd$ values similar to that of the estimated value of the depleted mantle at 1229 Ma ($^{143}Nd/^{144}Nd = 0.511317$, $^{87}Sr/^{86}Sr = 0.701883$) , with slightly enriched $^{87}Sr/^{86}Sr$ values. The samples of Fe-tholeiitic amphibolite (with N-MORB-like REE patterns) cluster above the regular and calcic metagabbroic rocks, with slightly more depleted $^{143}Nd/^{144}Nd$ values.

These trends are re-visualized on an εNd plot (figure 4.7) after DePaolo (1981), where the samples of regular and calcic metagabbroic rocks tend to cluster around the estimated Depleted Mantle evolution line at 1229 Ma and deviate towards lower εNd values, an effect attributed by DePaolo (1981, and many others) to influence from radiogenic crustal material. Whether this effect was induced during magmatism or metamorphism is currently uncertain. The samples of Fe-tholeiitic amphibolite plot well above (out of error) the Depleted Mantle curve, and the sample of mineralized labradorite metagabbro plots off the chart with an εNd value of +18.3.

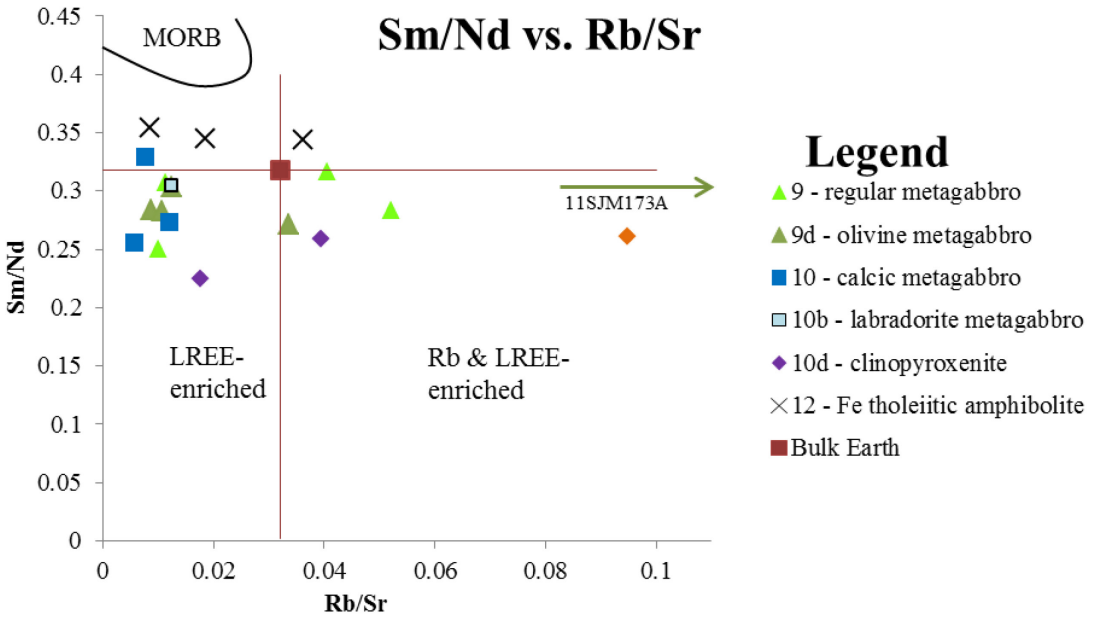

Figure 4.4 – Sm/Nd vs. Rb/Sr ratio plot after Norry and Fitton (1983). A majority of the regular and calcic metagabbroic rocks plot within the LREE-enriched quadrant relative to Bulk Earth trace element concentrations. The samples of Fe-tholeiitic amphibolite plot within the depleted quadrant. Sample 11SJM173A has a Rb/Sr value of 0.160.

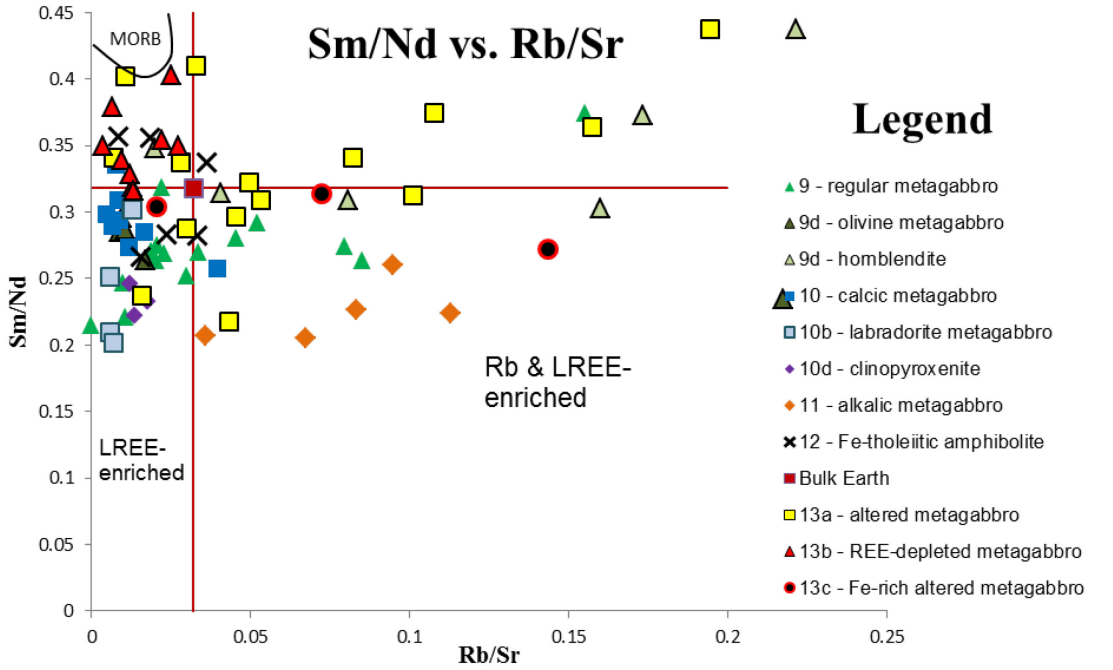

Figure 4.5 – Sm/Nd vs. Rb/Sr ratio plot after Norry and Fitton (1983) with all metagabbroic rocks collected from the Raglan Hills metagabbro. Note that the altered metagabbroic rocks (13a and 13b) tend to plot above the samples of regular and calcic metagabbroic rocks and into the LREE-depleted fields. The alkalic metagabbroic rocks (map unit 11) plot consistently within the Rb and LREE-enriched field, and the samples of Fe-tholeiitic amphibolite (map unit 12) are split into two groups: LREE-enriched and LREE-depleted, consistent with patterns observed in the REE and trace element patterns (figures 3.11 and 3.14, respectively). This plot shows that all samples, not only the ideal samples collected for isotopic analysis, follow similar enrichment trends.

Sample Name	11SM7003	11SJM056A	11SJM118	12SJM017A	11SM6001	11SM7002
Map Code	9a	9a	9a	9c	9d	9d
Rb (ppm)	14.56	5.45	5.18	1.41	3.35	3.99
Sr (ppm)	278.8	482	519.1	34.7	384	370.2
Nd (ppm)	10.82	4.81	7.23	11.6	9.44	9.33
Sm (ppm)	3.07	1.48	1.81	3.67	2.68	2.64
$^{143}Nd/^{144}Nd_{pres}$	0.512711	0.512791	0.512497	0.512718	0.512697	0.512705
$^{147}Sm/^{144}Nd_{pres}$	0.171633	0.185691	0.151397	0.191403	0.171459	0.171203
$^{143}Nd/^{144}Nd_{1229}$	0.511326	0.511293	0.511276	0.511173	0.511313	0.511323
εNd_{1229}	5.38	4.74	4.40	2.40	5.14	5.34
$87Sr/86Sr_{pres}$	0.705321	0.703634	0.703343	0.704340	0.703205	0.703306
$^{87}Rb/^{86}Sr_{pres}$	0.151	0.033	0.029	0.118	0.025	0.151
$^{87}Sr/^{86}Sr_{1229}$	0.702661	0.703058	0.702835	0.702271	0.702761	0.700647
Sample Name	11SJM173A	12SJM035A	12SJM167A	11SJM169A	12SJM011A	11SJM179A
Map Code	9d	9d	9d	10a	10b	10c
Rb (ppm)	26.82	2.13	8.86	7.93	3.29	2.04
Sr (ppm)	167.6	170.6	263.8	664.4	575.7	266.7
Nd (ppm)	11.5	10.84	16.26	5.49	5.99	10
Sm (ppm)	3.49	3.29	4.41	1.5	1.53	3.3
$^{143}Nd/^{144}Nd_{pres}$	0.512787	0.512831	0.512626	0.512637	0.512501	0.512893
$^{147}Sm/^{144}Nd_{pres}$	0.183736	0.183235	0.163931	0.165186	0.154610	0.199294
$^{143}Nd/^{144}Nd_{1229}$	0.511304	0.511352	0.511303	0.511304	0.511254	0.511285
εNd_{1229}	4.97	5.90	4.94	4.96	3.97	4.58
$87Sr/86Sr_{pres}$	0.709601	0.703357	0.703910	0.703986	0.703057	0.703329
$^{87}Rb/^{86}Sr_{pres}$	0.463	0.036	0.097	0.035	0.017	0.022
$^{87}Sr/^{86}Sr_{1229}$	0.701448	0.702721	0.702199	0.703379	0.702776	0.702940
Sample Name	11SM6002	12SJM013A	12SJM026A	11SJM028A	12SJM044A	12SJM160A
Map Code	10d	10d	11a	12a	12a	12a
Rb (ppm)	1.36	14.94	21.02	1.64	2.74	5.15
Sr (ppm)	76.6	379.3	221.5	192.9	147.3	141.8
Nd (ppm)	26.07	16.98	16.14	12.59	11.72	14.33
Sm (ppm)	5.87	4.4	4.22	4.46	4.05	4.93
$^{143}Nd/^{144}Nd_{pres}$	0.512401	0.512575	0.512564	0.513107	0.513091	0.513056
$^{147}Sm/^{144}Nd_{pres}$	0.136155	0.156766	0.157913	0.214219	0.208736	0.207957
$^{143}Nd/^{144}Nd_{1229}$	0.511302	0.511310	0.511290	0.511379	0.511407	0.511378
εNd_{1229}	4.92	5.07	4.68	6.42	6.97	6.41
$^{87}Sr/^{86}Sr_{pres}$	0.704477	0.705352	0.708244	0.703003	0.703102	0.704700
$^{87}Rb/^{86}Sr_{pres}$	0.051	0.114	0.275	0.025	0.054	0.105
$^{87}Sr/^{86}Sr_{1229}$	0.703573	0.703346	0.703409	0.702570	0.702155	0.702850

Table 4.1 – pertinent isotopic and trace element data for all samples (except 11SJM120A) collected for isotopic analysis from the Raglan Hills metagabbro, sorted by rock type (Map Code). See figures 4.4 to 4.8 and chapters 7.12 to 7.14 for applications.

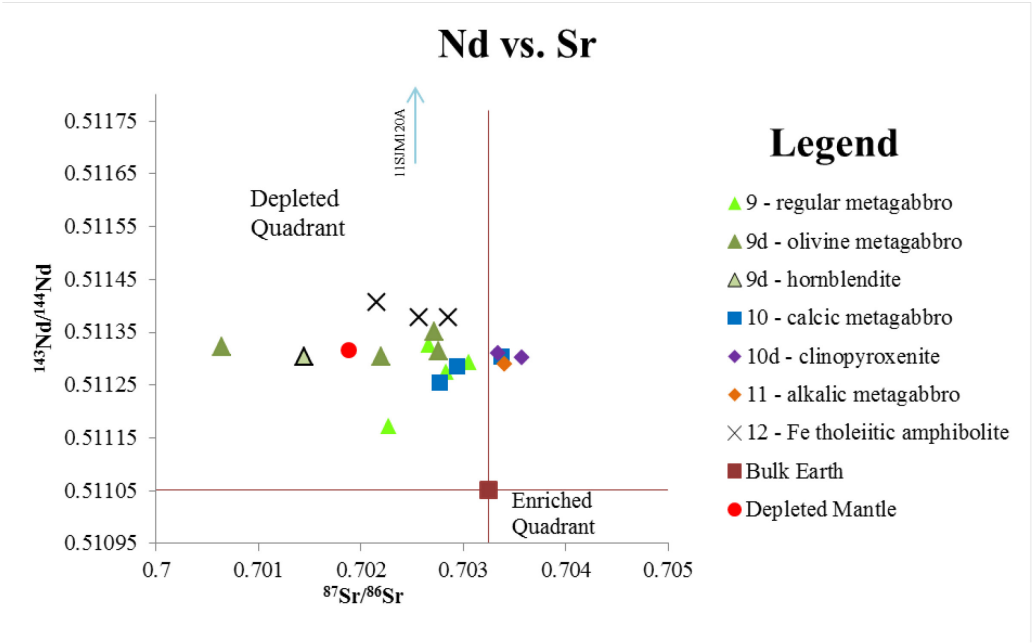

Figure 4.6 – Initial Nd vs. Sr isotope plot for all samples of metagabbroic rocks sampled for isotopic analysis from the Raglan Hills metagabbro. A majority of the samples collected from the Raglan Hills metagabbro plot within the Depleted Quadrant with respect to Bulk Earth isotopic values, with Nd isotopic concentrations similar to those of Depleted Mantle. Note that the mineralized sample of labradorite metagabbro collected from the Raglan Hills showing plots off the chart at $^{143}Nd/^{144}Nd = 0.511984$). Bulk Earth ($^{87}Sr/^{86}Sr = 0.703248$ and $^{143}Nd/^{144}Nd = 0.511051$) and Depleted Mantle ($^{87}Sr/^{86}Sr = 0.701883$ and $^{143}Nd/^{144}Nd = 0.511317$) values calculated for 1229 Ma from present reservoir values estimated by DePaolo and Wasserburg (1976) and DePaolo (1981).

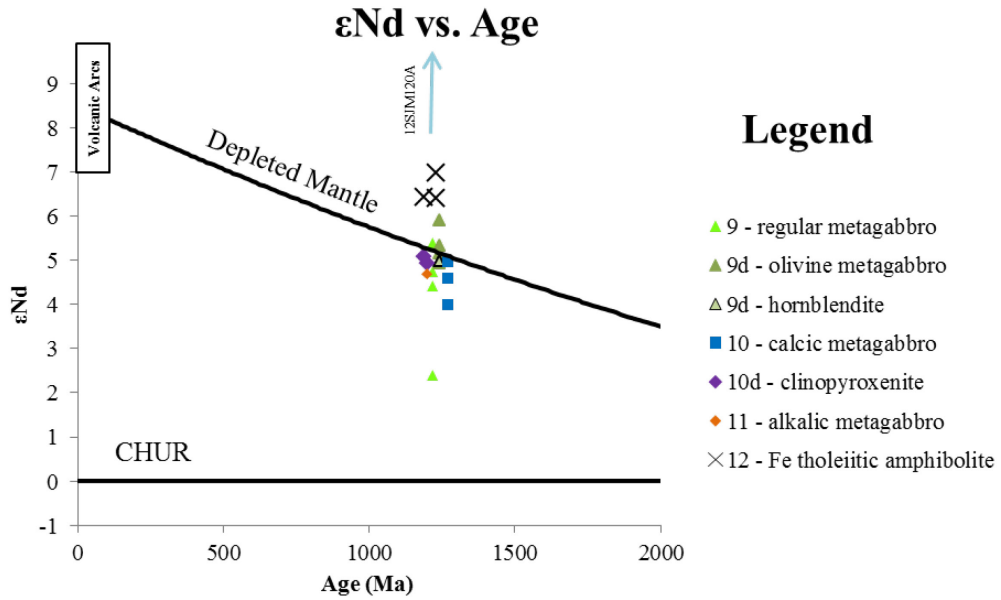

Figure 4.7 – εNd vs. Age plot after DePaolo (1981) containing all metagabbroic rocks samples from the Raglan Hills metagabbro for isotopic analysis. Note that sample 12SJM120A, a labradorite-bearing metagabbro from the Raglan Hills showing, has an εNd value of +18.3. Age of all samples has been assumed to be 1229 ± 5 Ma, (Pehrsson et al. 1996), however the age for the samples displayed has been adjusted slightly in order to avoid overlapping symbols. All εNd values have an error of ± 0.3.

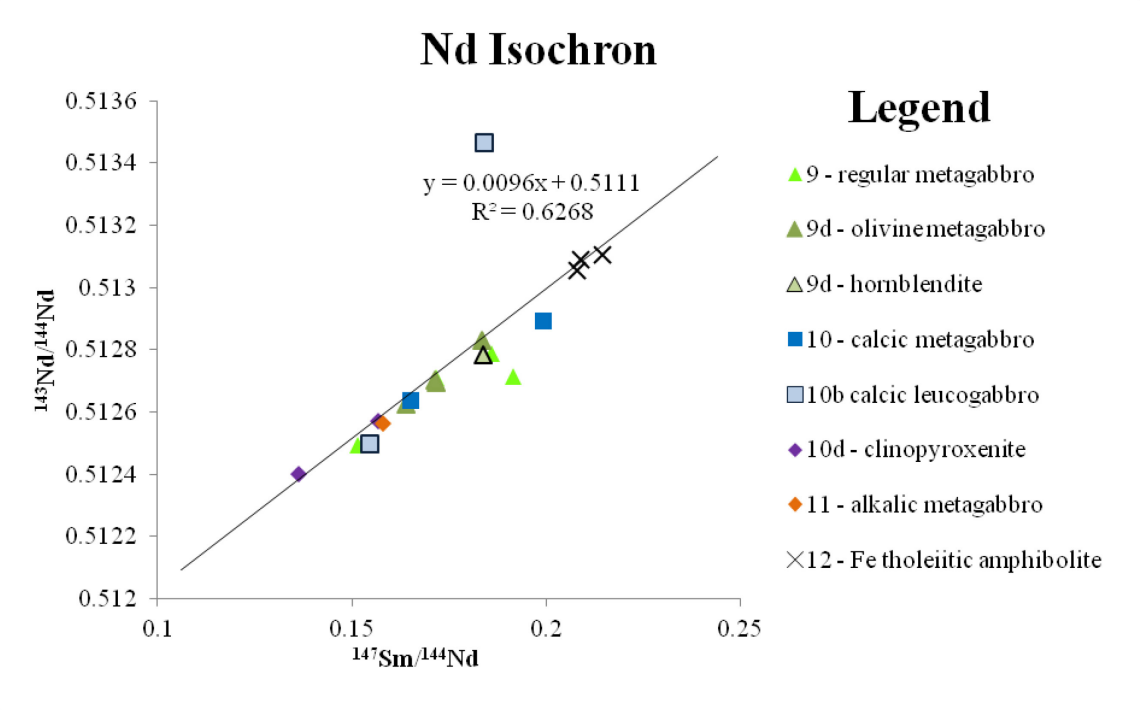

Figure 4.8 – Nd isochron diagram including all samples collected from the Raglan Hills metagabbro for isotopic analysis. This regression (with a poor R^2 value of 0.63) produces an age of 1465 Ma and an initial $^{143}Nd/^{144}Nd$ value of 0.510999, or εNd = +6.36, almost 2 epsilon units away from the Depleted Mantle value at that time (+4.47).

Plotting all of the samples from the Raglan Hills metagabbro together on a Nd isochron diagram produces an errorchron ($R^2 = 0.63$) with a proposed crystallization age of 1465 Ma and an initial $^{143}Nd/^{144}Nd$ value of 0.510999, much higher than that of the Depleted Mantle at that time (figure 4.8).

This problem requires further investigation into the magmatic and metamorphic history of the Raglan Hills metagabbro in order to produce meaningful results from isotopic analysis.

5 - Structural Geology

Roughly 150 structural measurements were collected from the Raglan Hills metagabbro including penetrative mylonitic foliations, localized shear zones (up to 5cm wide), and stretching lineations (figures 5.1 and 5.2). Analysis of these structures by combining equal area stereonet projections with sample locations has delineated several trends.

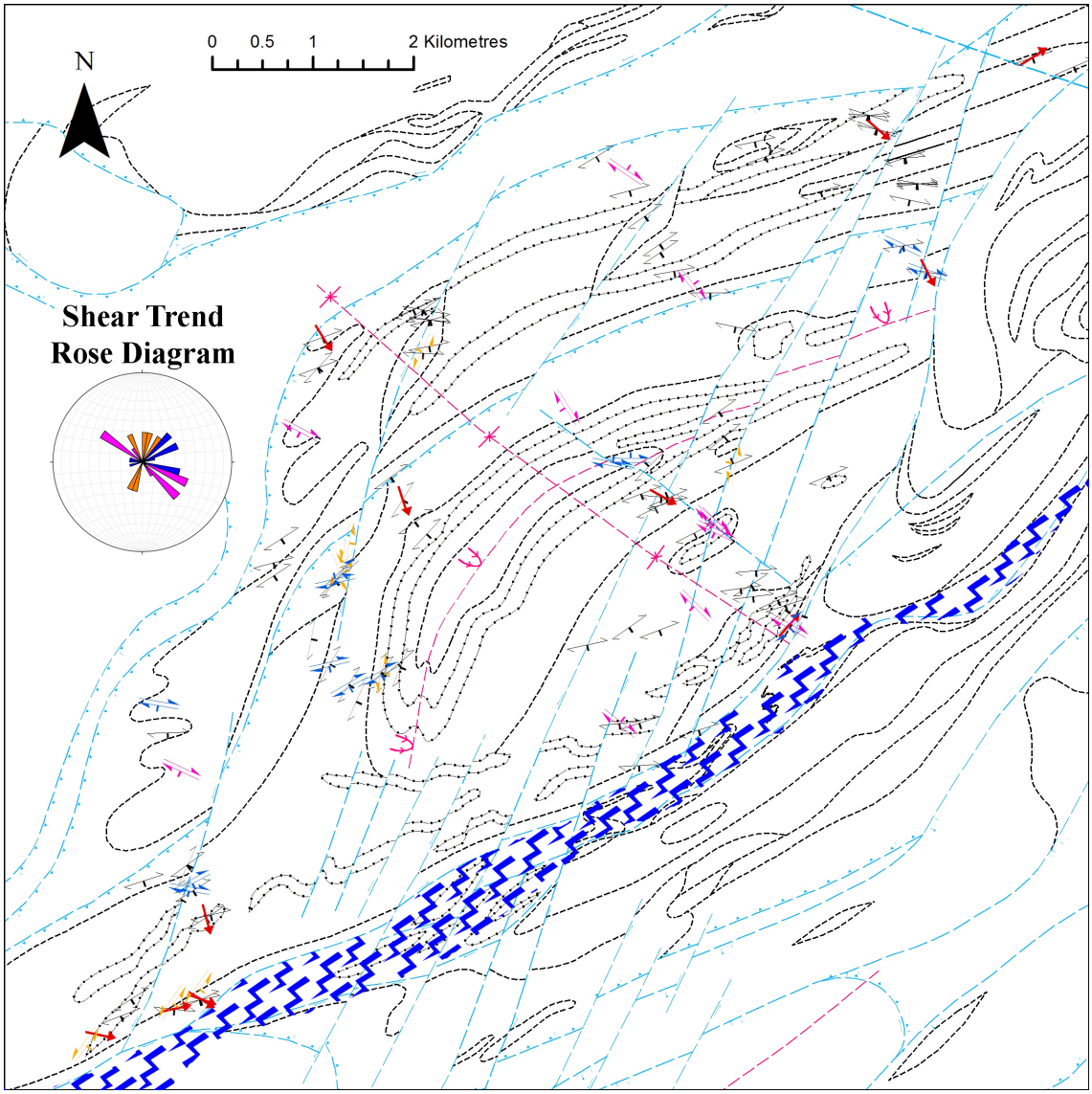

Figure 5.1 – Map of all structural measurements collected from within the Raglan Hills metagabbro with inferred contacts and faults. A Rose diagram is included which displays the strike measurements for all observed shear zones. Symbol colours: black = penetrative mylonitic foliation, red = stretching lineations, blue = east-by-northeast-trending dextral shear zones, orange = sinistral shear zones conjugate to the blue dextral shear zones, and pink = northwest-trending dextral shears and penetrative mylonitic foliations. These colours are consistent throughout all of the stereonets presented herein. McArthurs Mills shear zone indicated by blue lightning-bolt pattern.

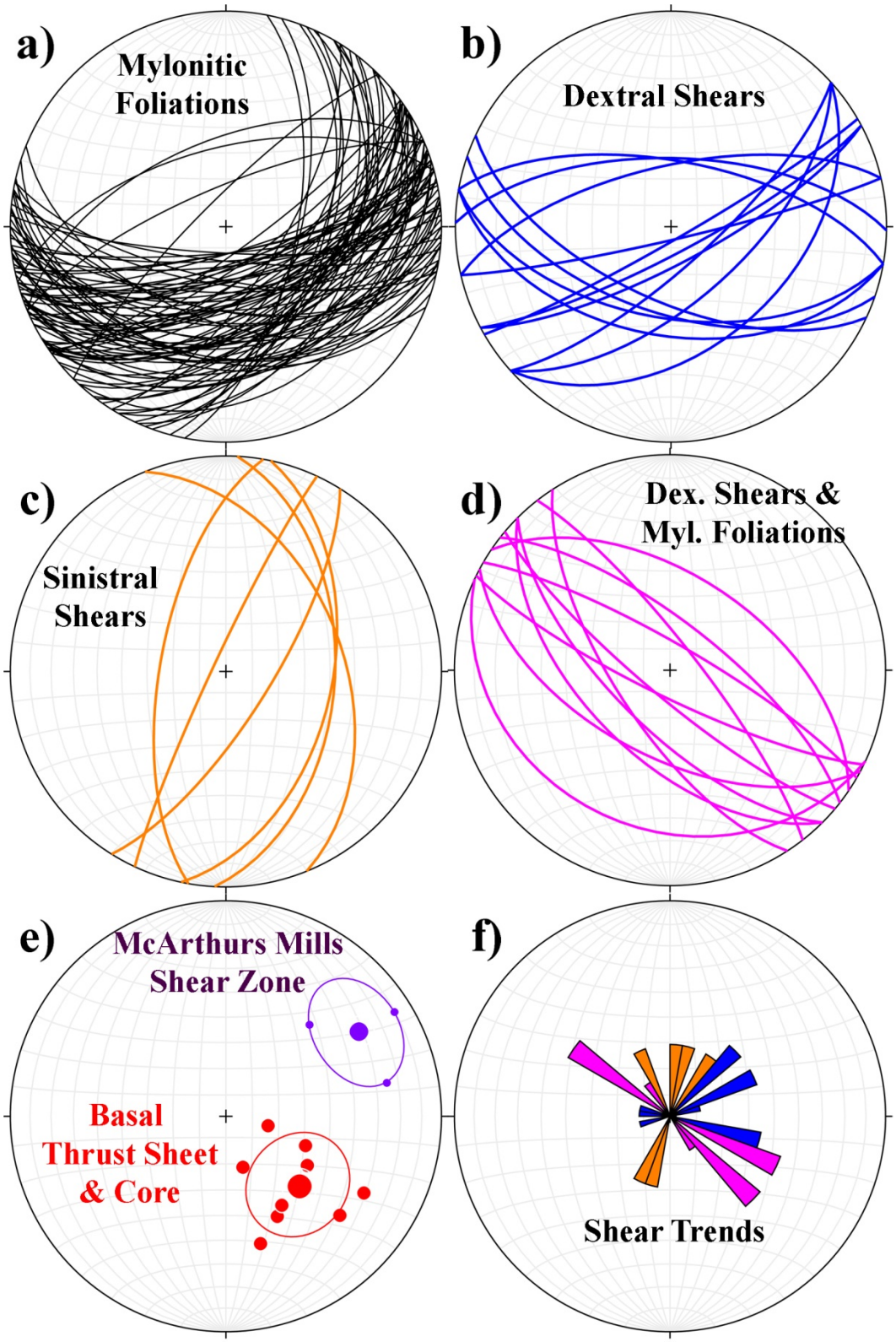

Figure 5.2 – equal area stereonets for the various structural measurements collected from within the Raglan Hills metagabbro, such as: a) penetrative mylonitic foliations, b) east-by-northeast-trending dextral shear zones, c) northeast-trending sinistral shear zones, d) northwest-trending dextral shear zones, and e) stretching lineations with "conical best

fir" vectors (larger point, encircled). f) A rose diagram displaying the preferred strike orientation for the three types of observed shear zones.

Small ductile shear zones have been observed throughout the intrusion which cross-cut each of the various rock-types. These shear zones produce strong localized mylonitic foliations, such that displacement along their strike may be identified through C-S fabrics and lithological displacements. Both sinistral and dextral displacements have been observed in the field, and it appears as though shear zones with sinistral displacement tend to have preferred orientations striking northeast, whereas the shear zones with dextral displacement display two different preferred orientations: one striking towards the east, the other striking to the northwest (figure 5.2b,c and d).

Stretching lineations measured within the Raglan Hills metagabbro tend to plunge moderately towards the southeast; however the stretching lineations measured near the McArthurs Mills shear zone tend to have a shallower plunge trending to the east.

As seen in figures 5.2a and 5.5, the strike of the penetrative protomylonitic to mylonitic fabrics observed throughout the Raglan Hills metagabbro varies across the intrusion from the west to the east. In the western portion of the intrusion, these foliations tend to strike northeast, and rotate clockwise to a more easterly strike in the outcrops towards the east of the intrusion. These foliations dip moderately to steeply towards the southeast, and locally dip steeply towards the northwest.

Although the penetrative mylonitic foliations throughout the intrusion all appear to follow common trend (rotation of strike from northeast to east, as described above), some distinction may be made between the foliations measured from different "domains" within the Raglan Hills metagabbro (figures 5.5 and 5.6). Some examples of the penetrative protomylonitic foliations are displayed in figure 5.7a-e.

Foliation measurements collected near the McArthurs Mills shear zone (along the southern margin of the intrusion) have dominantly steep dips, as do the measurements collected from outcrops of mylonitized Fe-tholeiitic amphibolite (figure 5.6). Also, the foliations measured near the McArthurs Mills shear zone appear to rotate counter-clockwise from west to east, opposite to the trend observed in the basalt thrust sheet and core of the intrusion. Measurements collected from within the "core" of the intrusion tend to dip moderately to steeply, and locally dip towards the northwest, whereas measurements collected from the "basal thrust sheet", a zone containing highly mylonitized and geochemically altered metagabbroic rocks, tend to display moderate dips (below 70 degrees).

There is textural evidence for northwest-directed thrusting in supracrustal rocks of the Bancroft Terrane to the north of the Raglan Hills metagabbro through asymmetrically boudinaged granitoid dikes (sigma clasts) contained within strong mylonitic fabrics which dip gently towards the southeast (Magnus 2013a, b). Similar evidence is seen within highly mylonitized altered metagabbroic rocks along northern margin of the intrusion. At station 11SJM099, an altered metagabbro with a strong, shallowly-dipping mylonitic fabric contains bands of melanocratic material which appears as though it has been boudinaged and drag-folded, indicating top-to-the-

northwest-directed displacement (thrusting) (figure 5.7f). Likewise, at station 11SJM059A, a granodiorite to monzogranite is in contact with altered metagabbro, and displays offshoot dikes which cut through the altered metagabbro (figure 5.7e). Both rock types have a similar strong mylonitic fabric which dips moderately to the southeast. The intrusive contact is parallel to this strong mylonitic foliation, and the offshoot dikes are displaced by the fabric indicating top-to-the-northwest-directed displacement (thrusting). These textures are unique to the altered metagabbroic rocks along the northeast margin of the Raglan Hills metagabbro, hence its designation as the "basal thrust sheet", as it is referred to herein.

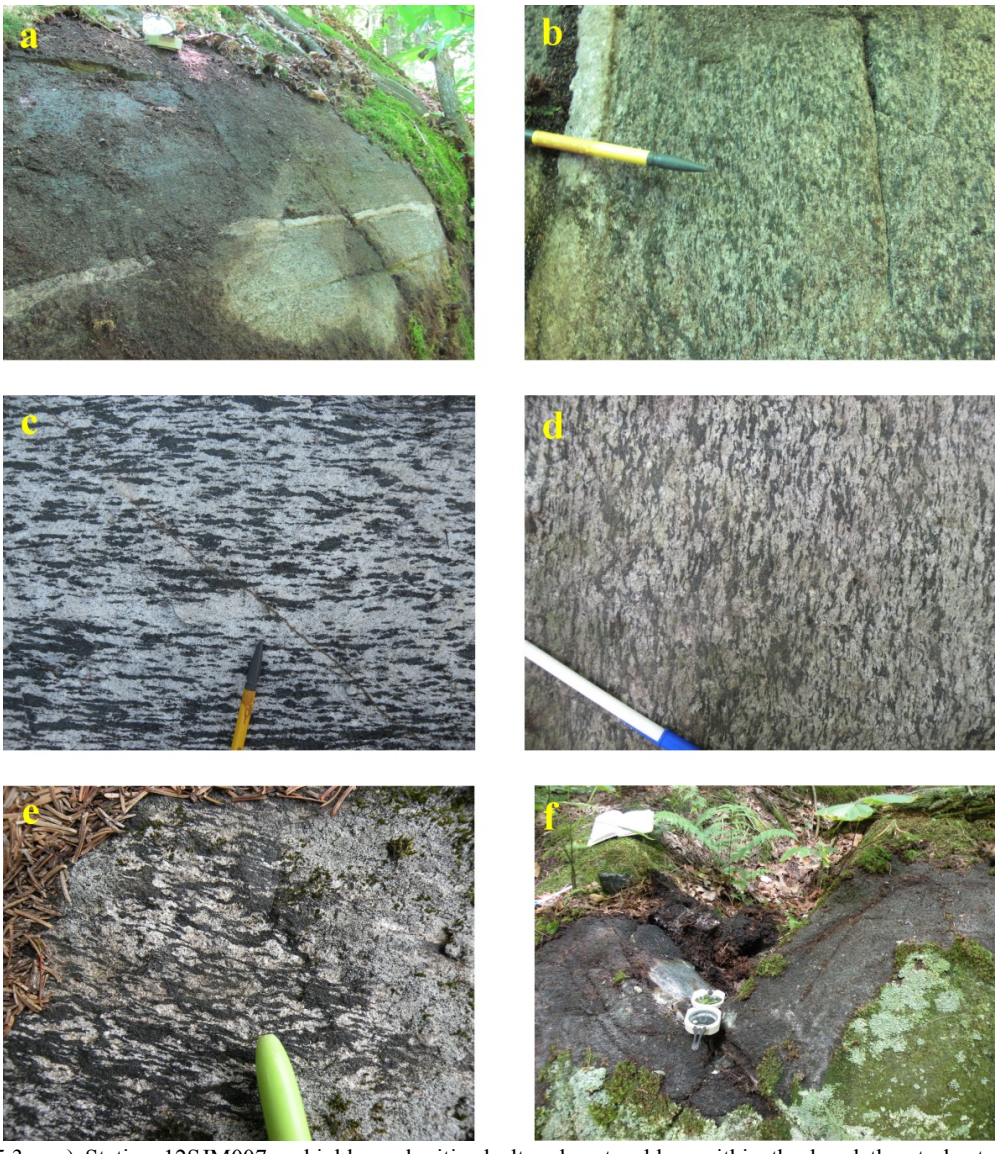

Figure 5.3 – a) Station 12SJM007, a highly mylonitized altered metagabbro within the basal thrust sheet, dipping moderately to the southeast, and a close-up shot of the fabric (b). c) Leucocratic regular metagabbro with a steeply dipping protomylonitic foliation striking east-northeast at station 11SJM118, within the core of the intrusion. d) Regular metagabbro with a steeply dipping protomylonitic foliation striking northeast at station 11SJM164, within the core of the intrusion. e) Regular metagabbro with a moderately dipping protomylonitic foliation striking northwest with indication for dextral displacement at station 12SJM176. f) A possible upright open fold at station 11SJM179 from within the core of the intrusion, with a fold axis plunging towards the south-southeast.

Textural evidence for northwest-vergent overturned folding occurs in the supracrustal rocks of the Bancroft Terrane north of the Raglan Hills metagabbro through map-scale structural analysis (Magnus 2013a, b). Also, the stations along County Road 514 (11SJM023, 024 and 025) which are located near the interpreted fold hinge contain strong mylonitic fabrics with asymmetrically-boudinaged granitoid dikes (described above) are folded in these outcrops, which suggests that this folding post-dates the thrusting

Analysis of airborne geophysical data (Ontario Geological Survey, 2010) shows an elongate ovoid shape in the centre (core) of the Raglan Hills metagabbro outlined by a positive magnetic anomaly, with its long axis oriented east-northeast, roughly parallel to the axial trace of the folds to the north of the intrusion. It has been shown through field work that this positive magnetic anomaly coincides with rocks of unit 9d – olivine metagabbro, which has been confirmed at various locations along the anomaly. Considering the orientation of primary igneous layering observed within the intrusion, and the repetition of rock types around the feature, this ovoid shape has been interpreted to represent a canoe-like structure formed by northwest-vergent folding, though whether the structure has been overturned or not is unknown. If this fold is assumed to be genetically related to the northwest-vergent folding to the north, it follows that this too post-dates an earlier thrusting event. However, thrusting may have continued during and/or after this folding event.

Geophysical evidence for another generation of folding has been observed through topological analysis of the positive aeromagnetic anomaly described above, in combination with analysis of the structural measurements collected from within the Raglan Hills metagabbro using equal-area stereonet techniques. The elongate ovoid shape in the core of the intrusion described through geophysical analysis (above) is warped, with its long axis trending north-northwest at its western end, bending towards an east-northeast trend at its eastern end.

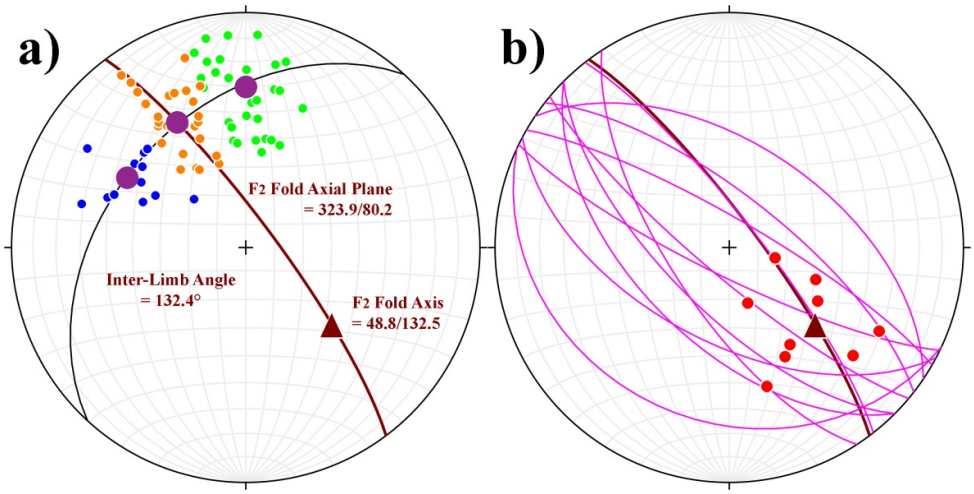

Figure 5.4 – a) π diagram for the mylonitic foliations measured within the core of the Raglan Hills metagabbro, and the resultant fold axial plane (brown plane, 323.9/80.2) and fold axis (brown triangle, 48.8/132.5). Blue points represent measurements from the "west limb", orange points represent measurements from the "hinge", green points represent measurements from the "east limb", and purple points represent the estimated average orientation of the two limbs. b) The resultant fold axial plane plots with a similar strike to the northwest-striking dextral shears observed within the same area as the interpreted F2 axial trace, and the resultant fold axis plots near the average vector for the stretching lineations measured from within the Raglan Hills metagabbro.

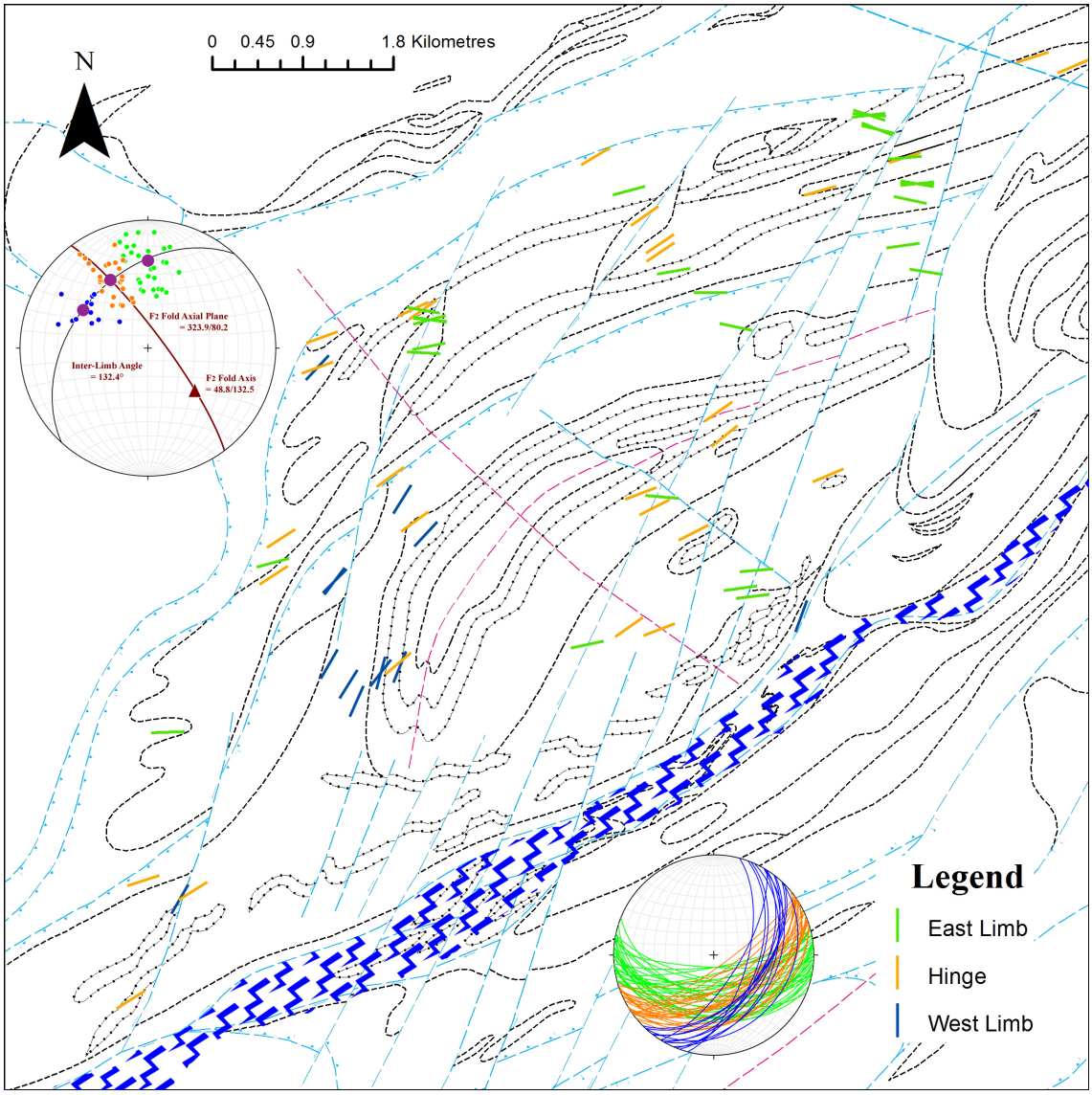

Figure 5.5 – map of all mylonitic foliation measurements collected from within the core and basal thrust sheet, colour-coded according to their orientation. Note that the general clockwise rotation of these foliations from west to east is not observed in the mylonitic foliations located near the McArthurs Mills shear zone (blue lightning bolt pattern), which strike towards the east and rotate slightly counter-clockwise from west to east, suggesting the morphology of the Raglan Hills metagabbro along its southern edge is primarily governed by shearing as opposed to thrusting and folding, which control the morphology of the basal thrust sheet and core of the intrusion. An equal area stereonet with all of the colour-coded penetrating mylonitic foliations, and a π-diagram including the calculated axial fold plane and fold axis (as in figure 5.4) have been included for reference.

This follows the trend observed in the mylonitic foliations described above, which also rotate (or bend) clockwise from west to east. After plotting these data as poles to planes, 1% contours were plotted on the stereonet to aid in picking points representative of the two limbs (one striking north-northeast, another striking east-northeast). Connecting a point on the π-girdle which bisects the limbs with the pole to the π-girdle produced a fold axial plane oriented roughly 318/70 with a fold axis plunging 46/112. This fold axial plane has an orientation similar to that of the northwest-striking dextral shears, and the fold axis has an orientation similar to the other lineations measured within the core of the Raglan Hills metagabbro.

Textural evidence for intense dextral ductile shearing along the McArthurs Mills shear zone has been observed within the Raglan Hills metagabbro and in supracrustal rocks contained within the shear zone (figure 5.7a-d) (Magnus 2013a,b). This is expressed along the southern margin of the intrusion through highly mylonitized metagabbroic rocks which locally display textures consistent with dextral displacement during ductile deformation, particularly at outcrops 11SJM027, 028, 029 and 030, located along Highway 28. Evidence for dextral displacement is also displayed by outcrops of Fe-tholeiitic amphibolite located within the core of the intrusion up to 700 metres away from the McArthurs Mills shear zone, such as station 12SJM045, which contains dextrally-rotated sigma-clasts (asymmetrically-boudinaged tonalite dikes). The northeast to east-northeast striking dextral shear zones located throughout the intrusion may also be genetically related to dextral shearing along the McArthurs Mills shear zone.

Unrooted folds that are dextrally rotated within the highly mylonitic fabric of the shear zone indicate that folding of the local rocks occurred prior to transpressional tectonism (figure 5.7a and b, station 11SJM032A).

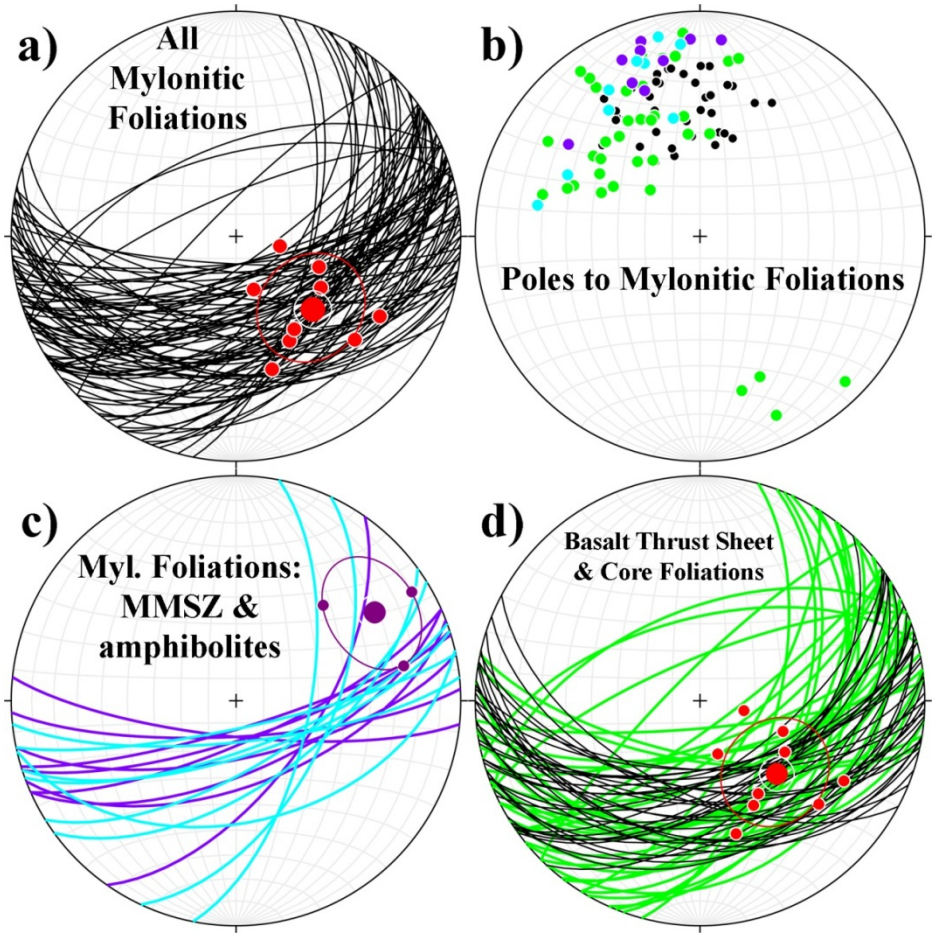

Figure 5.6 – Equal area stereonets displaying measurements collected from the three structural "domains" within the Raglan Hills metagabbro, including: a) a compilation of all penetrative protomylonitic to mylonitic foliations overlain by lineations (red points), c) all of the mylonitic foliations measured in close proximity to the McArthurs Mills shear zone (purple) plotted with measurements collected from mylonitic Fe-tholeiitic amphibolite throughout the intrusion overlain by lineations measured in close proximity to the McArthurs Mills shear zone (purple points), and d) planar fabrics from the "basal thrust sheet" (black) and "core" (green) of the Raglan Hills metagabbro.

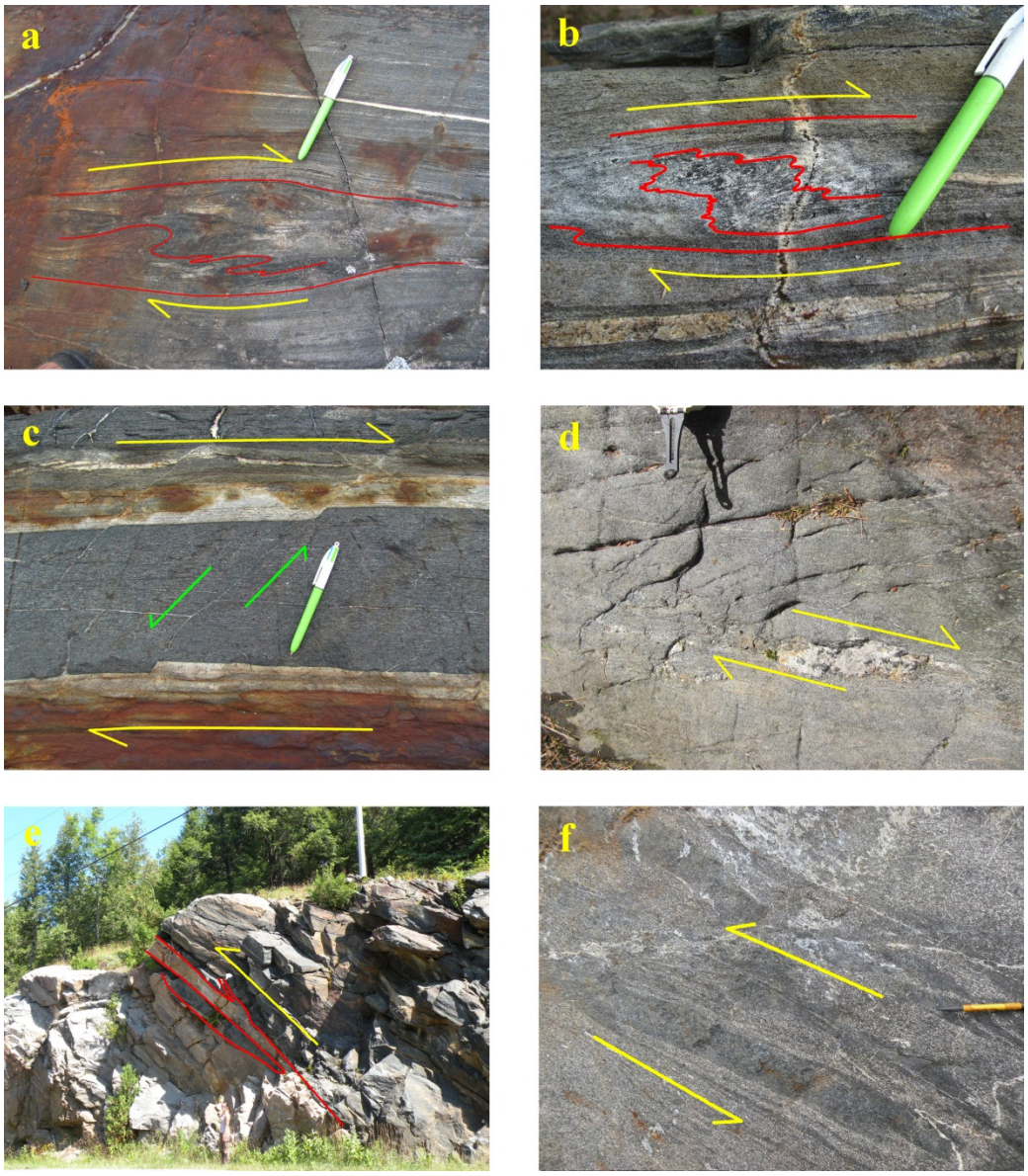

Figure 5.7 – a) and b) dextrally-rotated unrooted folds (outlined in red) in highly deformed metagabbro at station 11SJM032, within the McArthurs Mills shear zone. c) A sinistral offset (green arrows) conjugate to dextral deformation at station 11SJM032, within the McArthurs Mills shear zone. d) A dextral sigma-clast (boudinaged tonalite) within highly mylonitized Fe-tholeiitic amphibolite at station 12SJM045, within the core of the intrusion, roughly 700m from the southern edge of the intrusion (MacArthurs Mills shear zone). e) Granodiorite to monzogranite (outlined in red) cross-cutting altered metagabbro, both of which contain a strong mylonitic foliation dipping moderately to the south, with displacement of offshoot dikes indicating top-to-the-northwest directed displacement (thrusting), at station 11SJM059 along county road 514. f) Highly mylonitized altered metagabbro at station 11SJM099, with displacement and drag-folding of melanocratic bands indicating top-to-the-northwest directed thrusting.

6 - Metamorphism

Several outcrops south of the Raglan Hills metagabbro within the Grimsthorpe Domain of the Elzevir Terrane metavolcaniclastic package are composed of aluminum-rich rocks (Magnus 2013a, b). These rocks are interpreted to represent hydrothermally altered volcaniclastic rocks, and contain abundant knots of fibrolitic sillimanite, fine- to medium-grained garnet, biotite and plagioclase with minor potassium feldspar, quartz and fine-grained, anhedral staurolite (0.2mm). Local occurrences of garnet-sillimanite-bearing rocks in the metasedimentary rocks of the Bancroft Terrane directly north of the intrusion have also been recorded, with no observed staurolite. No kyanite or other occurrence of sillimanite was observed within the map area, and none of the rocks display evidence of retrogression from higher metamorphic facies (i.e. eclogite or granulite facies).

Based on the KFASH component system (Spear 1993), the rocks have likely passed the staurolite out reaction (staurolite = garnet + biotite + sillimanite + H_2O), and the persistence of trace anhedral staurolite suggests that this reaction did not go to completion. This reaction provides a lower limit for peak metamorphic conditions of roughly 600°C and 3 kilobars, however the upper limit is less well defined. Muscovite is not present in these rocks, but it is uncertain whether that is due to the muscovite out reaction (muscovite + quartz = sillimanite + K-feldspar), or if muscovite was never stable in the rocks. Since these supracrustal rocks confine the Raglan Hills metagabbro, the intrusion has likely experienced the same metamorphic history.

As described above, the rocks of the Raglan Hills metagabbro contain a plagioclase-hornblende dominant mineralogy. However, there are slight differences in mineralogy between the rock types that likely occur due to a combination of bulk geochemistry and degree of metamorphism. The rocks that display primary igneous textures and mineralogy, such as those containing medium- to coarse-grained anhydrous mafic minerals such as orthopyroxene, clinopyroxene and olivine, (rock types 9, 10, and 11), have likely not experienced extensive metamorphism. However, since the fully recrystallized rocks confine the core of the intrusion, the core likely experienced the same pressure and temperature conditions as the rocks that contain fine-grained granoblastic mineralogy (dominated by hornblende, plagioclase, biotite, epidote, scapolite and diopside) such as the Fe-tholeiitic amphibolite and the altered metagabbroic rocks.

A number of textural and geochemical patterns were observed within the Raglan Hills metagabbro which are of interest, however it is difficult to introduce these trends and their significance without further discussion, thus this section of thesis will resume with a discussion of the metamorphic processes (i.e. the final processes) which affected the Raglan Hills metagabbro, and continue toward the evidence which will help decipher the nature of its origin.

7 - DISCUSSION

7.1 - Metamorphism in the Core of the Intrusion

The metagabbroic rocks within the core of the Raglan Hills metagabbro contain minerals which display primary magmatic textures, such as euhedral plagioclase laths (in regular and alkalic metagabbroic rocks), the medium-grained equant diopside (pseudomorphed by amphibole) crystals observed in samples of calcic metagabbro (figures 3.1 and 3.4), the primary igneous layering of plagioclase-rich and plagioclase-poor regular and calcic metagabbro, and in particular the coronitic olivine metagabbro described in chapter 7.4. Along with the primary igneous textures, these rocks contain consistent major and trace element concentrations, which suggest that they have experienced weak isochemical metamorphism.

Plotting these samples on a calcium-aluminum-iron+magnesium (CAFM) ternary diagram shows a clear distinction between the regular and calcic metagabbroic rocks, shown by the green and blue fields in figure 7.1. Samples within the green space are generally composed of hornblende, plagioclase and biotite, with trace local scapolite, whereas samples within the blue space are generally composed of hornblende, plagioclase, diopside and epidote with trace local scapolite. Samples of felsic regular and calcic metagabbro tend to plot in about the same position, though the position of the calcic leucogabbro may be skewed by Fe-sulphide mineralization which occurs along with some of the outcrops of leucocratic metagabbro. The samples of alkalic metagabbro also tend to plot within the green space, which is supported by petrographic analysis which reveals that they are composed of hornblende, plagioclase and biotite (with minor titanite and ilmenite). Samples of olivine metagabbro and hornblendite that contain hornblende and plagioclase with minor cummingtonite and/or Fe-oxides plot within the brown field.

Texturally, metamorphism in these rocks is mainly expressed through massive to myrmekitic replacement of the mafic magmatic minerals (pyroxene and olivine) by hornblende, with minor biotite growth along the boundaries between amphibole and plagioclase, and minor replacement of plagioclase by epidote and scapolite. The persistence of primary magmatic minerals, especially those in samples of olivine metagabbro (map unit 9d), suggests that the mineral assemblages present in the core of the intrusion represent metastable assemblages during peak metamorphism.

Coarse-grained, euhedral plagioclase laths in the regular and calcic metagabbroic rocks appear dark grey to dark purple in hand sample, due to the high density of fluid inclusions visible under plane-polarized light. However, whether these fluid inclusions represent magmatic fluids or metamorphic fluids is currently unknown, and an in-depth study on these inclusions may shed some light on the magmatic and/or metamorphic fluids that were present during the formation and metamorphism of these rocks.

7.2 - Metamorphism at the Margins of the Intrusion

The metagabbroic rocks along the southern margin of the Raglan Hills metagabbro, near the McArthurs Mills shear zone, contain strong to intense mylonitic fabrics and display no

primary igneous textures, suggesting that these rocks have undergone extensive deformation. Their mineralogy is composed of fine-grained equigranular granoblastic hornblende and plagioclase with local diopside, epidote and scapolite. The granoblastic (not porphyroblastic) diopside in these rocks tends to have a light green colour under plane-polarized light, unlike the colourless diopside phenocrysts which are observed being pseudomorphed by hornblende in the calcic metagabbroic rocks. Similar mineralogy and textures (diopside growth, as opposed to diopside replacement) are observed in samples of metagabbroic rocks within the basal thrust sheet and in samples of Fe-tholeiitic amphibolite.

When plotted on a CAFM diagram, the altered metagabbroic rocks (collected from the basal thrust sheet and the McArthurs Mills shear zone) tend to plot below and to the left of the dotted red line, indicating that they are Ca-rich, though whether this reflects the bulk rock composition of their protoliths or Ca-enrichment during metamorphism is unknown (figure 7.2).

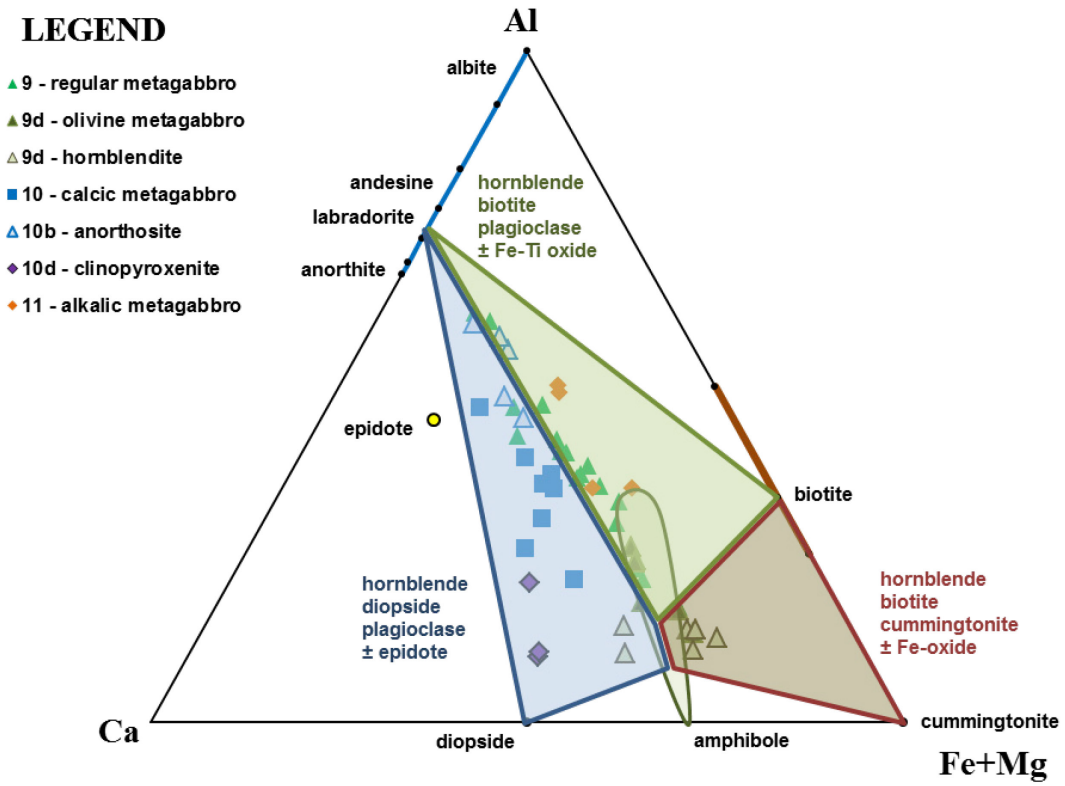

Figure 7.1 – ternary plot of molar ionic proportions for all unaltered regular, calcic and alkalic metagabbroic rocks collected from the Raglan Hills metagabbro. The samples of regular metagabbro (map unit 9) and alkalic metagabbro (map unit 11) tend to plot within the green space, whereas the samples of calcic metagabbro tend to plot in the blue space. The more felsic samples of the regular and calcic metagabbroic rock types converge toward a similar composition close to the labradorite composition within the plagioclase series (blue line). Samples of olivine metagabbro and hornblendite plot within the brown space, composed of hornblende and biotite with cummingtonite and/or Fe-oxides. Biotite (brown line) and amphibole (green line) end member compositions, cummingtonite, diopside and epidote compositions have been added for reference.

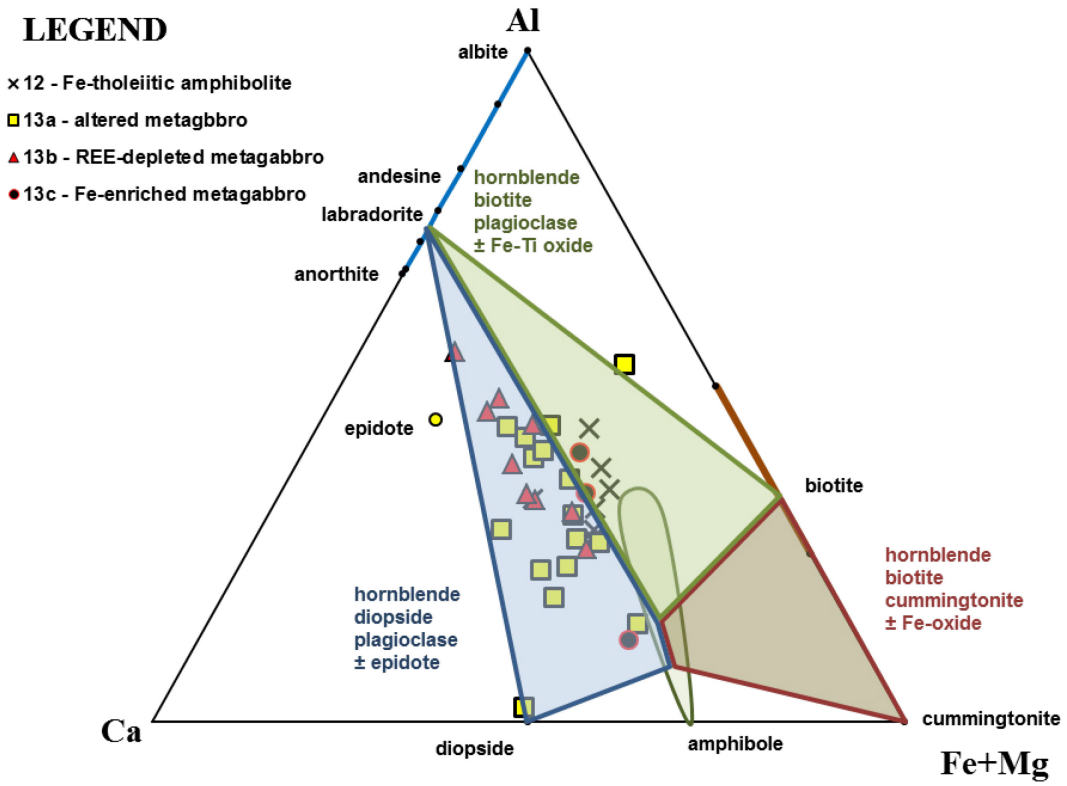

Figure 7.2 – ternary plot of molar ionic proportions for all altered metagabbroic rocks and Fe-tholeiitic amphibolite samples collected from the Raglan Hills metagabbro. A majority of these samples plot within the blue space, which represents compositions similar to calcic metagabbro.

This correlation between deformed metagabbroic rocks and more progressed metamorphic recrystallization suggests that the rocks which are more deformed contain mineral assemblages that are representative of the metamorphic conditions experienced by the Raglan Hills metagabbro, and therefore may be used to help constrain these metamorphic conditions. For example, in the samples of non-deformed calcic metagabbro collected from the core of the intrusion, the diopside present is likely magmatic, and is being replaced by hornblende during metamorphism. In contrast,the diopside in the highly deformed samples of altered metagabbro and Fe-tholeiitic amphibolite appears to have grown during metamorphism, and therefore that mineral assemblage is more representative of the local metamorphic facies, whereas the samples containing diopside pseudomorphed by hornblende represent a reaction that did not go to completion, likely due to a lack of hydrous fluid.

7.3 - Case Study: Iron and Oxidation

Ferric [Fe^{3+}] and ferrous [Fe^{2+}] iron were measured by using two separate analytical methods: total iron as Fe_2O_3t by X-Ray Fluorescence and [Fe^{2+}] as FeO by chemical titration analysis. Assuming that the titration targeted only ferrous iron, the molar concentration of [Fe^{3+}]

as Fe_2O_3 should be calculable by subtracting [Fe^{2+}] from [Fe^{3+}t]. This method produced realistic values for ferric and ferrous iron, except for samples with abundant sulphide mineralization, which in two cases produced negative weight percentages of Fe_2O_3. Of course if there were a conventional modern method with which to obtain [Fe^{2+}] and [Fe^{3+}] concentrations simultaneously, the author would have more confidence that the following observations are valid.

Plotting all of the samples of metagabbroic rocks collected from the Raglan Hills metagabbro on a ternary plot of molar ionic proportions of [Fe^{2+}], aluminum (divided by 2 to better fill the space of the diagram) and [Fe^{3+}] reveals a trend along which a majority of the samples lie, which forms a straight line between the aluminum corner of the diagram towards the [Fe^{2+}] – [Fe^{3+}] edge of the diagram at roughly 78% [Fe^{2+}] (figure 7.3). Some of the rock-types scatter across this line: the samples of olivine metagabbro and hornblendite tend to plot toward the [Fe^{2+}] side (apart from samples 12SJM015, 12SJM017 and 12SJM200A), whereas the samples of clinopyroxenite plot consistently on the [Fe^{3+}] side; the samples of Fe-tholeiitic amphibolite commonly plot on the [Fe^{3+}] side, and the samples of Fe-rich altered metagabbro and the samples of Fe-sulphide-mineralized calcic leucogabbro plot on both sides of the line.

Plotting these points on a [Fe^{2+}] vs. [Fe^{3+}] binary diagram shows the same trend and produces a [Fe^{3+}]/[Fe^{2+}] slope of 0.2825 (figure 7.4). In order to utilize these data, the points have been converted to epsilon iron values (deviation from the slope 0.2825, $\varepsilon Fe = [Fe^{3+}]/[Fe^{2+}] - 0.2825$), where positive values are rich in molar [Fe^{3+}] and negative values are rich in [Fe^{2+}] (figure 7.5). Plotting these values on a map shows that samples with near zero εFe values are located throughout the intrusion, samples with negative values (yellow) are located almost exclusively within the core, and samples with positive values (red) are located in close proximity to northeast-striking sinistral shear zones (figure 7.6).

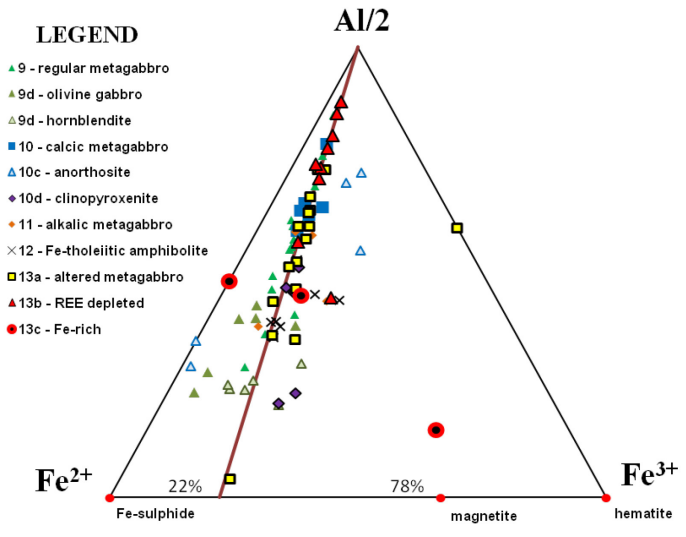

Figure 7.3 – ternary diagram of molar ionic proportions for all unaltered metagabbroic rocks collected from the Raglan Hills metagabbro, including Fe-oxide and Fe-sulphide compositions for reference. Note that a majority of the samples lie along a line that is defined by roughly 22% [Fe^{3+}] / 78% [Fe^{2+}] = 0.2825 (see below, figure 7.4).

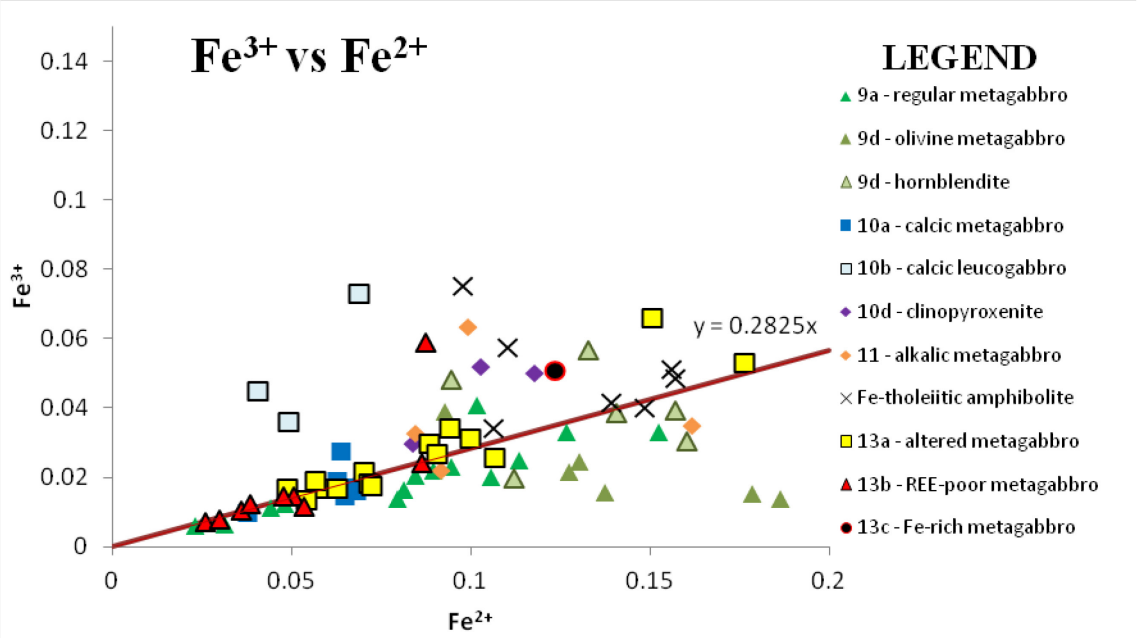

Figure 7.4 – binary diagram of molar ionic proportions for all metagabbroic samples collected from the Raglan Hills metagabbro. The samples fit a line (equivalent to the line in figure 7.3) with a slope of 0.3942.

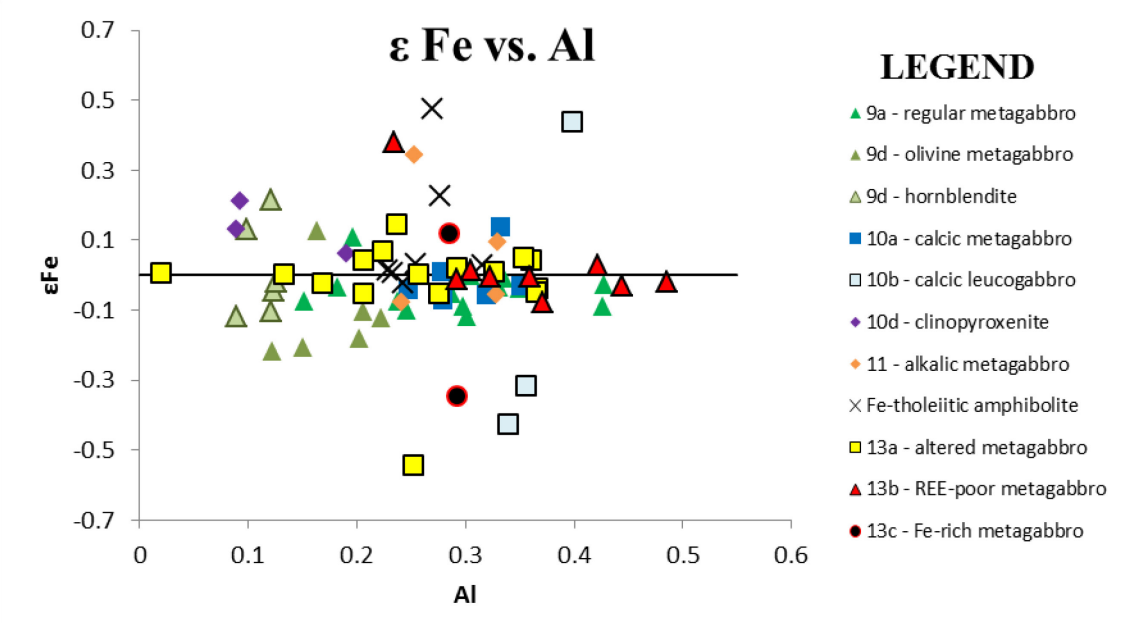

Figure 7.5 – plot of epsilon iron ($\varepsilon Fe = ([Fe^{3+}]/[Fe^{2+}]) - 0.2825$) vs. molar concentration of aluminum. The $\varepsilon Fe = 0$ value (0.2825) was taken from the slope of the line of best fit, calculated in figure 7.4.

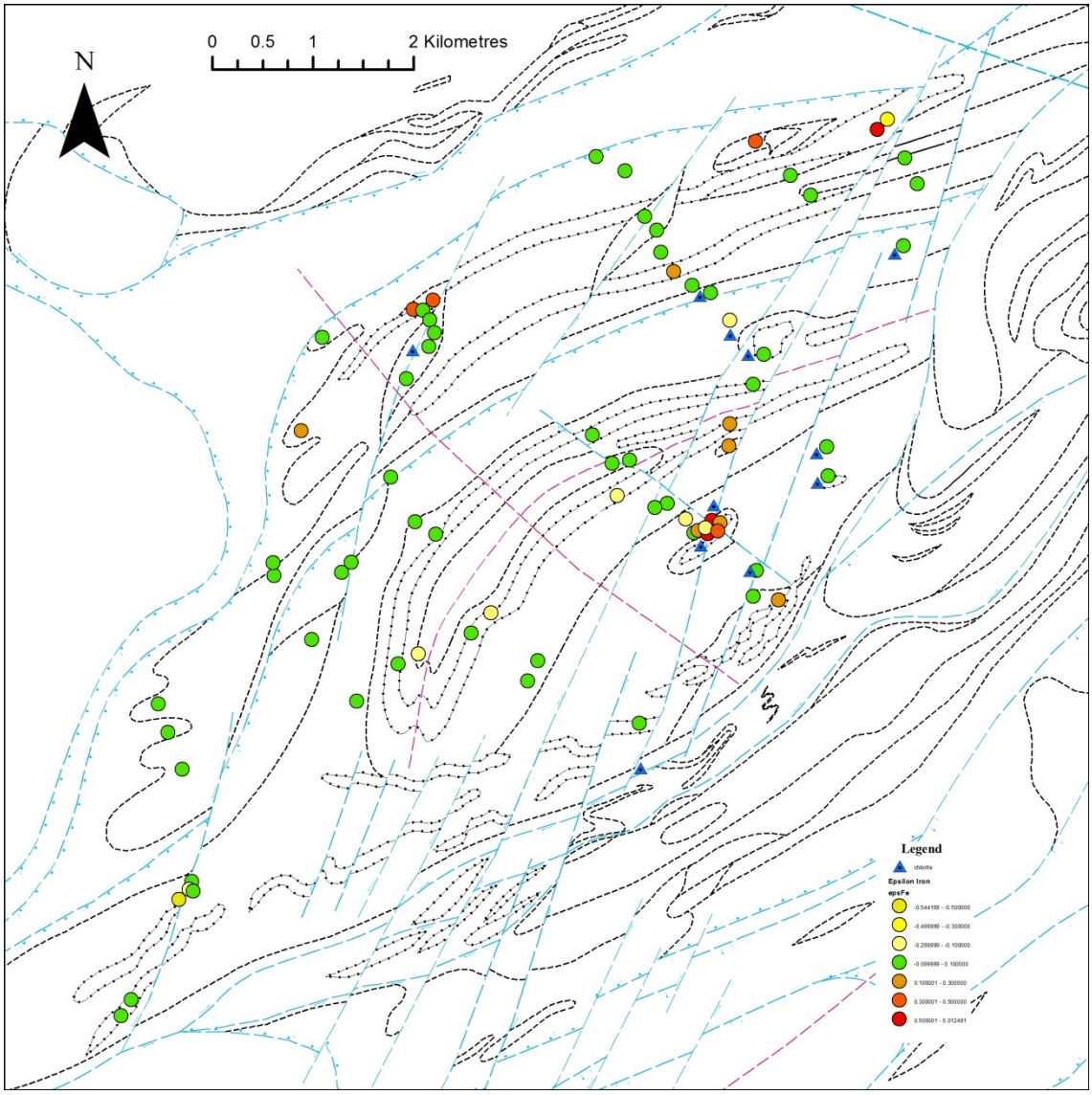

Figure 7.6 – map of all metagabbroic samples collected for whole rock geochemical analysis with symbols coloured according to their εFe value. Note that the samples which have a value of roughly 0 (green) plot throughout the intrusion, whereas those that are below 0.1 (yellow) plot almost exclusively within the core of the intrusion, and those that are above 0.1 (red) plot near major shear zones. All occurrences of chlorite (generally fine-grained radiating clots of magnesium-rich chlorite) marked with blue triangles.

7.4 - Case Study: Coronitic Olivine Metagabbro

Outcrops of olivine metagabbro are located near positive aeromagnetic anomalies within the core of the intrusion, and each occurrence of this rock type contains similar mineralogy and displays similar igneous textures and metamorphic fabrics which are all unique within the Raglan Hills metagabbro. These rocks are composed mainly of medium to coarse-grained euhedral dark brown pyroxene (maximum 5mm) with minor interstitial dark purple twinned plagioclase (rich in fluid inclusions) and orange olivine, and lack sulphide mineralization. The primary magmatic minerals (pyroxene, olivine and plagioclase) are separated by coronae composed of enstatite and tschermakite, a texture that is uncommon in mafic intrusive rocks of the Central Metasedimentary Belt, and may provide useful information for the magmatic and metamorphic history of the Raglan Hills metagabbro.

7.4.1 - Pyroxene thermometry

Lindsley (1983) developed experimentally-calibrated two- and three-pyroxene thermometers for use with volcanic, intrusive and high grade metamorphic rocks using the ternary model-system $CaSiO_3$ – $MgSiO_3$ – $FeSiO_3$ (which include corrections related to other components, including Na, Al, Cr, and Ti), improving upon previous binary system thermometers which could only use two out of the three major end member components. These thermometers are based on the theory that the composition of pyroxene that crystallizes from magma is dependent on the pressure and temperature conditions or crystallization, and that two to three different kinds of pyroxene may crystallize simultaneously; one Ca-rich (augite), one Mg and Fe-rich (orthopyroxene) and occasionally an intermediate pyroxene (pigeonite). Upon relatively slow cooling, these crystals typically exsolve minor components as a second pyroxene phase. For instance, a crystal of augite will typically exsolve minor iron and magnesium as enstatite lamellae, or a crystal of enstatite/clinoenstatite will exsolve minor calcium as augite or diopside. So, using mineral chemistry and textural evidence, one should be able to plot pyroxene compositions onto Lindsley's trapezoid and interpret temperatures related to crystallization, exsolution, and possibly metamorphism, assuming that the crystals have remained a closed system during metamorphism (figure 7.10).

The pyroxene crystals in samples of olivine metagabbro are generally augite in composition (figure 7.8), and host exsolution lamellae of enstatite and minor ilmenite (figure 7.7). The lamellae of enstatite are less than 3 μm thick and oriented parallel to (100), hosted in augite lamellae of maximum 30 μm thick. Exsolved crystals of ilmenite have two preferred orientations: parallel to the enstatite lamellae (100), and parallel to the mineral cleavages (110) and $(\bar{1}10)$.

One of the requirements for using Lindsley's thermometer is that the exsolved pyroxene crystals must be re-integrated, taking into consideration the abundance and thickness of lamellae and a phenomena called granule exsolution, during which exsolved pyroxene migrates from the core and crystallizes in discrete grains along the crystal faces of the original pyroxene crystal. Considering the enstatite lamellae are roughly 3μm thick or less, and the sheath of enstatite around the crystals is roughly 50μm maximum, and that this orthopyroxene makes up roughly

10% of the entire pyroxene grain, the crystals have been integrated to 10% of the enstatite end member composition with 90% of the augite end member composition (figure 7.9).

This integrated composition plots at around 1150°C on a trapezoid calibrated at 5 kilobars (figure 7.10), and plots at about 1125°C at 1 atmosphere of pressure, and 1175°C at 15 kbar, which shows that the effect of pressure is relatively minimal for pyroxene of this composition, especially given the 50°C accuracy of this graphical projection method (Lindsley 1983). This likely represents a temperature of crystallization for these crystals of pyroxene at about 1150°C.

The analyses of non-integrated augite plot around 900°C, as do several analyses of enstatite, whereas a majority of the analyses of enstatite plot between 700 and 550°C. These temperatures likely represent two events: exsolution during magmatic cooling at around 900°C, since this is much higher than the local maximum metamorphic temperature of 700°C (Magnus 2013a); and metamorphic exsolution at around 600°C.

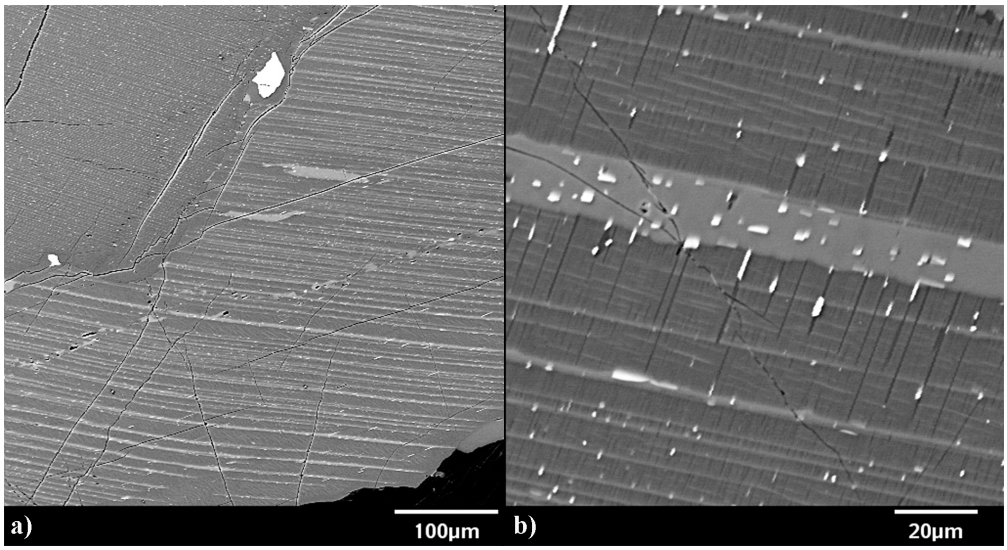

Figure 7.7 – back-scattered electron images of a) enstatite (light grey) lamellae exsolved from augite (dark grey), with two grains of ilmenite (white) along a grain boundary with another crystal of pyroxene, and several areas of "secondary" enstatite exsolution, and b) close-up of enstatite (light grey) lamellae exsolved from augite (dark grey) with grains of ilmenite (white) oriented parallel to the enstatite lamellae and perpendicular to the lamellae in fractures (mineral cleavage).

Two distinct forms of exsolution have been observed: straight laminae and "blotchy" exsolutions (figure 7.7a, large grey patches parallel to lamellae) which tend to overprint the straight laminae, with single blotches which generally overlap several straight laminae and encapsulate crystals of ilmenite. The straight laminae have been interpreted to represent the exsolution during magmatic cooling, which were then overprinted by the secondary blotchy exsolution during metamorphism.

Diffusion of cations between augite and enstatite during metamorphism likely caused their respective compositions to become more refined, pushing the enstatite laminae closer to the pure orthopyroxene edge of the triangle (towards lower temperatures) and pushing the augite laminae closer to the diopside field (also towards lower temperatures). This effect would create the compositional variation in augite and enstatite analyses, with the less "pure" compositions

representing pre-metamorphic compositions, and the more "pure" compositions representing compositions at the closing temperatures for Ca, Fe and Mg diffusion in pyroxene.

This method has several limitations: the change in volume between augite and enstatite compositions is not considered, exsolution of titanium as ilmenite is not considered, and the development of mineral cleavage (likely due to ilmenite exsolution) is not considered. All of these factors may affect diffusion rates of the major elements, and likely control the efficiency and form of exsolution within pyroxene. Also, no crystals of enstatite with minor exsolutions of augite have been located, which are useful to double-check the temperatures determined with the crystals of augite.

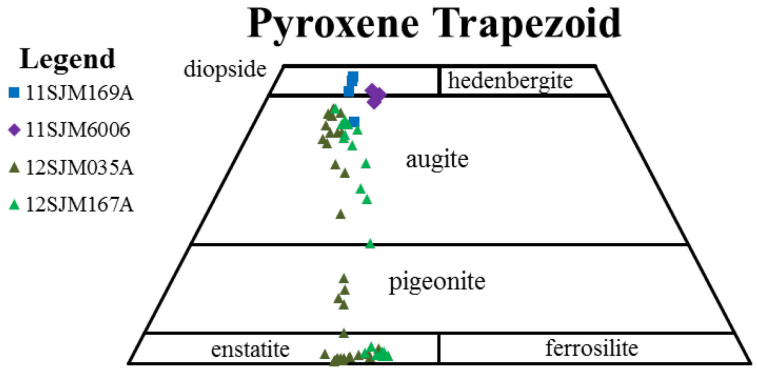

Figure 7.8 – pyroxene classification trapezoid, with all data collected using electron microprobe from samples of calcic metagabbro (11SJM169A), clinopyroxenite (11SJM6006), and olivine metagabbro (12SJM035A and 12SJM167A). Note that the analyses from samples of olivine metagabbro cluster in two zones: enstatite and Ca-rich augite, and analyses which plot in between are the result of probing very thin exsolution lamellae of enstatite in augite (figure 7.7), producing a false mixing effect. Results were projected onto the end-member quadrilateral according to Lindsley (1983). Trapezoid after Morimoto (1989).

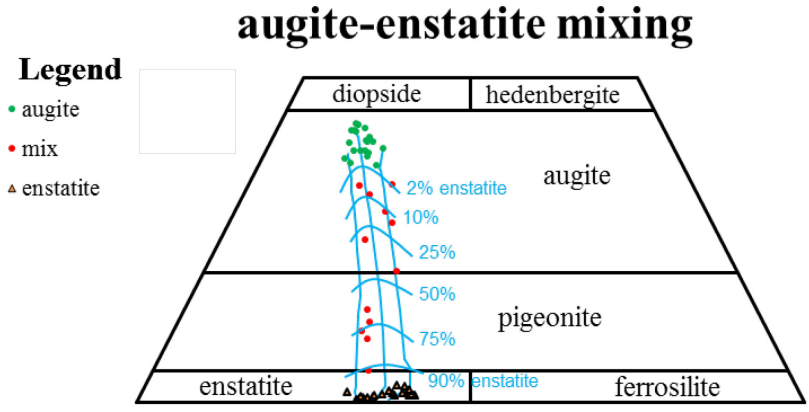

Figure 7.9 – plot of augite, enstatite and mixed analyses from samples of olivine metagabbro. The mixed analyses occur due to the thin (<3 μm) lamellae of enstatite relative to the thicker (~30 μm) host augite lamellae, which are thinner than the size of the electron beam used for measurement.

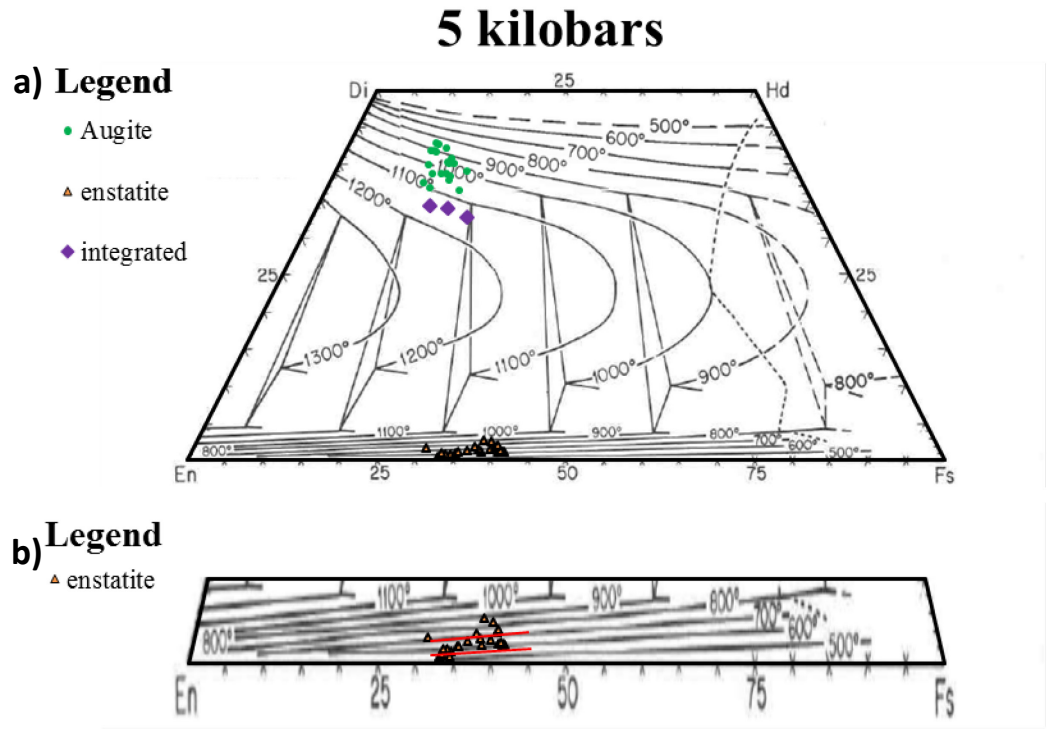

Figure 7.10 – a) analyses of augite and enstatite from samples of olivine metagabbro, along with three integrated pyroxenes assuming a mix of 10% enstatite and 90% augite (considering their relative lamellae thicknesses), plotted on a polythermal diagram at 5 kilobars developed by Lindsley (1983). Note that the integrated pyroxene compositions plot at about 1150°C, which may represent the rough temperature at which pyroxene first crystallized. These analyses plot at roughly the same temperatures on a diagram calibrated for 10 kilobars, and therefore the pressure between 5 and 10 kilobars does not significantly affect the temperature of crystallization for pyroxene of this composition. b) enlarged view of the trapezoid up to 5% of the wollastonite end member, including the analyses of enstatite, which tend to plot between 700 and 550°C, with some spread up to 900°C and down to 500°C.

7.4.2 - Coronae and Metamorphism

A large outcrop of coronitic olivine metagabbro was observed at station 12SJM035, and by scanning the outcrop with a handheld magnetometer several magnetic portions of the outcrop were located which are composed of hornblendite. Several other outcrops of hornblendite have been described within the Raglan Hills metagabbro (Magnus 2013a), though none of these outcrops display contact relationships with the other gabbroic rock types. A sample of the contact between olivine metagabbro and hornblendite was collected from this station for petrographic and geochemical analysis in order to better understand the transition between rock types and metamorphism within the Raglan Hills metagabbro in general.

Two stages of metamorphism were observed within the olivine metagabbro, the first of which is represented by coronitic texture ubiquitous throughout the olivine metagabbro. The mafic minerals (augite and olivine) and crystals of plagioclase are separated by coronitic reaction rims composed of enstatite and tschermakite, such that no crystal of plagioclase is in direct contact with olivine (figures 7.11 and 7.12), though plagioclase has been observed in direct contact with enstatite. The crystals of augite and olivine are sheathed by enstatite, which is

sheathed by hornblende (tschermakite), which is in contact with plagioclase. Biotite is locally present in association with hornblende. The crystals of plagioclase are dark grey/purple, contain abundant fluid inclusions and commonly display twinning.

One exsolution reaction, one phase transition and one terminal reaction are responsible for the coronae present in the olivine gabbro, illustrated in figure 7.14:

All crystals of pyroxene also have a very thin sheath of enstatite, likely formed during exsolution (granular exsolution, see chapter 7.4.1) (figure 7.14b).

All crystals of olivine are surrounded by a sheath of enstatite, likely formed by the following reaction (figure 7.14c):

$$olivine + SiO_2 = enstatite$$

A band of green tschermakite separates enstatite from plagioclase, likely formed by the (unbalanced) reaction (figure 7.14c):

$$plagioclase + enstatite + H_2O + K^+ = tschermakite + silica + H^+$$

The olivine to enstatite reaction described above requires an influx of SiO_2, which may have either occurred during metamorphism (hydrothermal SiO_2) or during crystallization from a silica-undersaturated magma (Bowen and Anderson 1914).

The high density of fluid inclusions visible in all of the plagioclase crystals suggests that they likely acted as a conduit for the hydrous fluids that drove these reactions. The source of the hydrous fluid is currently unknown, but it may have been contained in fluid inclusions or along grain boundaries as late stage magmatic fluid, it could have come from an unknown hydrous magmatic phase, or very small amounts of external fluid may have been introduced to the rocks post-crystallization. A geochemical study on the fluid inclusions in plagioclase may help determine the source of the fluid responsible for the development of the tschermakite coronae.

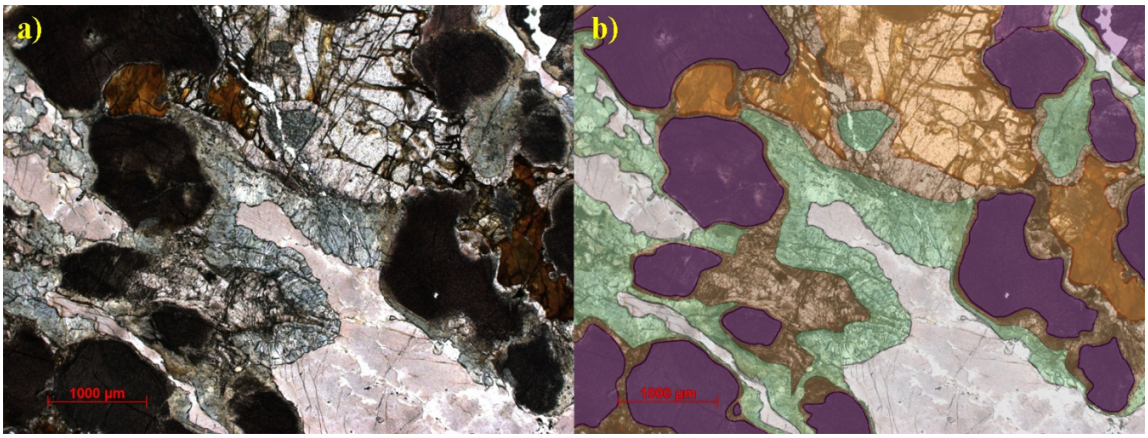

Figure 7.11 – a) photomicrograph of olivine gabbro from station 12SJM035 in plane polarized light and b) colour-enhanced image of the same photomicrograph. Colours: purple = augite (with enstatite lamellae), brown = enstatite, orange = olivine, green = tschermakite, and grey = plagioclase. Note that the enstatite-hornblende coronae are thickest between plagioclase and olivine, and thinnest between plagioclase and augite. Also note the high density of fluid inclusions in the crystals of plagioclase.

Figure 7.14 contains compatibility diagrams which schematically illustrate these reactions. First, in figure 7.14a, the original stable magmatic phase assemblage is plagioclase, olivine and pyroxene (integrated composition as described above). Figure 7.14b shows the exsolution of pyroxene into augite and enstatite components, and figure 7.14c shows the reaction between plagioclase and pyroxene to create tschermakite. The development of coronae indicates that the minerals (especially plagioclase and olivine) were not stable, and the development of the coronae was likely facilitated by the addition of limited H_2O into the system, indicating an open system. Since these diagrams still appropriately represent the observed mineral reactions, the topology is outlined by "pseudo-tie lines", rather than regular tie lines that represent stable mineral assemblages in closed systems.

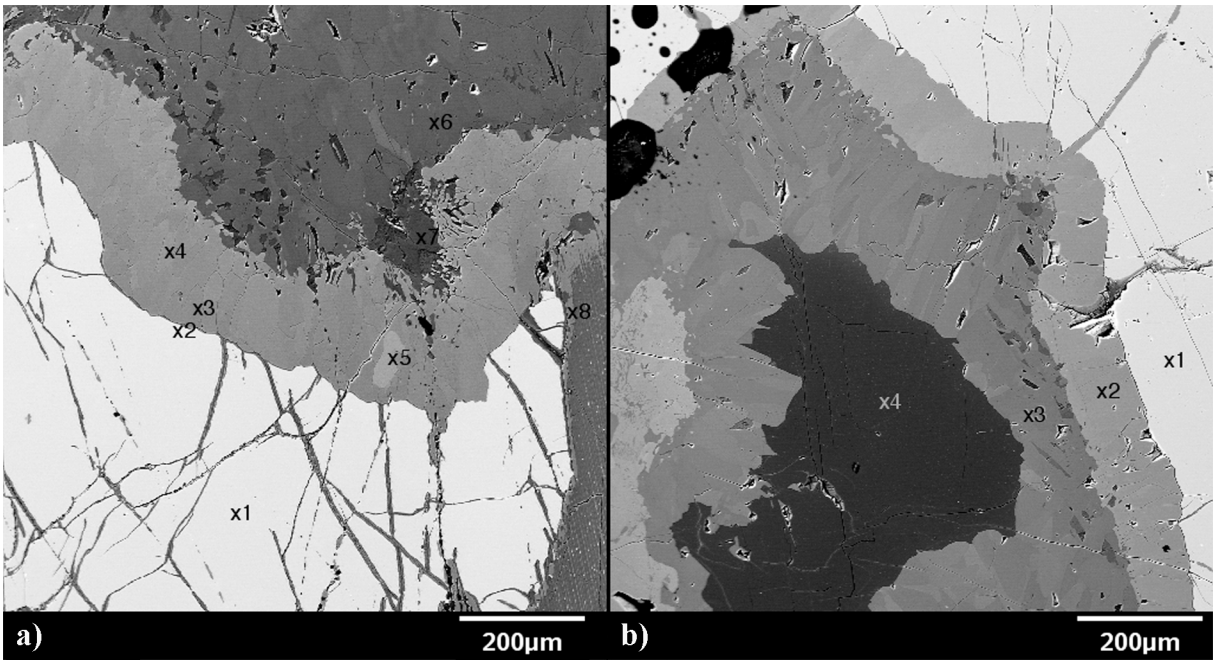

Figure 7.12 – back-scattered electron images of a) olivine (white) in contact with augite (dark grey, bottom right near point 8) sheathed with a layer of orthopyroxene (grey) and tschermakite (dark grey), and b) olivine (white, point 1), enstatite (grey, point 2), tschermakite (dark grey, point 3) and plagioclase (very dark grey, point 4). Analyses for spots x1 to x4 are provided in table 7.1.

The second stage of metamorphism is represented by elongate lenses of magnetic hornblendite dispersed throughout the outcrop. These rocks are composed almost entirely of green hornblende, with minor cummingtonite, Fe-Ti oxides and trace tourmaline. The exact morphology and orientation of these lenses is unknown, due to lichen coverage and the dark nature of both this rock and the olivine metagabbro causing optical distinction between them on a hand-sample scale difficult.

Figure 7.13 shows a photomicrograph of a slide cut from the contact between olivine metagabbro and hornblendite, where a distinct reaction front is plainly visible. This photomicrograph shows a crystal of pyroxene (with exsolution lamellae) which has been partially replaced by green hornblende and Fe-Ti oxides, which have pseudomorphed the former grain of pyroxene. Also visible in this photomicrograph are crystals of colourless clinoamphibole (cummingtonite) which are located along the edges of and interstitial to the pyroxene

pseudomorphs, also associated with Fe-Ti oxides. This was likely formed by the following (unbalanced) reaction.

$$enstatite + SiO_{2(\text{liquid})} + H_2O = cummingtonite$$

The Fe-Ti oxides associated with the hornblende and cummingtonite likely formed as a result of high fO_2(oxygen fugacity) during metamorphism, which may have caused iron from the pyroxenes to exsolve as oxides rather than participate in the phase transformation. As seen in table 7.1, the Mg# (ratio of magnesium to total magnesium plus iron) increases from olivine to enstatite to tschermakite, and although no data was collected from the hornblende and cummingtonite from this sample, they will likely have even higher concentrations magnesium relative to iron.

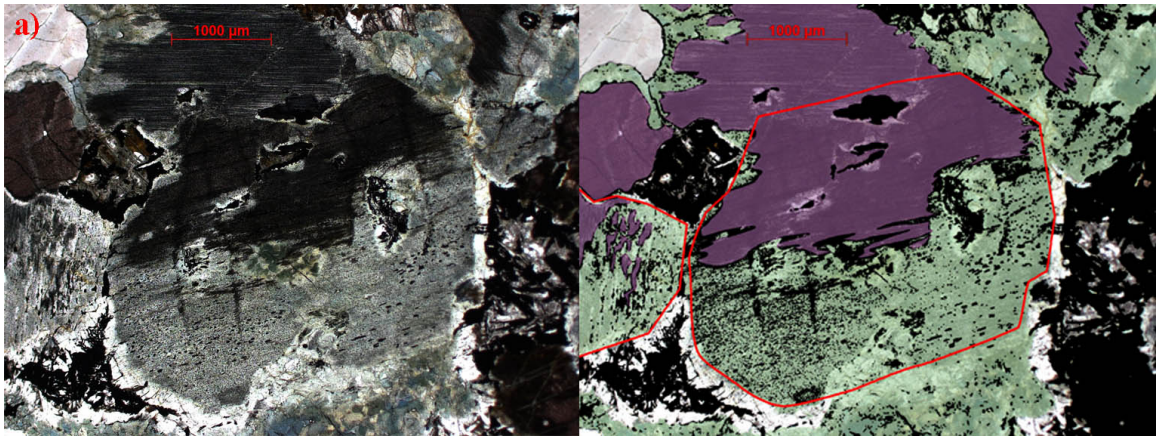

Figure 7.13 – photomicrograph of altered olivine gabbro from station 12SJM035 in plane polarized light, and b) a colour-enhanced image of the same photomicrograph, with partially replaced crystals of augite (with enstatite lamellae) outlined in red. Note that the altered portions of the crystals contain a much higher concentration of opaque minerals, likely Fe-Ti oxides (ilmenite). Colours: purple = augite, grey = plagioclase, green = hornblende, and black = opaque minerals. Note that the colourless minerals (apart from plagioclase in the upper left corner) are crystals of amphibole, not orthopyroxene.

Analysis	**x1**	**x2**	**x3**	**x4**
Mineral	**60% forsterite**	**67% enstatite**	**tschermakite**	**39% andesine**
SiO_2	36.42	54.53	41.84	59.12
Al_2O_3	0.00	0.55	17.56	26.81
FeO	34.34	19.77	11.18	0.10
MgO	28.65	24.32	12.86	nm
Mg#	59.90	68.56	92.05	-
MnO	0.40	0.44	0.19	nm
CaO	0.02	0.78	10.55	8.26
Na_2O	0.00	0.00	3.60	7.25
K_2O	0.00	0.00	0.21	0.03
NiO	0.08	0.02	0.06	nm
TiO_2	0.02	0.02	0.07	nm
TOTAL	99.92	100.42	98.17	101.68

Table 7.1 – spot analyses from sample 12SJM035A of coronitic olivine metagabbro. Spot locations shown in figure 7.12b. All values are in weight %, aside from Mg#, which is dimensionless. Abbreviation: nm = not measured. $Mg\# = 100\ x\ (Mg^{2+}/(Mg^{2+} + Fe^{2+}))$.

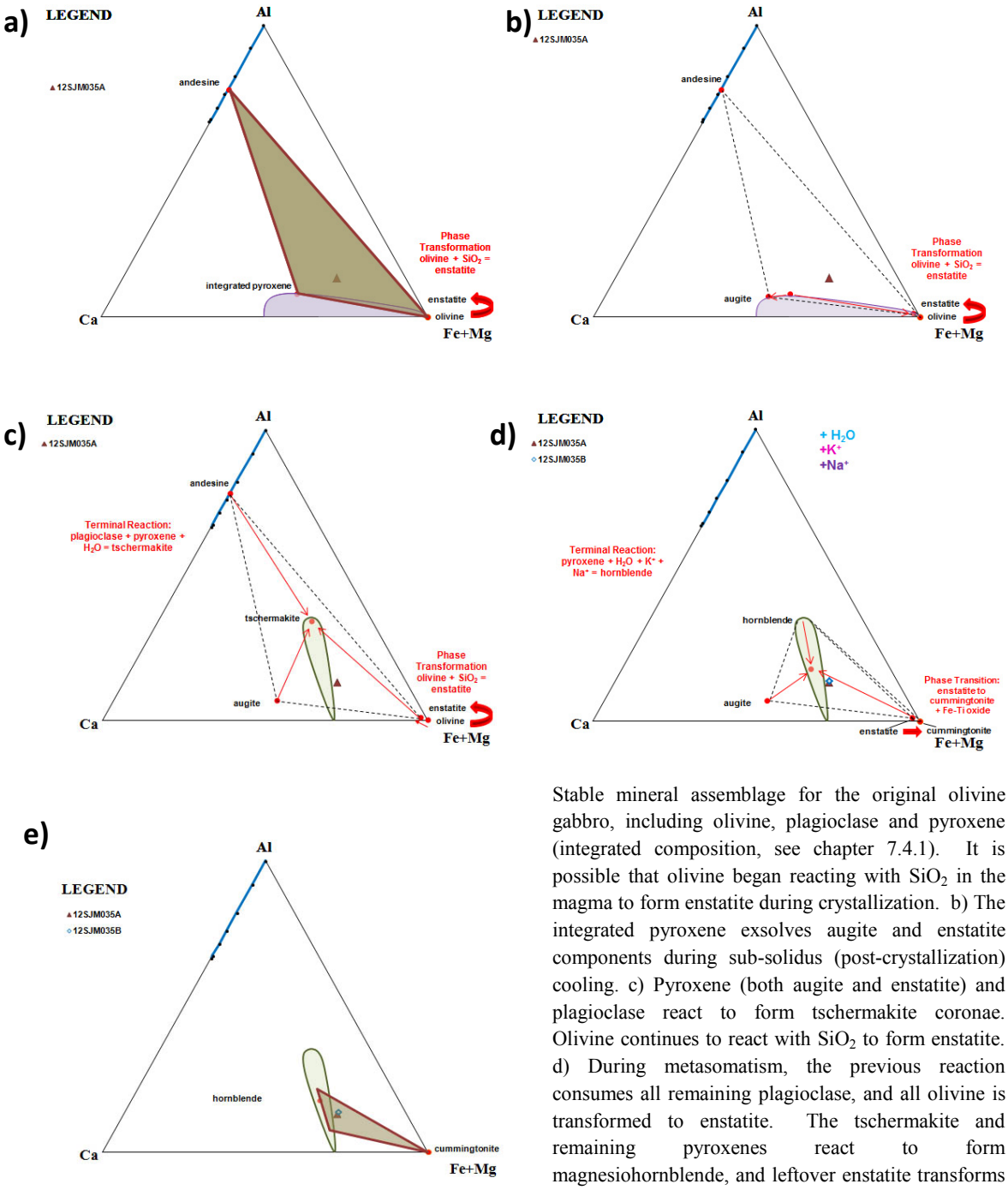

Figure 7.14 – Petrogenetic model for the generation of coronitic olivine metagabbro and hornblendite, illustrated through the ternary system calcium-aluminum-iron+magnesium, with observed mineral compositions and pseudo-stability fields plotted. a) Stable mineral assemblage for the original olivine gabbro, including olivine, plagioclase and pyroxene (integrated composition, see chapter 7.4.1). It is possible that olivine began reacting with SiO_2 in the magma to form enstatite during crystallization. b) The integrated pyroxene exsolves augite and enstatite components during sub-solidus (post-crystallization) cooling. c) Pyroxene (both augite and enstatite) and plagioclase react to form tschermakite coronae. Olivine continues to react with SiO_2 to form enstatite. d) During metasomatism, the previous reaction consumes all remaining plagioclase, and all olivine is transformed to enstatite. The tschermakite and remaining pyroxenes react to form magnesiohornblende, and leftover enstatite transforms to cummingtonite through hydration and releases iron to form Fe-Ti oxides. e) The final observed mineral assemblage in the sample of hornblendite (12SJM035B) consisting of hornblende, cummingtonite and Fe-Ti oxides.

Plagioclase has been completely consumed by the terminal reaction described earlier, and thus a new terminal reaction between tschermakite and any remaining pyroxene likely formed the green amphibole that constitutes the majority of the hornblendite. These reactions have been plotted on ternary phase diagrams in figure 7.14d-e. Both of these diagrams include the bulk chemistry of both the olivine metagabbro and the hornblendite, which are almost identical in Al-Ca-FeMg compositional space. The transformation from olivine metagabbro to hornblendite is a metasomatic reaction, and so it is important to note that the system was open during metamorphism. Although the pseudo-tie lines drawn in figure 7.14d-e accurately represent the observed reactions, they do not necessarily represent stable mineral assemblages, but rather mineral reactions in a chemically dynamic environment. The change in major and trace element geochemistry is described below.

Plotting the olivine metagabbro and hornblendite on REE and trace element diagrams (figure 7.15) shows that ΣREE concentrations are similar between rock types, though slightly depleted in the hornblendite, whereas the hornblendite is enriched in alkali metals such as cesium, rubidium and potassium as well as large ion lithophile elements such as lead.

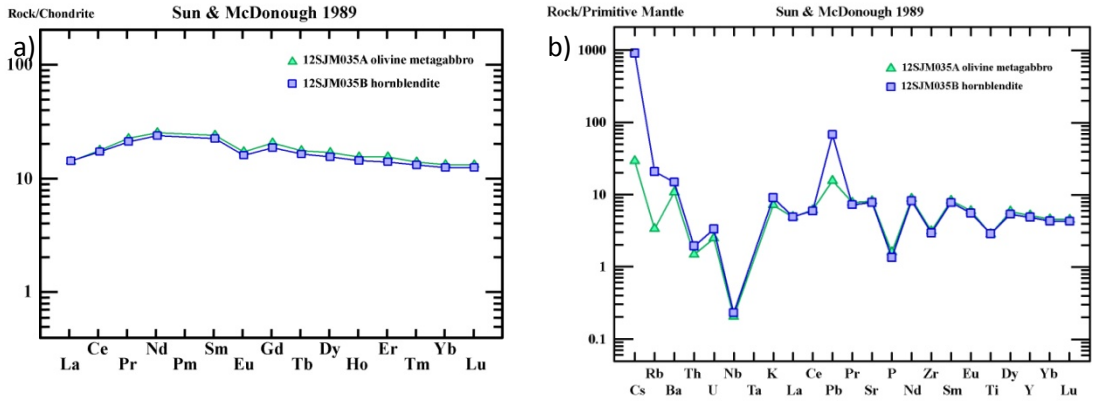

Figure 7.15 - REE plot normalized to chondritic values and b) trace element plot normalized to primitive mantle values, including samples 12SJM035A and 12SJM035B (olivine metagabbro and hornblendite, respectively). Note that the total REE concentrations in the hornblendite (blue squares) are slightly depleted compared to those of the olivine metagabbro, but their relative concentrations are the same (parallel topology). Also, the sample of hornblendite contains much higher concentrations of cesium, rubidium and lead. All normalization according to Sun and McDonough (1989)

The enrichment and depletion of elements is better displayed on an isocon diagram (after Grant 2005). For this diagram, the ratio between elements in each rock is plotted as a point on the diagram, aside from Al_2O_3, which is assumed to have stayed immobile during alteration, and is plotted as a dotted black line against which each of the other elements may be compared. This shows that many of the divalent cations (Ca, Mg, Sr, REEs, Fe_t, Fe^{2+} etc.) are more abundant in the original rock, whereas the monovalent cations (K, Rb, Cs, or large ion lithophile elements), ferric iron (Fe^{3+}), chalcophile elements and volatile elements (LOI) are more abundant in the altered rock (hornblendite).

The transition from [Fe^{2+}] to [Fe^{3+}] from the olivine metagabbro to hornblendite suggests that the fluids present during alteration were oxidizing, which is supported by the appearance of

Fe-Ti oxides in the hornblendite as described above, and is consistent with the εFe data presented in chapter 7.3. The addition of volatiles is also consistent with the metamorphic reaction described above, which is required to produce such abundant amphibole in the altered rock. The addition of chalcophile elements and lead, and the depletion in Sr coupled with enrichment in Rb may both have significant implications for mineralization and isotope systematics.

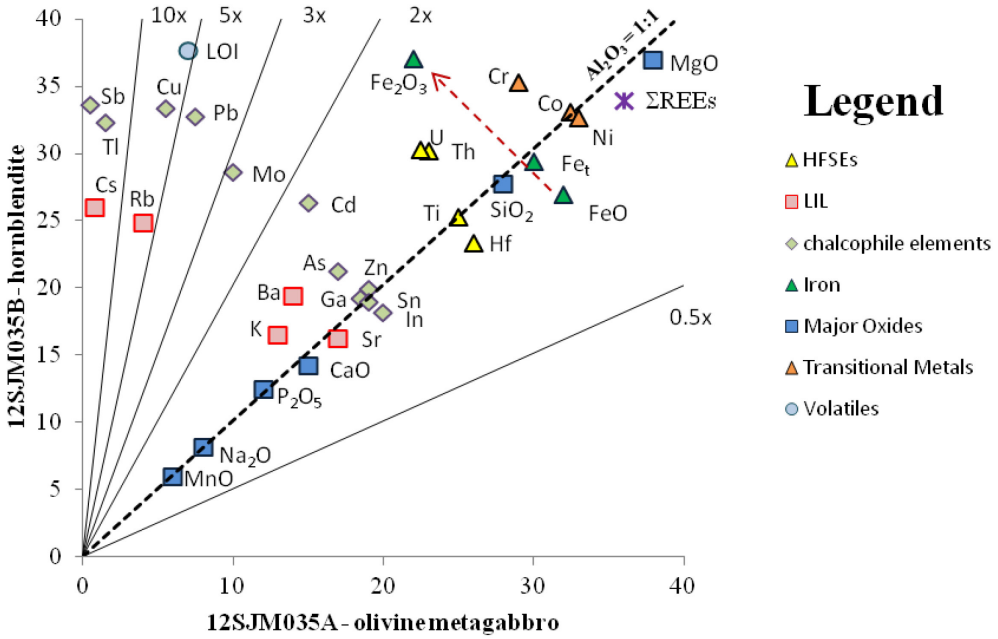

Figure 7.16 – Isocon plot (after Grant 2005) comparing concentrations of different major and trace elements in the coronitic olivine metagabbro (x-axis) and its metamorphosed equivalent, the hornblendite (y-axis). Aluminum is assumed to have been immobile during alteration (dotted black line), and plotted along with other reference lines with which to compare the enrichment and depletion of other elements between rock types. The red arrow illustrates the change from ferrous to ferric iron between the olivine metagabbro and the hornblendite.

7.5 - Altered Metagabbro

As described above, several types of altered metagabbro occur throughout the Raglan Hills metagabbro. These rocks which mostly concentrated within the basal thrust sheet tend to contain major and/or trace element concentrations that are not consistent with the major rock types within the intrusion, and are interpreted to be the result of metasomatism.

The rocks of unit 13a, "altered metagabbro", display recognizable metagabbroic textures, but their major and/or trace element concentrations are anomalous and make identification of their protolith difficult. These rocks also commonly display textural evidence for metasomatism, such as quartz-calcite-sulphide veining or "washed out" textures.

The rocks of unit 13b also commonly display recognizable metagabbroic textures (with the exception of station 12SJM005, which appears migmatitic), and have distinctly low silica and/or rare earth element concentrations. These rocks are located within the basal thrust sheet, proximal to major sinistral offsets and along the boundary between the basal thrust sheet and the core of the intrusion. Due to their proximity to major structures, it is likely that the structures acted as conduits for metasomatizing fluids which mobilized silica and the rare earth elements.

The rocks of unit 13c are commonly homogenous, locally foliated, fine-grained, granoblastic and melanocratic, composed mainly of green hornblende, biotite, diopside and Fe-Ti oxide minerals. They occur along positive magnetic anomalies that lie parallel to the northern boundary of the intrusion, within the basal thrust sheet. Their major and trace element concentrations are highly varied, such that the rocks may resemble olivine metagabbro, clinopyroxenite, or Fe-tholeiitic amphibolite, and have likely been metasomatized, which makes the genesis of these rocks highly convoluted. Therefore it is uncertain whether these rocks represent altered ultramafic dikes or Fe-tholeiitic amphibolite dikes, or whether these anomalies lie along structurally-controlled metasomatic zones with highly oxidizing fluids.

7.6 – Chlorite Distribution

Although the majority of the Raglan Hills metagabbro is composed of mineralogy consistent with amphibolite facies metamorphism, there are numerous occurrences of magnesium-rich chlorite throughout the core and basal thrust sheet of the intrusion that have been interpreted as retrograde metamorphic features. As seen in figure 7.6, chlorite tends to occur proximal to major sinistral offsets, which may suggest that deformation along these structures may occurred under lower pressure and temperature conditions than the majority of the intrusion.

7.7 - Metamorphic Implications for the Granitoid Rocks

As described in chapter 3.6, the granitoid rocks located in the basal thrust sheet of the Raglan Hills metagabbro are tonalitic to granodioritic to monzogranitic in modal mineralogy, which may in part be explained by crystal fractionation processes, but the observed mobility of large ion lithophile elements during metamorphism, specifically potassium and rubidium, may have also affected the current mineralogy of the meta-granitoid rocks and their classification on diagrams which include the LIL elements.

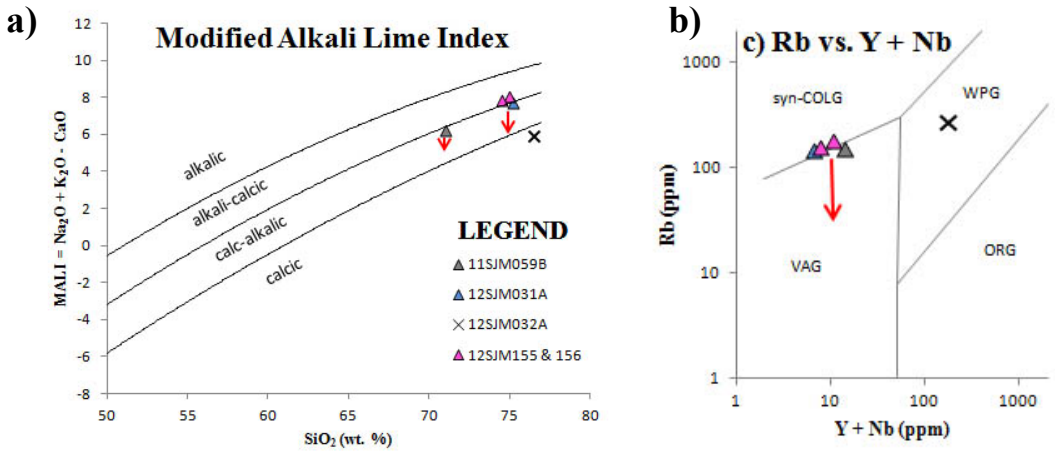

Figure 7.17 – granitoid classification diagrams revisited. Considering the mobility (and general enrichment) of K and Rb in local rocks during metamorphism, the samples of meta-granitoid rocks may actually belong in the calc-alkalic field on a MALI diagram (a) and in the volcanic arc granitoid field on a Rb vs. Y + Nb diagram (as well as a Rb vs. Yb + Ta diagram, not shown here). This classification as a volcanic arc granitoid is consistent with the same classification achieved in REE granitoid discrimination diagrams.

Figure 7.17 contains two granitoid classification diagrams, including a Modified Alkali Lime Index and a Rb vs. Y + Nb diagram, both utilized in chapter 3.6. Considering the general enrichment of local rocks in K and Rb during metamorphism (chapter 7.4), the placement of the metagranitoid rocks in these diagrams should shift to less K and Rb-rich fields. On the MALI diagram, the samples should plot more within the calc-alkalic field, and on the Rb vs. REE diagram, the samples should plot more within the VAG field, which is more consistent with their placement on REE discrimination diagrams (figure 3.23).

7.8 - Summary: Metamorphism and Metasomatism

The metasomatism observed in the olivine metagabbro has several implications for metamorphism throughout the rest of the Raglan Hills metagabbro and the surrounding country rocks.

The original magma which crystallized the olivine metagabbro was likely H_2O undersaturated, due to the apparent absence of primary hydrous phases (all biotite and hornblende are interpreted as metamorphic minerals) causing the formation of coronae rather than hornblendite during metamorphism, and external fluids were required to form hornblendite through metasomatism.

The original magma which crystallized the olivine metagabbro likely evolved from silica-undersaturated (crystallizing olivine) to silica-saturated, causing the formation of enstatite rims around the crystals of olivine. This may have been induced by assimilation of siliceous rocks or mixing with a siliceous magma.

The elongate lens morphology of the hornblendites indicates their formation was likely structurally controlled, and these structures likely acted as the main conduits for external hydrous fluids.

Metasomatism of the olivine metagabbro did not significantly affect its major element concentrations, and so the other metagabbroic rocks within the core of the intrusion likely underwent “isochemical” metamorphism with respect to the major elements.

The large ion lithophile elements, such as potassium and rubidium, were mobile during metamorphism, which may affect the geochemical classification of rocks, such as pushing gabbroic rocks from the sub-alkaline field to the alkaline field on a Total-Alkali Silica (TAS) diagram, or changing granitoid rocks from “volcanic arc granitoids” to “syn-collision granitoids” on granitoid discrimination diagrams that use Rb.

The chalcophile elements were mobile, becoming more enriched in the hornblendite. This may be significant for studying other metasomatized and mineralized gabbroic rocks in the Raglan Hills intrusion.

Although the concentration of iron did not change significantly during metasomatism, the iron is more oxidized (ferric) in the hornblendite, causing these rocks to appear as positive aeromagnetic anomalies within the core of the Raglan Hills metagabbro. This feature allows the ultramafic rocks to be delineated using geophysical interpretation.

Several geochemical and mineralogical trends are present within the intrusion that have implications for the nature of metamorphism and the metamorphic fluids which affected the Raglan Hills metagabbro.

The mineralogy of the recrystallized rocks in the intrusion, such as the Fe-tholeiitic amphibolites, or some of the altered rocks in the basal thrust sheet, is consistent with amphibolite-facies metamorphism (plagioclase – hornblende – diopside – titanite), which is supported by a metamorphic analysis performed on the country rocks by Magnus (2013b).

This results in a lower limit for peak metamorphic conditions of roughly 600°C and 3 kilobars, with a rough estimate for an upper limit of 700°C and 8 kilobars.

A majority of the metamorphosed rocks within the intrusion have similar Fe^{3+}/Fe^{2+} ratios (28% Fe^{3+} / 72% Fe^{2+} = 0.2825), controlled by an unknown buffer. Since this ratio is consistent throughout most of the intrusion (spatially), the buffer was likely within the rock rather than the metamorphic fluids.

The samples with lower ratios (higher [Fe^{2+}]) tend to be the least metamorphosed rocks, such as the coronitic olivine metagabbro, whereas those with higher ratios (higher [Fe^{3+}]) tend to be located within zones of high deformation and/or metasomatism, such as within the basal thrust sheet, or proximal to the McArthurs Mills shear zone and its conjugate sinistral offsets.

The basal thrust sheet contains several unique types of altered metagabbroic rocks, which suggests that a variety of metasomatic fluids were transported through this zone of moderate to strong deformation.

Weak retrograde metamorphism may have been related to structural effects on local pressures and temperatures.

The absence of any textural evidence for previous greenschist facies metamorphism suggests that either the Raglan Hills metagabbro was emplaced under amphibolite facies conditions and remained under those conditions until the termination of the Ottawan Orogeny, or that the Raglan Hills metagabbro was emplaced at a shallow crustal level, however, because the magma was likely H_2O undersaturated, recrystallization was restricted until metamorphic fluids were introduced to the intrusion under amphibolite facies conditions.

7.9 - Structural Geology

Evidence for four distinct phases of deformation was described for the rocks in the Raglan Hills area by driven by compressional, transpressional and extensional tectonism (Magnus 2013b). These include:

D_1 – compressional, ductile (1190-1170 Ma, Shawinigan Orogeny)

D_2 – compressional, ductile (1080-1020 Ma, Ottawan Orogeny)

D_3 – transpressional, ductile (1080-1020 Ma, Ottawan Orogeny)

D_4 – extensional, ductile (late Ottawan to post-Ottawan Orogeny)

Time ranges given above are after Rivers (1997) and Carr et al (2000), and include both deformation and metamorphism. Note the almost 60 million-year time span of the Ottawan Orogeny.

7.9.1 - Thrusting and Folding

Both compressional phases consist of parallel northwest-vergent features such as thrust faults and recumbent to overturned folds, with thrust planes and axial fold planes striking roughly east-northeast and dipping moderately towards the southeast. There is evidence to suggest that folding occurred after thrusting, however thrusting and folding may have occurred during both the Shawinigan and Ottawan orogenies, making a temporal distinction between different compressional structures difficult.

The transpressional phase cross-cuts earlier thrust faults and folds, with the locus of deformation in the McArthurs Mills shear zone, a roughly one kilometre wide zone of intense dextral ductile deformation that is located along the southern margin of the Raglan Hills metagabbro (figure 7.18).

The extensional phase was only observed to the south of the Raglan Hills metagabbro, and is evidenced by normal ductile shearing along planes parallel to the McArthurs Mills shear zone and axial planar cleavage in the metavolcanic rocks of the Elzevir Terrane, indicating that these previous structures were likely reactivated during this late extensional event. No evidence for normal faulting was observed within the Raglan Hills metagabbro or in the country rocks north of the intrusion.

Evidence for thrusting, folding and transpressional shearing (but not normal shearing) has been observed within the Raglan Hills metagabbro (chapter 5).

For instance, several rocks located proximal to the northwest boundary of the intrusion show evidence for top-to-the-northwest thrusting within a zone of moderate to strong deformation and metasomatism herein called the “basal thrust sheet”.

One fold axis was identified through geophysical analysis: the elongate ovoid positive magnetic anomaly within the centre of the metagabbro, which is likely composed of olivine metagabbro and hornblendite, has been interpreted as a canoe-like upright to inclined synform, with a fold axis that plunges inward towards the center of the canoe. The fold axial plane appears to have been folded, as it trends north-northeast in the western part of the synform, and changes to an east-northeast trend at the eastern end of the synform, a shape roughly parallel to the curvature of the northern margin of the intrusion (and the basal thrust sheet). Protomylonitic to mylonitic foliations within the core of the metagabbro are oriented parallel to these features as well, and have been interpreted as representing the fold axial planar foliation.

Structural analysis of these folded protomylonitic foliations has provided a secondary fold axial plane oriented roughly 324/80, which is parallel to several protomylonitic fabrics observed both in the field and through geophysical analysis. Hence, these features have been

interpreted as representing the fold axial planar foliation to the secondary fold. The calculated fold axis for this secondary fold is roughly 49/132, which is roughly parallel to most of the stretching and mineral lineations measured throughout the basal thrust sheet, core, and country rocks north of the intrusion.

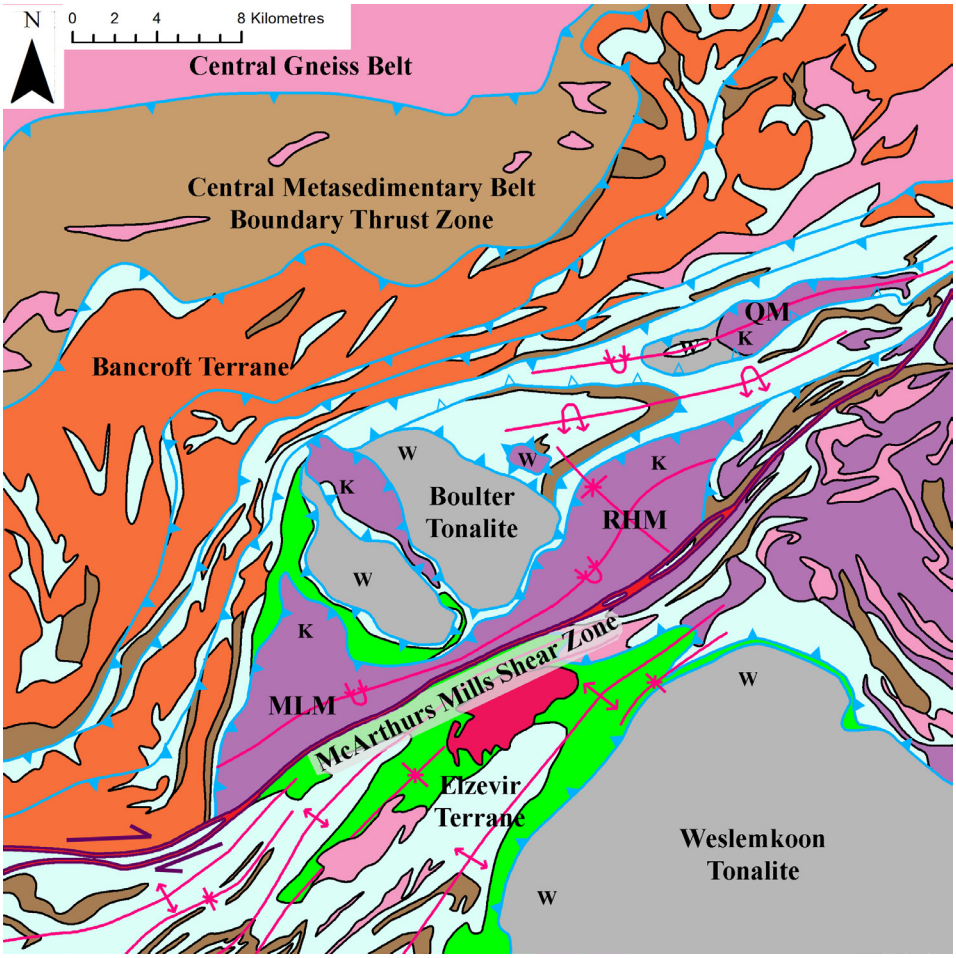

Figure 7.18 – Sketch map of Raglan Hills area, including portions of the Laurentian Margin, Bancroft Terrane and Elzevir Terrane (from northwest to southeast, respectively). The Laurentian Margin and the Bancroft Terrane are separated by the CMBBTZ, and the Bancroft Terrane and Elzevir Terrane are separated in part by the McArthurs Mills Shear Zone (MMSZ) and in part by a south-west vergent thrust fault which overlies the Elzevir volcaniclastic package (green). The change in structural style across the MMSZ from thrust-dominated in the northwest to fold-dominated in the southeast suggests the MMSZ is the youngest major structural feature. Abbreviations: RHM = Raglan Hills metagabbro, MLM = Mallard Lake metagabbro, QM = Quadeville metagabbro. Structural klippes and windows are indicated with Ks and Ws respectively.

Although the secondary folding event post-dates the earlier canoe-shaped synform, there is no evidence to suggest that there was a significant difference in the timing of their formation. In fact, what likely happened is that while the metagabbro was being thrust northwestward (producing the basal thrust sheet and primary fold), the intrusion was juxtaposed against the Boulter Tonalite, a large felsic intrusion located to the northwest of the Raglan Hills intrusion.

Thus, the thrusting and both fold events likely occurred due to compressional stress in the same direction. The absolute timing of the folding and thrusting is unknown, though thrusting

was most likely initiated during the Shawinigan Orogeny, with some possible folding, and the thrusts may have been reactivated during the Ottawan Orogeny. These data and interpretations are consistent with those of Hanmer and McEachern (1992).

7.9.2 - Ductile Shearing

The three distinct shear features described earlier (chapter 5, figure 5.1) comprise a classic example of composite foliations formed in ductile shear zones.

The east-northeast-trending dextral shear planes that are parallel to the northern and southern margins of the intrusion represent the S-planes, which are likely reactivated thrust planes and fold axial planar foliations produced during the earlier compressional deformation.

The southeast-striking dextral shears are roughly parallel to the F_2 fold axis calculated earlier, and it is possible that the F_2 axial planar foliations were reactivated as dextral C-planes during shearing.

The north-northeast-striking sinistral shear zones are unique within the local structural history, and likely also formed as conjugate sinistral fractures during large-scale dextral shearing, a feature commonly observed in quartz and feldspar porphyroclasts in ductile shear zones (Hatcher 1995). Proximal to the margins of the intrusion, these fractures appear brittle, with sharp displaced contacts along their strike, and commonly host plagioclase-hornblende ± diopside veinlets, indicating that they formed under extensional conditions, and may have facilitated partial melting of metagabbroic rocks in the basal thrust sheet (Si and REE-depleted, Al-rich rocks such as those at station 12SJM005). In the core of the intrusion, trace retrograde Mg-rich chlorite occurs proximal to these sinistral fractures, which suggests that these fractures may have "ventilated" the metagabbro, dropping the local temperature and pressure to upper greenschist facies conditions.

Station 12SJM159 displays textural evidence for syn-tectonic magmatism that is unique within the Raglan Hills metagabbro (figure 3.8). This outcrop is composed of variably deformed alkalic metagabbro, including lenses of non-deformed magmatic-textured metagabbro in sharp contact with protomylonitic metagabbro, appearing as though fresh magma was injected into already-crystallized and deformed gabbro. This alkalic metagabbro has been observed cross-cutting both regular metagabbro, which shows no evidence for deformation at the time of crystallization, and highly deformed Fe-tholeiitic amphibolites, which contain almost no primary textures, and therefore cannot provide textural evidence for syn-tectonic magmatism. . Whether this deformation (and coeval magmatism) occurred during the Shawinigan Orogeny or the earlier Elzevir Orogeny (~1250-1190 Ma, Rivers 1997) is currently unknown, though a geochronological study of the alkalic metagabbro may solve that problem.

Structural analyses have provided evidence that the Raglan Hills metagabbro was affected by three of the four phases of deformation described by Magnus (2013a,b) for the

surrounding country rocks, excluding the youngest phase of deformation (normal shearing), and a possible earlier phase of deformation has been described (D_0 – syn-magmatic deformation).

Northwest-vergent thrusting and folding occurred throughout the Shawinigan and Ottawan orogenies, which transported the Raglan Hills metagabbro toward the Laurentian Margin and apparently anchored it against the rheologically stiff Boulter tonalite, which has a profound effect on the morphology of the intrusion and its structural features.

Dextral ductile deformation with a locus of deformation along the southern margin of the Raglan Hills metagabbro produced local intense mylonitic fabrics accompanied by metasomatic alteration of the different metagabbroic rocks in the intrusion. This shearing likely reactivated previous foliations (belonging to earlier thrusting and folding events) to produce a large-scale composite foliation fabric consisting of three dominant shear orientations: two dextral shear directions which comprise the classic C-S fabric, and one sinistral shear direction with an apparent extensional component.

Textural evidence suggests that some of the youngest stages of magmatism may have occurred during local tectonic activity, which may be coincident with the Elzevirian Orogeny.

The timing of peak metamorphism in the Raglan Hills metagabbro is unknown, and therefore the local metamorphic conditions prevalent during the Shawinigan and Ottawan orogenies are currently unknown, with the exception that during the last observable deformation event (dextral shearing), the Raglan Hills metagabbro was subjected to amphibolite facies metamorphic conditions with localized retrograde metamorphism controlled by the extensional component of the late dextral shear event. However, evidence for similar metamorphic conditions has been observed in the local thrusted and folded country rocks, so it is likely that the Raglan Hills metagabbro was subjected to amphibolite facies metamorphism throughout those events as well.

7.10 - Igneous Petrology

Four distinct gabbroic rocks have been identified within the Raglan Hills metagabbro, the regular metagabbro, calcic metagabbro, alkalic metagabbro and Fe-tholeiitic amphibolite. Field observations, petrography and geochemistry have helped sort out their petrogenesis and petrogenetic sequence.

7.10.1 - Regular and Calcic Metagabbro

Except for their calcium concentrations, both the regular and calcic metagabbroic rocks contain very similar major and trace element concentrations. When plotted on a Jensen diagram, both of these rock types plot near the intersection between high Fe tholeiitic basalt, high Mg tholeiitic basalt and basaltic komatiite (samples with Eu* close to 0), with more intermediate and felsic rocks spreading into the calc-alkaline field, and the more mafic rocks spreading variably into the komatiite field, whereas the other rock types plot solely within the tholeiitic field.

Relative trace element concentrations in these rocks display strong negative Nb-Ta anomalies and moderate positive Pb anomalies, with variable enrichment in LILs and depletion in

HFSEs. These trace element patterns are typical of igneous rocks derived from a volcanic arc setting, and are attributed to enrichment in mobile elements (Pb and LILs) in the mantle source from dehydration of various components of the subducted plate. All of these rocks (except for the samples of clinopyroxenite) display negative P anomalies as well, which may indicate that P was not enriched in the mantle source, or apatite fractionation occurred during crystallization.

Relative rare earth element concentrations in these rocks display generally flat patterns (La = Lu = 10 to 30 x chondritic values), with more negatively-sloping patterns in the intermediate to felsic rocks (La>Lu). Positive to negative europium anomalies are present in the felsic to mafic rocks, respectively, which is attributed to the preferential substitution of Eu for Ca in plagioclase over the other REEs (Brownlow, 1996), and only slightly negative Ce anomalies are perceptible in a few of the samples of calcic metagabbro, which may support the theory that assimilation of carbonate material by regular gabbroic magma formed the calcic gabbroic rocks, due to the strong negative Ce anomalies present in seawater and in local calcite marbles. However, since the anomalies visible in the calcic metagabbro are very slight, their significance is at the mercy of the detection limits for measuring the rare-earth elements, and thus cannot be used to support the aforementioned theory.

Analysing their major element geochemistry relative to their Eu* values has shown that fractional crystallization played a significant role in the petrogenesis of both of these rock types (figures 4.1, 4.2 and 4.3). It is important to note that the rocks with an Eu* close to zero plot close to the intersection between high Fe tholeiitic basalt, high Mg tholeiitic basalt and basaltic komatiite on a Jensen diagram, which might represent the initial non-fractionated liquid composition (figure 3.13).

For the regular metagabbro, plagioclase was likely the sole fractionated component (with minor pyroxene fractionation; olivine only appears as an interstitial phase and therefore was not significant during fractionation), which is supported by the abundance of euhedral plagioclase laths with interstitial mafic material which locally show cumulate textures consistent with magmatic layering (fractionation).

However, it appears that diopside and apatite were fractionated during crystallization of the calcic metagabbro, which is indicated by the abundance of euhedral diopside phenocrysts present in the samples of calcic metagabbro with interstitial anhedral plagioclase, and the presence of apatite in samples of cumulate-textured clinopyroxenite. This diopside and apatite fractionation would have caused a relative accumulation of plagioclase in the residual melt, creating a parallel Eu* trend to the rocks of the regular metagabbro, along with depleting the residual melt in phosphorous, producing a negative P anomaly.

The genesis of the calcic metagabbro is somewhat convoluted, though either processes in the magma chamber or in the melt source must be to blame. Four theories investigated by the author are:

1. Calcium was added to the magma by assimilation of country rock carbonate material.

2. The conditions (pressure, temperature) during crystallization were occasionally changed such that Ca was enriched in the melt by crystal fractionation processes.

3. The melt source for these magmas was variably enriched in calcium.

4. The conditions (pressure, temperature) during melting were occasionally changed such that Ca was more mobile.

Negative anomalies for the HFSEs (Zr, Hf, Ti, and exaggerated Nb and Ta anomalies) for both regular and calcic metagabbro suggest that either a refractory phase kept these elements in the melt source, or a HFSE-bearing phase was fractionated out of the magma early in the crystallization history, prior to assimilation.

An important feature of the calcic metagabbroic rocks is their lack of euhedral plagioclase laths, particularly in the mesocratic samples, relative to their regular metagabbroic counterpart, which contain abundant euhedral plagioclase laths. This may suggest that hydrous fluids were present during the crystallization of the calcic metagabbro, which tend to suppress silica polymerization required to crystallize framework silicates such as plagioclase (source). If this is true, the coincidence between Ca-rich and fluid-rich magma suggests that assimilation of country rocks (locally dominated by carbonate and silicate metasedimentary rocks) by regular metagabbro may have produced calcic metagabbro. However, the effect of carbonate-rich fluids on crystallization processes is in general poorly understood, and thus the remaining genetic theories may still be valid (2, 3, 4). The occurrence of calcic metagabbro around the margins of the metagabbro may support this theory (1), however as described in chapters 5 and 7.9, the morphology of the intrusion was largely influenced by thrusting and shearing, which may have tectonically eroded the true magmatic contacts of the intrusion.

Layered calcic metagabbro also occurs in the core of the intrusion in close association with the bands of olivine metagabbro, which may have implications for the genetic relationship between the calcic and regular metagabbro. Considering the likelihood that crystal fractionation and accumulation played a major role in the formation of these rocks and the possibility that assimilation of carbonate material may have caused the formation of the calcic metagabbro, a genetic model for the formation of these rocks and their close spatial relationship must accommodate both of these processes.

7.10.2 - Alkalic Metagabbro

The alkalic metagabbro is (as the name suggests) an iron-rich alkalic rock which is enriched in large-ion lithophile elements, light rare earth elements and high field strength elements with respect to the regular and calcic metagabbroic rocks. These rocks tend to be located near the margins of the intrusion, in close association with Fe-tholeiitic amphibolite. These rocks display negative Nb-Ta anomalies; much less extreme than those of the regular and calcic metagabbroic rocks and less exaggerated positive Pb and negative P anomalies.

Trace element concentrations indicate that plagioclase and apatite were likely fractionated during crystallization of these rocks. Plagioclase fractionation is apparent in station 12SJM159, which contains both melanocratic and leucocratic alkalic metagabbro, which appear

to grade into one another through fractionation of coarse euhedral plagioclase laths. However, no apatite has been positively identified in these rocks.

7.10-3 - Fe-tholeiitic Amphibolite

The Fe-tholeiitic amphibolite is a fine-grained granoblastic Fe-rich tholeiitic rock which displays MORB-like trace element and REE patterns with variably enriched and depleted LREEs and LILs, and display only small negative Nb-Ta anomalies and small positive Pb anomalies. The Fe-tholeiitic rocks also display slightly negative HFSE anomalies (Zr, Hf, Ti) similar to those observed in samples of regular and calcic metagabbro, but absent in samples of alkalic metagabbro. These rocks also contain particularly high $^{143}Nd/^{144}Nd$ ratios relative to the other rocks in the Raglan Hills metagabbro, and tend to be located above positive aeromagnetic anomalies near the margins of the intrusion in dike-like arrangements (which have likely been dismembered during deformation).

7.10.4 - Temporal Relationships

Relative age relationships on an outcrop scale provide a simple magmatic sequence for the Raglan Hills metagabbro.

Both Fe-tholeiitic amphibolite and alkalic metagabbro cross-cut the regular and calcic metagabbro, therefore the regular and calcic metagabbroic rocks are the oldest magmatic rocks in the intrusion.

Alkalic metagabbro cross-cuts the Fe-tholeiitic amphibolite, therefore it is the youngest magmatic rock in the intrusion.

7.11 - Emplacement Model

Considering the current morphology and interpreted igneous layering and cross-cutting relationships, a genetic model for the Raglan Hills metagabbro has been developed (figures 7.19 and 7.20). This model is focuses on crustal processes, and does not include any mantle processes involved (i.e. mantle component geometry, melt conditions or transport through the mantle to the crust). The diagrams in this model are oriented perpendicular to the long axis of the intrusion, which could likely have extended for tens of kilometres.

The model begins with metamorphosed carbonate rocks (marble) located in the hypothetical Elzevirian back-arc basin (figure 7.19a). Extension likely produced planes of high strain (low stress) which could provide pathways for magma transportation through the crust.

The early stages of magmatism would have been restricted to the pathways opened up by extension (figure 7.19b). Lateral extension of the magma transportation would likely have occurred parallel to sedimentary bedding, which may have been erased in the carbonate rocks due to recrystallization, however intercalated beds of metamorphosed siliciclastic rocks would have preserved the structure of primary bedding.

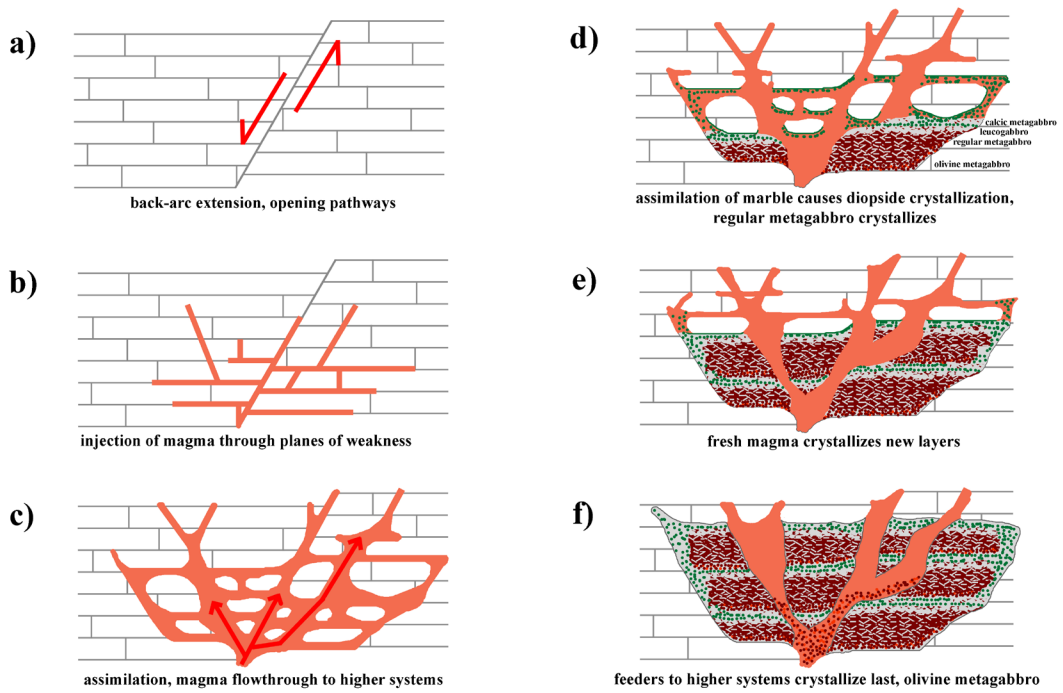

Figure 7.19 – model for the emplacement of the Raglan Hills metagabbro beginning with extension and development of pathways in metacarbonate-dominated host rocks (a to c), followed by crystallization of the regular and calcic metagabbro (d to f). Crystal colours: burgundy = augite, grey = plagioclase, orange = olivine, and green = diopside.

As more magma is introduced to the system, the host metasedimentary rocks were likely eroded and assimilated by the magma (figure 7.19c). Considering the large volume of gabbro observed in the current form of the Raglan Hills metagabbro, and the large volume of regular metagabbroic rocks that display little evidence for assimilation, the Raglan Hills metagabbro likely represents a conduit that fed magma higher into the crust, flushing out magma affected by assimilation.

As the magma cools, crystallization begins in quiescent zones within the conduit (figure 7.19d). The regular metagabbro (including olivine metagabbro) were likely crystallized from magma unaffected by assimilation. Interaction between wall-rocks along the sides and roof of the intrusion may have caused Ca-enrichment in the magma, stabilizing diopside while hydrous fluids boiling out of the assimilated metasediments may have repressed plagioclase formation.

Continued introduction of magma causes continued excavation into the host metasedimentary rocks and subsequent assimilation and crystallization (figure 7.19e).

As the influx of magma slows down, the intrusion solidifies, first in the more restricted pathways and terminating in the less restricted pathways (figure 7.19f). The true number of layers within the Raglan Hills metagabbro is currently unknown.

Figure 7.20a is a simplified illustration of the intrusion post-crystallization, including regular metagabbro in shades of green and calcic metagabbro in dark blue, with leucogabbro in

light blue. In reality the layers and arrangement of rock types in this intrusion were likely less planar and uniform.

Following complete crystallization of the regular and calcic gabbro, extension resumed and Fe-tholeiitic magma was fed into structures located near the (current) edges of the intrusion (figure 7.20b).

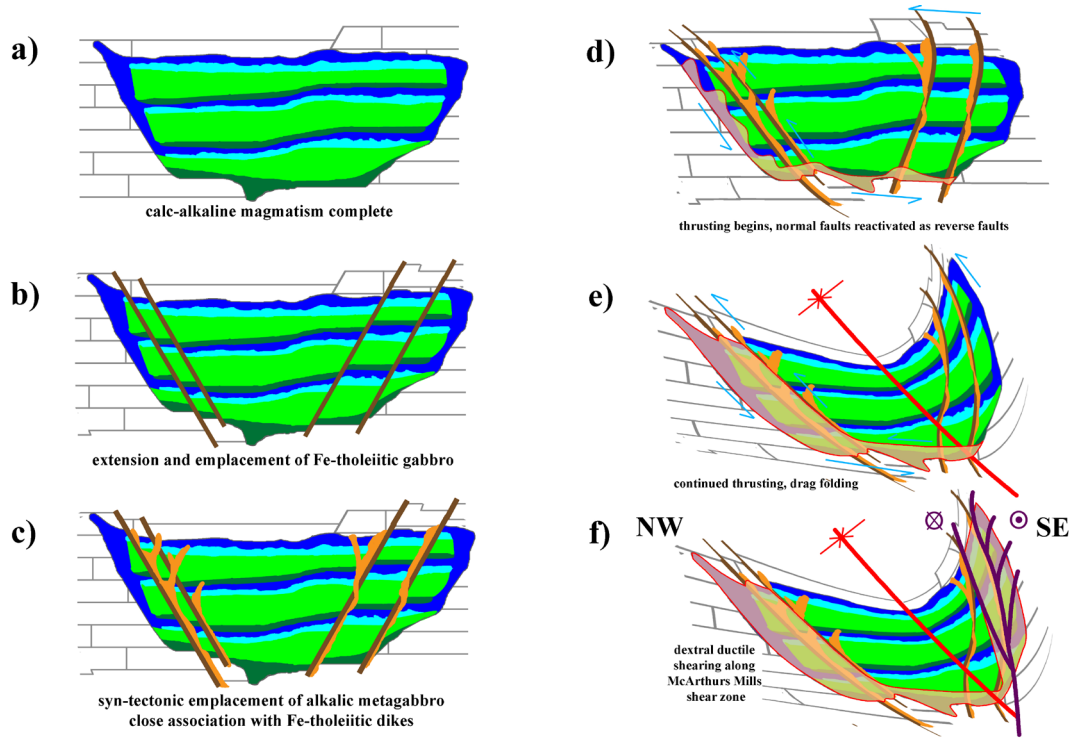

Figure 7.20 – a) simplified arrangement of regular and calcic metagabbro following step f in figure 7.19. Rock type colours: dark green = olivine metagabbro, green = regular metagabbro, light blue = leucogabbro, dark blue = calcic metagabbro. b) emplacement of Fe-tholeiitic dikes, followed by c) emplacement of alkalic gabbro. Northwest-directed thrusting and folding (d and e) deform the intrusion and cause the formation of the basal thrust sheet (transparent pink overlay). f) dextral shearing along the McArthurs Mills shear zone causes more alteration.

Due to their close spatial relationship with the Fe-tholeiitic dikes, alkalic gabbro likely took advantage of the same structures, and locally cross-cut the tholeiitic gabbro (figure 7.20c). Although the alkalic metagabbro shows evidence for syn-tectonic emplacement, it is uncertain whether it was extensional or compressional.

As the Composite Arc Belt (e.g. Elzevir terrane) collided with the Laurentian margin, deformation along the Central Metasedimentary Belt boundary thrust zone initiated as northwest-vergent thrusting and folding. The intrusion likely acted as a single thrust sheet, providing a pathway for metamorphic fluids along its base, creating the metasomatized basal thrust sheet (transparent pink overlay in figure 7.20d).

Continued northwest-vergent deformation also formed a synformal structure, which is apparent through analysis of the airborne geophysical patterns in the current core of the intrusion (figure 7.20e).

Dextral shearing occurred along the southern margin of the intrusion, which mylonitized and metasomatised the metagabbro (figure 7.20f).

There is currently no evidence to suggest that any tectonic events significantly affected the Raglan Hills metagabbro following dextral shearing, which likely occurred during the Ottawan Orogeny. Preferential weathering of marble over gabbroic rocks has caused the intrusion to comprise a topographic high, with roughly 150 metres of relief between its lowest and highest elevation.

7.12 - Geochronology

Absolute temporal relationships between the different rock types within the Raglan Hills metagabbro may be estimated using geochronological methods, such as U-Pb zircon analysis, and Nd-Sm and Rb-Sr whole rock isotopic analyses.

Pehrsson et al. (1996) collected one sample of "coarse, ophitic isotropic sample from a 5 m thick layer in the banded part of the gabbro", located within the basal thrust sheet of the intrusion. This sample yielded two populations of zircons: one group of irregular pale yellow to colourless clear crystals and fragments, and a group of complex polycrystalline aggregates which have been interpreted as metamorphic zircon which replaced baddeleyite. Analysis of these grains produces three distinct ages: 1229 ± 5 Ma, 1154 ± 7 Ma, and 1046 ± 20 Ma. The oldest age, 1229 ± 5 Ma, was interpreted as the date of magmatic crystallization, whereas the two younger ages were interpreted as dates of metamorphic zircon growth, and correspond to the Shawinigan and Ottawan orogenies, respectively.

A sample of tonalite to granodiorite was collected from station 11SJM059 (also labelled sample 11RME-0024) from within the basal thrust sheet of the Raglan Hills metagabbro (Geospec Consultants 2013), which cross-cuts altered metagabbroic rocks and has been transposed into the northwest-vergent thrust foliation. Analysis of this sample produced a discordia line with an upper intercept of 1213.4 ± 5.4 Ma, which has been interpreted as a minimum estimate for the emplacement age of the tonalite dike. The high degree of discordance for the zircons analyzed makes analysis of the younger (metamorphic) ages difficult, but the Pb^{207}/Pb^{206} ages are consistent with metamorphic growth during both the Shawinigan and Ottawan orogenies. Since this dyke cross-cuts the intrusion (likely altered regular or calcic metagabbro), this crystallization age of 1213 Ma places a minimum constraint on the crystallization age of the intrusion itself.

Both the metagabbro and granodiorite emplacement ages are consistent with regional geochronological data as presented by Rivers (1997). The emplacement ages for the gabbro and the volcanic-arc affinitive tonalite (1229 and 1213 Ma, respectively) are roughly coincident with the emplacement of the Levant gabbro-diorite (+ tonalite) intrusive suite (1250-1227 Ma), which likely represents stitching plutons emplaced during the earlier phases of the Elzevirian Orogeny (1250-1190 Ma) (Easton 1992). The younger (metamorphic) ages determined from the sample of metagabbro also coincide with the Shawinigan and Ottawan orogenies (1190-1170 Ma and 1080-1020 Ma, respectively).

As described above (chapter 4.2), plotting all of the samples analysed for Nd-Sm isotopes from this study onto an isochron diagram produces an age of roughly 1465 Ma with a highly depleted initial $^{143}Nd/^{144}Nd$ ratio 2 epsilon units above the depleted mantle at that time. However, since textural analysis has shown that the alkalic metagabbro and Fe-tholeiitic amphibolite are both younger than the regular and calcic metagabbro, these rock types should be separated for the purposes of geochronological study.

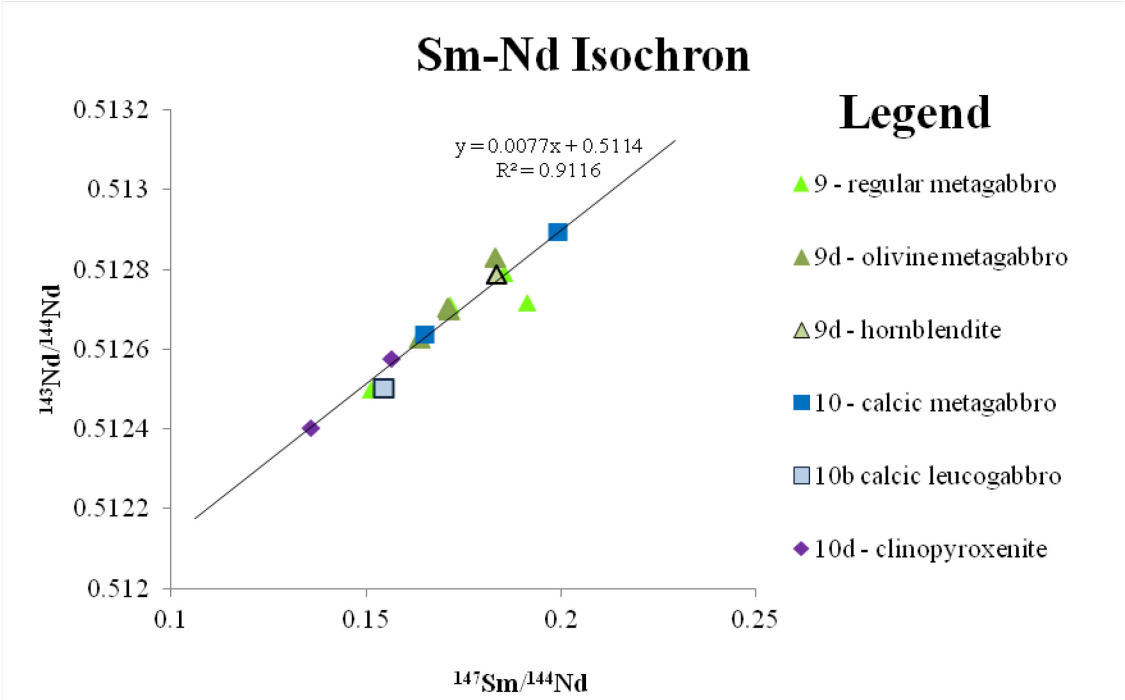

Figure 7.21 – Sm-Nd isochron diagram for all samples of regular and calcic metagabbro collected from the Raglan Hills metagabbro. The resultant line of best fit, with an R^2 value of 0.91, produces an age of ~1171 Ma, much younger than the crystallization date estimated using U-Pb zircon analysis. Note that the sample of mineralized calcic leucogabbro (11SJM120A) has been removed from the data set, due to its anomalously high $^{143}Nd/^{144}Nd$ ratio, likely caused by hydrothermal alteration during mineralization.

The Sm-Nd isochron diagram in figure 7.21 includes all samples of regular and calcic metagabbro collected from the Raglan Hills metagabbro for isotopic study, excluding sample 11SJM120A, a mineralized calcic leucogabbro, that has an anomalously high $^{143}Nd/^{144}Nd$ ratio. Regression through the remaining points yields an age of roughly 1171 Ma, and a regression through these points without sample 12SJM017A (green triangle which lies below the line of best fit) yields an age of roughly 1284 Ma. These ages bound the U-Pb age of 1229 Ma, and thus indicate that the rare earth elements have remained relatively immobile in the whole rock system for the regular and calcic metagabbroic rocks in the core of the intrusion. The varied isotopic ratios observed for the samples may have been caused by assimilation of crustal material, or an isotopic heterogeneous mantle source. The limited spread in values for the Fe-tholeiitic amphibolite, and lack of data for the alkalic metagabbro make interpretation of their source using isotopes difficult. However, the samples of Fe-tholeiitic amphibolite have consistently high $^{143}Nd/^{144}Nd$ ratios, with an average εNd value of +6.6 (1.4 epsilon units higher than the depleted mantle), which is outside the margin of error of the depleted mantle line. Since these samples

come from various parts of the intrusion (from the core, basal thrust sheet and near the McArthurs Mills shear zone) and these samples show regular REE patterns, it is unlikely that the enrichment in radiogenic Nd was caused by post-magmatic alteration, and is more likely a signature from the melt source or the conditions of melting.

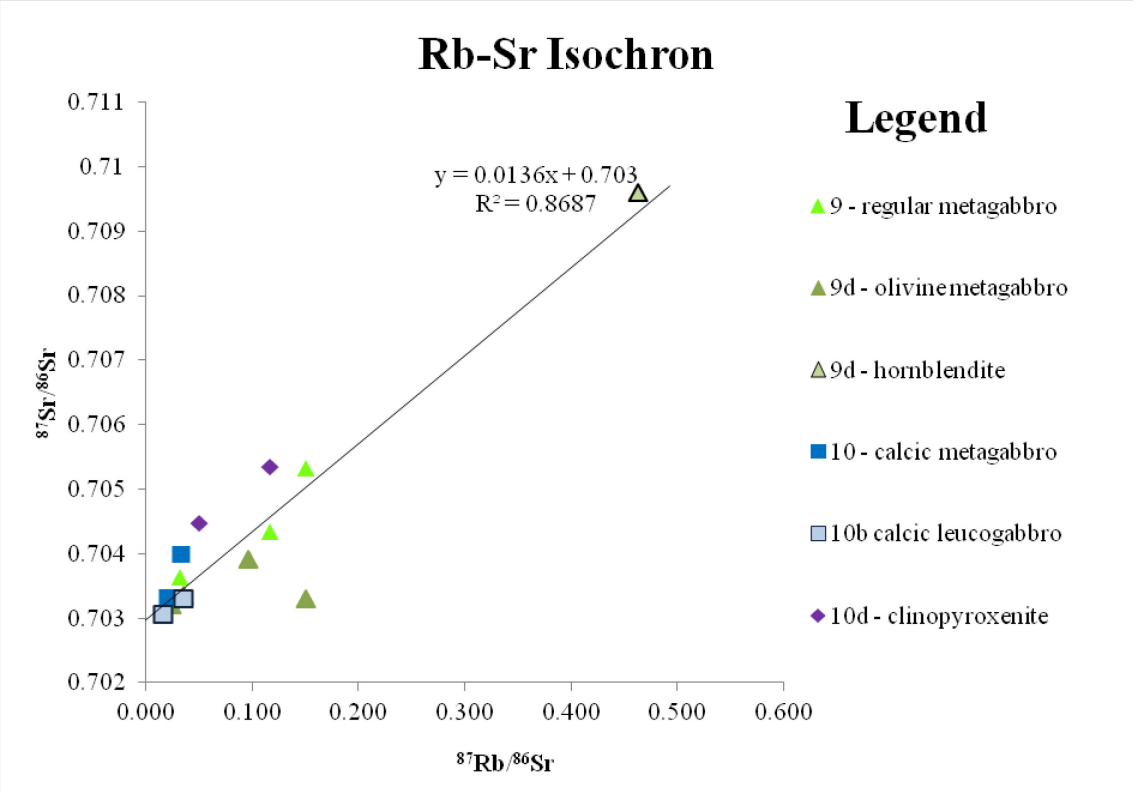

Figure 7.22 – Rb-Sr isochron diagram for all samples of regular and calcic metagabbro collected from the Raglan Hills metagabbro. The resultant line of best fit, with an R^2 value of 0.87, produces an age of ~955 Ma, much younger than the crystallization date estimated using U-Pb zircon analysis. Note that this correlation is controlled mainly by the sample of hornblendite (11SJM173A) which plots far away from the remaining samples.

Plotting the same samples on a Rb-Sr isochron diagram (figure 7.22) produces a different result. Regression through the samples produces an age of roughly 1056 Ma, much younger even than the 1229 Ma crystallization age obtained from U-Pb zircon analysis. This age is coincident with the Ottawan Orogeny (1080-1020 Ma), and suggests that the whole rock system was open with respect to alkali metal and alkali earth metal mobility during metamorphism (see Chapter 7.7), and the system was likely open during the Elzevirian and Shawinigan orogenies as well. This age is not reliable for an exact date however, since the exact behavior of isotopic partitioning during metamorphism is unclear, though this definitely shows that the isotopes were at least mobile.

These isotope systematics are consistent with the geochemical trends observed in sample 12SJM035 as described above, which also shows that the alkali metals and alkali earth metals were mobile during metamorphism, whereas the rare earth elements were immobile, and only changed in relative concentration with respect to the mobile elements.

7.13 - Case Study – Sr Leaching

In an attempt to obtain Rb-Sr data applicable to primary igneous processes, three samples of regular and calcic metagabbro were processed with a leaching technique developed by Cousens (1993) for use with Miocene volcanic rocks that showed evidence for post eruptive mobility of Rb and Sr. The theory behind this method was that by leaching a sample of altered igneous material using acids at low to moderate temperatures, the minerals (and associated strontium) which were introduced during metamorphism would be dissolved first, leaving a residuum composed of minerals which crystallized from the original melt, specifically pyroxene and plagioclase, which accommodate strontium at the expense of calcium. This was applied to a sample of coronitic olivine metagabbro (11SJM6001), a sample of diopside-bearing calcic metagabbro (11SJM169A), and a sample of clinopyroxenite (11SJM6002). The leaching process was executed as follows:

- 200 mg of powder was measured from each sample
- Leached in hot 2N HCl (hotplate for 2 days), repeated thrice
- Leached in hot 50% HF (hotplate for 1 hour), performed once
- After each leach step, the residual powder was washed twice with distilled H_2O
- Final residual powder was dissolved using the same method described in chapter 2.5
- When fully dissolved in 6N HCl, 10% of each sample was split into a separate vial and spiked with 200 mg of mixed $^{87}Rb/^{84}Sr$ spike
- Spiked and non-spiked samples were washed through columns using the same method described in chapter 2.5
- measured Sr and Rb concentrations and isotopic ratios in the spiked samples and Sr isotopic ratios in the non-spiked samples

Both spiked and non-spiked Sr runs failed for the sample of clinopyroxenite (11SJM6002), and the non-spiked Sr run failed for the sample of calcic metagabbro (11SJM169); however all of the runs for the sample of coronitic olivine metagabbro were successful and produced reliable data. The failed runs were likely due to a lack of Sr on the filaments, probably caused by over-exposing the samples to hydrofluoric acid, which may have dissolved the pyroxenes prior to the final leaching step.

The resultant initial $^{87}Sr/^{86}Sr$ ratio for sample 11SJM6001 was 0.701678, with a 2-sigma error of $1x10^{-6}$, which is considerably less than the original un-leached value of 0.702761. This brought the sample closer to the estimated value for the depleted mantle at 1229 Ma (figure 7.23). This shows that leaching these high-grade metamorphic rocks may produce similar results to

those obtained by Cousens (1993), and therefore it may be possible to examine other meta-intrusive and meta-volcanic rocks in the central metasedimentary belt and to study the Rb-Sr isotopic properties of the local mantle source during the Proterozoic era.

If one were to repeat this process, it is suggested that the samples be exposed to hydrofluoric acid for less time, or perhaps not at all, to avoid dissolving the magmatic pyroxene and leaching too much strontium. Also, it might be wise to use more than 200 mg of sample, in order to maximize the concentration of Sr in the final residual sample.

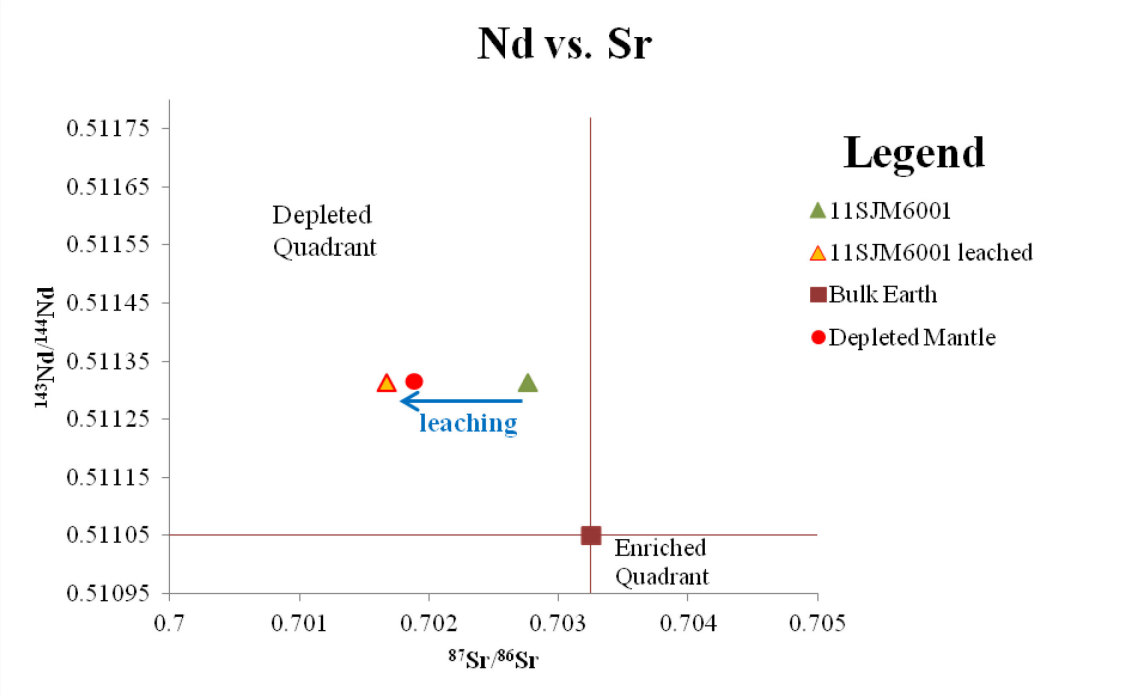

Figure 7.23 – applying the leaching technique to sample 11SJM6001 of coronitic olivine metagabbro produced a less radiogenic $^{87}Sr/^{86}Sr$ value, bringing the sample closer to the estimated value of the depleted mantle at 1229 Ma.

7.14 - Mantle Source Characteristics and Melting Conditions

The elemental and isotopic mantle-source plots presented in chapter 4.2 both suggest that the mantle source for the melts which formed the different gabbroic rocks in this intrusion were derived from a mantle source depleted in radiogenic Nd and Sr, as well as LREE and LILs relative to the bulk earth composition. Also, the rocks were derived from a source with a fairly narrow range of isotopic compositions, with variance in isotopic ratios largely attributable to assimilation of crustal material and metasomatism.

As described earlier, the negative Nb and Ta anomalies in combination with the positive Pb anomalies present in each of the rock types indicate that the mantle source for these rocks must have been metasomatized prior to melting. Since the Fe-tholeiitic metagabbro has the highest εNd values, and thus was derived from a more depleted (un-altered) mantle source, and it was derived from a fairly high degree of partial melting (due to its MORB-like characteristics), this rock-type may be the closest representative to the depleted mantle source available. By projecting a curved line through the most immobile elements (rare earth elements and high field

strength elements) on a trace element diagram (figure 7.24), a trace element pattern for the local unaltered depleted mantle has been estimated, against which the enrichment and depletion of elements for each rock-type may be compared.

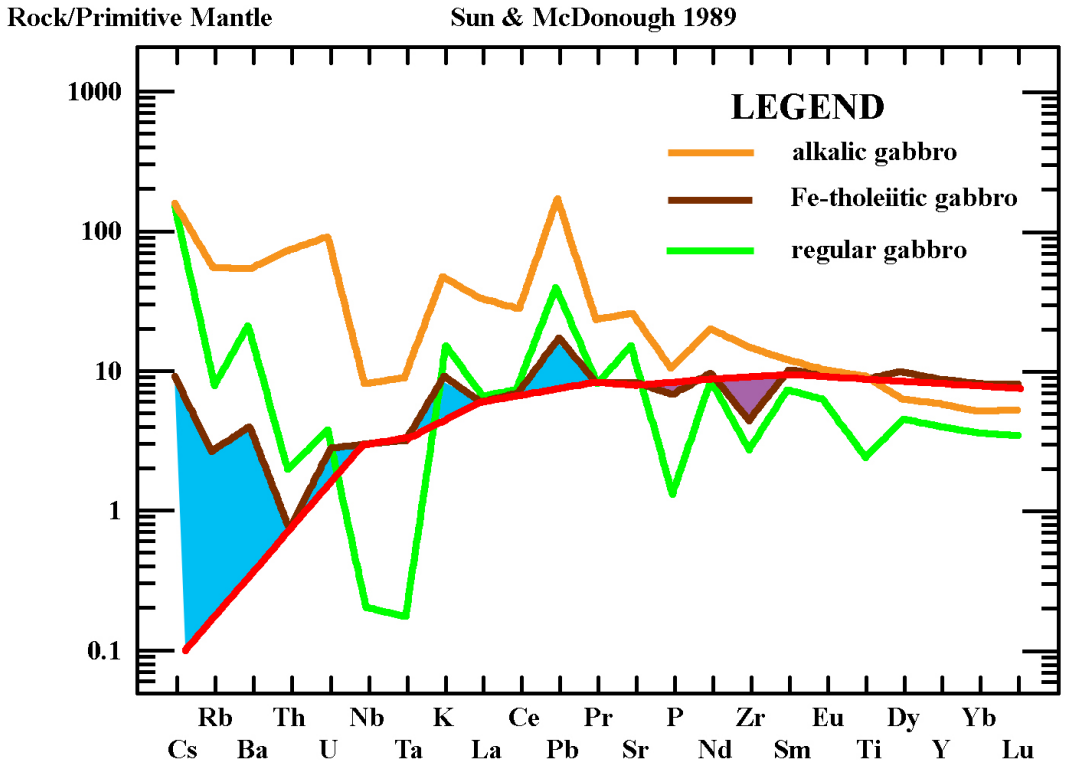

Figure 7.24 – trace element diagram including typical patterns for regular, Fe-tholeiitic and alkalic metagabbroic rocks with the smallest europium anomalies (Eu* = 0, least fractionated samples). The red line represents the closest estimate to the depleted mantle composition prior to metasomatic alteration. Blue areas represent elements that are enriched relative to the depleted mantle composition, whereas purple areas represent elements that have been depleted in the resultant rocks, likely due to fractional crystallization. Note that the patterns for the regular gabbro and alkalic gabbro are progressively rotated clockwise with respect to the Fe-tholeiitic gabbro, which may likely be attributed to different degrees of partial melting. All patterns normalized to primitive mantle values according to Sun and McDonough (1989).

The progressive clockwise rotation of these patterns from the Fe-tholeiitic gabbro to the regular gabbro to the alkalic gabbro may be attributed to differences in degrees of partial melting, with the Fe-tholeiitic gabbro derived from the highest degree of partial melting, and the alkalic gabbro derived from the lowest degree of partial melting. Considering temporal relationships between the gabbroic rocks, the mantle source apparently changed from one with lower εNd values (+5.1 for regular metagabbro) to one with higher εNd values (+6.3 for Fe-tholeiitic gabbro), and back to a lower εNd value (+4.7 for alkalic metagabbro). However, this does not require a dynamic mantle source, but may be related to partial melting of a heterogeneous mantle source.

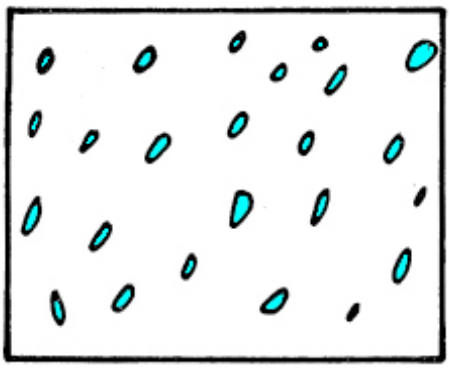

model I:
large-scale homogeneities;
small-scale heterogeneities

Figure 7.25 – model for mantle heterogeneity modified after Allègre et al. (1980). In this case, the blue batches represent bits of metasomatized mantle, and the bulk of the mantle (white) is unaltered depleted mantle. Preferential melting of the hydrous, metasomatized batches may have produced the regular and alkalic metagabbroic rocks with lower percentages of partial melting, whereas higher percentages of partial melting would have produced a melt of chemistry dominated by the unaltered depleted mantle component.

Model I proposed by Allègre et al. (1980) for heterogeneity in the mantle (figure 7.25) sufficiently explains this model, in which the local mantle is homogenous on a large scale, dominated by unaltered depleted mantle, though heterogeneous on a small scale, with localized batches of metasomatized mantle. Lower degrees of partial melting might have preferentially sampled more of the metasomatized mantle, since metasomatic alteration might have produced hydrous phases in the altered patches, whereas higher degrees of partial melting might have sampled more of the unaltered depleted mantle to produce the Fe-tholeiitic gabbro.

The degree of heterogeneity (i.e. the abundance of altered mantle batches) may have also contributed to the variably depleted and enriched geochemical signatures. As illustrated in figure 7.26, mantle directly above the subducted slab would have likely contained more metasomatized material (source for regular and alkalic magma), which would likely grade upwards into a less metasomatized mantle (source for Fe-tholeiitic, MORB-like magma). A brief thermal pulse could have caused partial melting of the less-altered mantle asthenosphere to produce the Fe-tholeiitic magma, which is anomalous amongst the higher volumes of regular and alkalic gabbroic rocks in the intrusion.

A study on the lead and oxygen isotope concentrations may help to better describe the composition of the metasomatized batches, i.e. whether the metasomatizing fluids were derived from subducted oceanic crust or subducted continental material (HIMU or EMI/EMII mantle array end-members respectively) or a mixture of both.

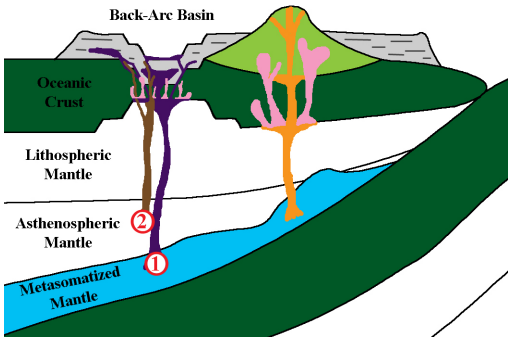

Figure 7.26 – tectonic model for the emplacement of the Raglan Hills gabbro, including the forearc trench, the subducted slab, mantle components and supracrustal components. The regular, calcic and alkalic magmas were likely derived from a metasomatized mantle source (spot 1), whereas the Fe-tholeiitic magma was likely derived from a less altered source (spot 2). Both sources likely contained heterogeneities, however the batches of altered mantle were likely larger and/or more abundant in the mantle closer to the subducted slab.

7.15 - Comparison to Regional Gabbroic Rocks

Two major suites of gabbroic rocks are present in the Central Metasedimentary Belt of Ontario: the Killer Creek gabbro suite and the Lavant diorite-gabbro suite.

The gabbroic rocks of the Killer Creek suite (1300-1270 Ma) tend to have higher concentrations of TiO_2 and P_2O_5 Cu relative to their counterparts of the Lavant suite, and have been interpreted as having been generated in an island-arc setting (Easton 1992). Similar enrichment in TiO_2 and P_2O_5, and to a lesser extent Cu is typical of rocks of the alkalic metagabbro in the Raglan Hills intrusion. However, since the alkalic rocks in the Raglan Hills intrusion represent the latest stage of magmatism, they are not related directly to the Killer Creek gabbroic rocks, but may have been created from similar processes and/or similar mantle sources.

However, samples of the Lavant metagabbro collected by Gemmell (2009) display varied enrichment and depletion of both Ti and P, indicating that fractional crystallization of apatite and some HFSE-bearing phase occurred during crystallization of these magmas, similar to that described in this study for the Raglan Hills metagabbro which only displays strong negative P and Ti anomalies, whereas the alkali Glamorgan metagabbro studied by Jessett (2010) displays only very slight negative anomalies of these elements. This indicates that fractionation of P and Ti-bearing phases operated differently within separate gabbroic rocks of the Lavant group, and it is possible that similar fractionation processes occurred in rocks of the Killer Creek suite, making this geochemical distinction between the groups very vague and perhaps obsolete.

Textural descriptions of the Killer Creek and Lavant suite gabbroic rocks are quite similar, both containing ultramafic (pyroxenite and hornblendite) to more intermediate phases (gabbro and diorite) with minor occurrences of anorthosite, indicating that similar processes of fractional crystallization of the major silicate phases occurred in both suites. Perhaps the only way to distinguish between the two suites and individual intrusions within them is to perform geochronological and isotope geochemical analyses on each individual intrusion.

Isotopic studies on the Lavant and Glamorgan intrusions, by Gemmell (2009) and Jessett (2010) respectively, produced Nd-Sm isochron ages of 1243 Ma (Lavant) and 1273 Ma (Glamorgan) with εNd values of roughly +5.1, within analytical error of the value for the depleted mantle value at 1250 Ma of +5.14 (DePaolo 1981). This fits perfectly with the Raglan Hills metagabbro, which produced a Nd-Sm isochron age of 1284 Ma with an εNd value of +5.11. Of course, the U-Pb zircon crystallization age for the Raglan Hills metagabbro obtained by Pehrsson et al. (1996) is 1229 Ma, indicating that the Nd-Sm isochron technique over-estimates the age of this intrusion. Similarly, the ages determined for the Lavant (1224±2 Ma, Corfu and Easton 1997) and Glamorgan (1246±3Ma Pehrsson et al. 1996) intrusions are overestimated. This at least shows that the intrusions are related at least temporally, so their geochemical differences may provide evidence for the genesis of the suite as a whole and the potential differences in local mantle composition.

The study by Pehrsson et al. (1996) also obtained U-Pb ages from the Glamorgan (their Trooper Lake), and Chenaux gabbroic intrusions, and concluded that along with the Raglan Hills gabbro, they were all emplaced between 1246 and 1227 Ma. Together with the Lavant and

Glamorgan intrusions, plus a potential many other local intrusions for which there is currently no geochronological data, these intrusions constitute a rather large volume of mafic magmatism that occurred within roughly a 20 million year period. Following an interpretation proposed by Easton (1992), the study by Smith et al. (2001) proposed that collectively, the Bancroft, Elzevir and Sharbot Lake terranes constituted a superterrane which formed a back-arc basin to a Frontenac volcanic arc, and that the emplacement of the Lavant gabbroic suite occurred during extensive rifting of this basin. A problem with this model is that there are no volcanic rocks, arc or otherwise, within Frontenac terrane and it is unclear how much older crust, if any, is present within the Elzevir superterrane. The only inherited zircons found in the gabbros studied by Pehrsson et al (1996) came from the Faraday metagabbro, which yielded a Shawinigan age.

Whether this back-arc basin was created by an early (pre-1280 Ma) rifting of the Frontenac-Adirondack belt away from the Laurentian margin, or whether the rocks of the Central Metasedimentary Belt represent a mature oceanic island arc that was rifted prior to reaching the Laurentian margin is currently unknown. The consistently non-radiogenic Nd-Sm and Rb-Sr isotopic ratios of the Raglan Hills and other gabbroic intrusions suggest that they had minimal interaction with old crustal material upon ascension, which also makes the development of the Central Metasedimentary Belt proximal to the Laurentian margin difficult to support. However, the theory has not been proven wrong, so it must still be considered a possibility.

7.16 - Mineral Potential and Mineralization

One of the many features which make the Raglan Hills metagabbro interesting is the presence of several small, yet highly concentrated occurrences of Ni-Cu mineralization. Two of these occurrences were sampled and studied in order to determine the petrogenesis of the mineralization and ultimately to assess the Ni-Cu mineralization potential for this gabbro and other gabbroic rocks of the Central Metasedimentary Belt.

7.16.1 - Raglan Hills Showing

The first and most substantial occurrence is the historic Raglan Hills showing, located at 306140E, 5008130N (UTM coordinates in NAD83, zone 18) within the southern limb of the core of the intrusion (figure 7.27). This showing is also proximal to a lens-shaped positive aeromagnetic anomaly, although none of the rock-types observed at the showing are particularly magnetic.

Five distinct rock types have been observed in the several outcrops which comprise this showing, as described in Magnus (2013b) (figure 7.28).

1. calcic metagabbro

A medium to coarse-grained protomylonitic rock composed primarily of plagioclase and hornblende (replacing clinopyroxene, with titanite), with minor epidote. Sulphide minerals are mostly concentrated around anastomosing ductile shear bands (2-5 cm thick) that are observed in the most western outcrop.

2. labradorite metagabbro

A medium-grained rock composed of euhedral, roughly equant labradorite grains with interstitial hornblende, biotite and sulphide. Mineralized and un-mineralized examples of this rock outcrop throughout the entire showing, in some places with a moderately developed foliation defined by the alignment of interstitial hornblende crystals.

3. anorthosite

A fine to medium-grained rock composed almost entirely of labradorite with minor hornblende and trace biotite. Contacts with the labradorite metagabbro are visible close to sample location 12SJM200C, which appear uneven and diffuse, possibly indicating magma mixing.

4. hornblendite

A fine-grained rock composed almost entirely of hornblende, with minor epidote and biotite, which occurs as a north by north west-trending lens in labradorite metagabbro, which has been displaced dextrally along the strike of a tonalite dike.

5. tonalite

A granitoid dike (+ tourmaline) with a fine-grained, foliated core and coarse-grained zones along its sharp contacts with labradorite metagabbro and hornblendite. The hornblendite lens appears to be displaced dextrally along the strike of the tonalite dike, suggesting that the dike was emplaced into a fracture along which dextral displacement had occurred.

Aside from the displacement visible along the strike of the tonalite dike, anastomosing ductile shear zones up to 5cm wide cross cut both the calcic and labradorite metagabbroic rocks and a penetrative southeast-striking protomylonitic fabric. These shear zones host veins of pyrrhotite, which appears to have been remobilized from pre-existing sulphide mineralization. White mica and iron-rich chlorite are also associated with these veins, possibly related to the same fluids that altered pyrrhotite to marcasite.

Sulphide mineralization, consisting of pyrrhotite with minor chalcopyrite and pyrite, and trace pentlandite, is located mostly within the labradorite metagabbro. These mineralized rocks are composed of medium-grained (<0.7 cm) euhedral blocky plagioclase crystallized with interstitial (net-textured) sulphides, trace hornblende and biotite. These samples contain up to roughly 4000 ppm copper, 3000 ppm nickel, 50 ppb gold, 60 ppb platinum and 30 ppb palladium (table 7.2).

A classical interpretation of the net-textured pattern is that the crystals of labradorite crystallized from a melt and sank into a pod of monosulphide solution prior to its crystallization. This requires that the magma had become saturated in sulphur prior to the crystallization of silicates from the magma, and that plagioclase was denser than the magma and more importantly, the sulphide solution, which is unlikely. However, since the Raglan Hills metagabbro has been interpreted as a layered intrusion, it is possible that low density phases such as plagioclase might be juxtaposed against high density phases such as a monosulphide solution.

In order to assess whether the magma which crystallized the Raglan Hills metagabbro could naturally produce abundant Cu-Ni sulphides, it is important to review the chemistry of the most primitive, un-fractionated magma present in the intrusion, which have also experienced the

least metasomatism. The samples which fit this requirement are the samples of olivine gabbro which display a Eu* = 0, and preferably minimal P and HFSE anomalies as well. These samples include 11SJM6001, 11SJM7002 and 11SJM7004, all collected from diamond drill core proximal to the Raglan Hills showing (First Nickel holes FNB-006 and FNB-007). Li and Ripley (2005) developed a multi-parameter equation calibrated using several separate published datasets for the sulphur concentration at sulphide saturation (SCSS) for mafic silicic magmas which is dependent on P, T and several compositional components, and remains the most up-to-date estimate for sulphur saturation. Using the equation:

$$lnX_S = 1.229 - 0.74\left(\frac{10^4}{T}\right) - 0.021(P) - 0.311\, x\, lnX_{FeO} - 6.166X_{SiO_2} - 9.153X_{Na_2O} + K_2O - 1.914X_{MgO} + 6.594X_{FeO}$$

The resultant SCSS is: $X_S = 511 - 533\ ppm$ for the three samples of olivine gabbro.

With current sulphur concentrations of 216 to 243 ppm (assuming this concentration has not changed during metamorphism), the samples were well under saturation during crystallization, which is supported by the absence of sulphide minerals present in the samples. As a physical rule, after a liquid has become oversaturated in a component, it will not become naturally undersaturated, and will instead exsolve that component and remain at a concentration of stable saturation, thus this magma likely never reached its SCSS. This is supported by the presence of nickel in the samples (166-178 ppm), which would have fractionated out of the silicate melt had it become S-saturated and produces a monosulphide solution. However, these samples contain only 2.5-5.1 ppm Cu, which may only be explained by a Cu-poor parental melt, since it has already been shown that sulphide minerals have not been fractionated out of this magma.

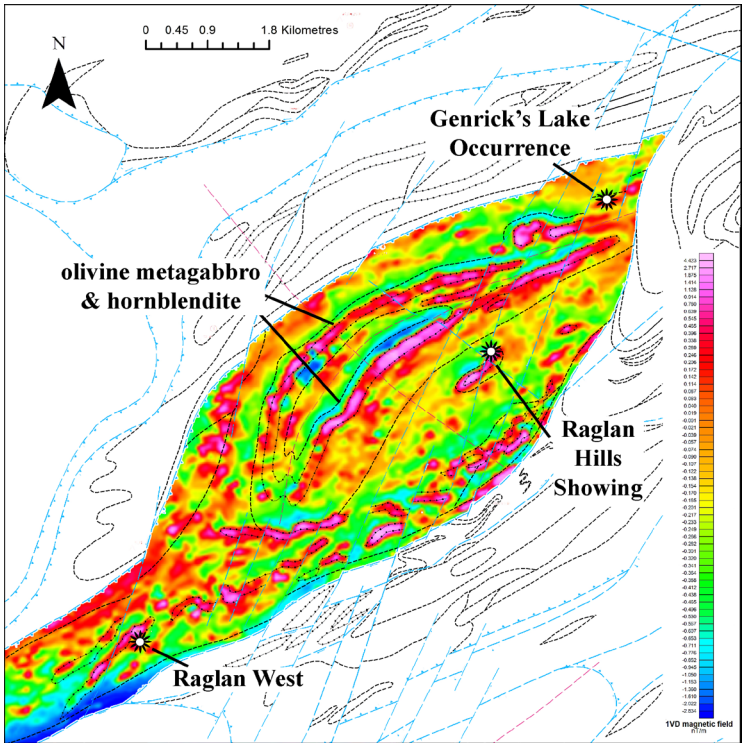

Figure 7.27 – map of the Raglan Hills area, with the 2nd derivative aeromagnetic map highlighting the core of the intrusion. The Raglan Hills and Raglan West showings are indicated, along with the Genrick's Lake occurrence, which was not sampled for this study. It is recommended that exploration for Ni-Cu sulphide mineralization focus around the positive aeromagnetic anomalies associated with olivine metagabbro and hornblendite.

Sample	**11SJM120A**	**11SJM120B**	**12SJM200E**	**12SJM200F-1**	**12SJM200F-2**	**12SJM150A**
Rock Type	labradorite metagabbro	labradorite metagabbro	labradorite metagabbro	labradorite metagabbro	labradorite metagabbro	metapyroxenite
Al_2O_3	19.99	22.96	25.61	19.58	20.55	5.12
CaO	11.9	13.21	11.438	8.472	8.639	15.296
FeO	4.96	3.54	2.92	28.85	23.87	8.06
Fe_2O_3	6.37	3.27	3.92	-0.99	2.11	2.48
K_2O	0.42	0.45	0.35	0.23	0.24	0.3
MgO	4.49	4.1	1.61	0.81	0.49	14.72
MnO	0.09	0.07	0.039	0.027	0.018	0.209
Na_2O	2.65	2.55	3.48	2.38	2.46	0.7
P_2O_5	0.02	0.02	0.029	0.013	0.012	0.022
SiO_2	46.1	47.77	47.58	33.74	34.47	51.61
TiO_2	0.83	0.62	0.59	0.16	0.19	0.51
LOI	1.64	1.08	1.8	5.73	5.68	1.41
Total	99.45	99.65	99.37	99	98.73	100.43
CO_2	<0.03	0.06	0.01	0.03	0.03	0.18
S	2.57 wt. %	0.8 wt. %	2.18 wt. %	12.8 wt. %	12.6 wt. %	1019 ppm
Cu	1252.4	399.7	3272	3385	3826	73.4
Ni	1092.1	299.9	464.2	3262.3	3080.9	423.8
Au	7	<6	51	13	23	<6
Pd	9.3	3.3	15.1	67.3	63	<1.3
Pt	15.3	4.3	1.2	28.2	21.2	<0.4
ΣREEs	23.67	23.41	9.20	7.21	7.04	26.78

Sample	**12SJM150C**	**11SJM6001**	**11SJM7002**	**11SJM7004**	**11SJM6002**	**11SJM6006**
Rock Type	altered metagabbro	olivine metagabbro	olivine metagabbro	olivine metagabbro	clinopyroxenite	clinopyroxenite
Al_2O_3	14.57	12.84	11.89	11.69	5.12	5.38
CaO	2.814	11.04	11.21	11.39	22.18	21.75
FeO	8.04	9.17	9.37	9.88	8.48	7.38
Fe_2O_3	-1.34	2.76	3.02	2.36	4.94	4.98
K_2O	1.84	0.4	0.4	0.39	0.15	0.1
MgO	3.48	11.35	11.72	11.79	10.23	10.53
MnO	0.136	0.18	0.2	0.19	0.17	0.16
Na_2O	0.08	2.18	2.12	2.01	0.68	0.74
P_2O_5	0.153	0.02	0.03	0.02	1.34	0.47
SiO_2	65.43	49.31	49.03	49.26	44.71	45.9
TiO_2	0.71	0.57	0.58	0.58	1.36	1.53
LOI	4.26	0.22	0.49	0.27	0.89	1.49
Total	100.17	100.05	100.06	99.84	100.24	100.43
CO_2	0.26	0.15	0.36	0.16	0.62	0.78
S	3.4 wt. %	224 ppm	243 ppm	216 ppm	4473 ppm	2970 ppm
Cu	1216.1	2.9	5.1	2.5	1564	621.1
Ni	1704.9	167.6	178.1	166.6	188.1	149.6
Au	<6	<6	<6	<6	44	8
Pd	1.3	<1.3	<1.3	<1.3	6.4	1.3
Pt	0.9	<0.4	<0.4	1.3	8.5	4.4
ΣREEs	13.04	44.20	43.97	43.85	117.86	89.44

Table 7.2 – geochemical data for samples with significant Ni-Cu contents, including samples from the Raglan Hills showing (11SJM120 and 12SJM200), the Raglan West showing (12SJM150), samples of olivine metagabbro and clinopyroxenite. All oxides and LOI reported in weight percent, and all elemental values and ΣREEs reported in ppm, except Au, Pd and Pt in ppb.

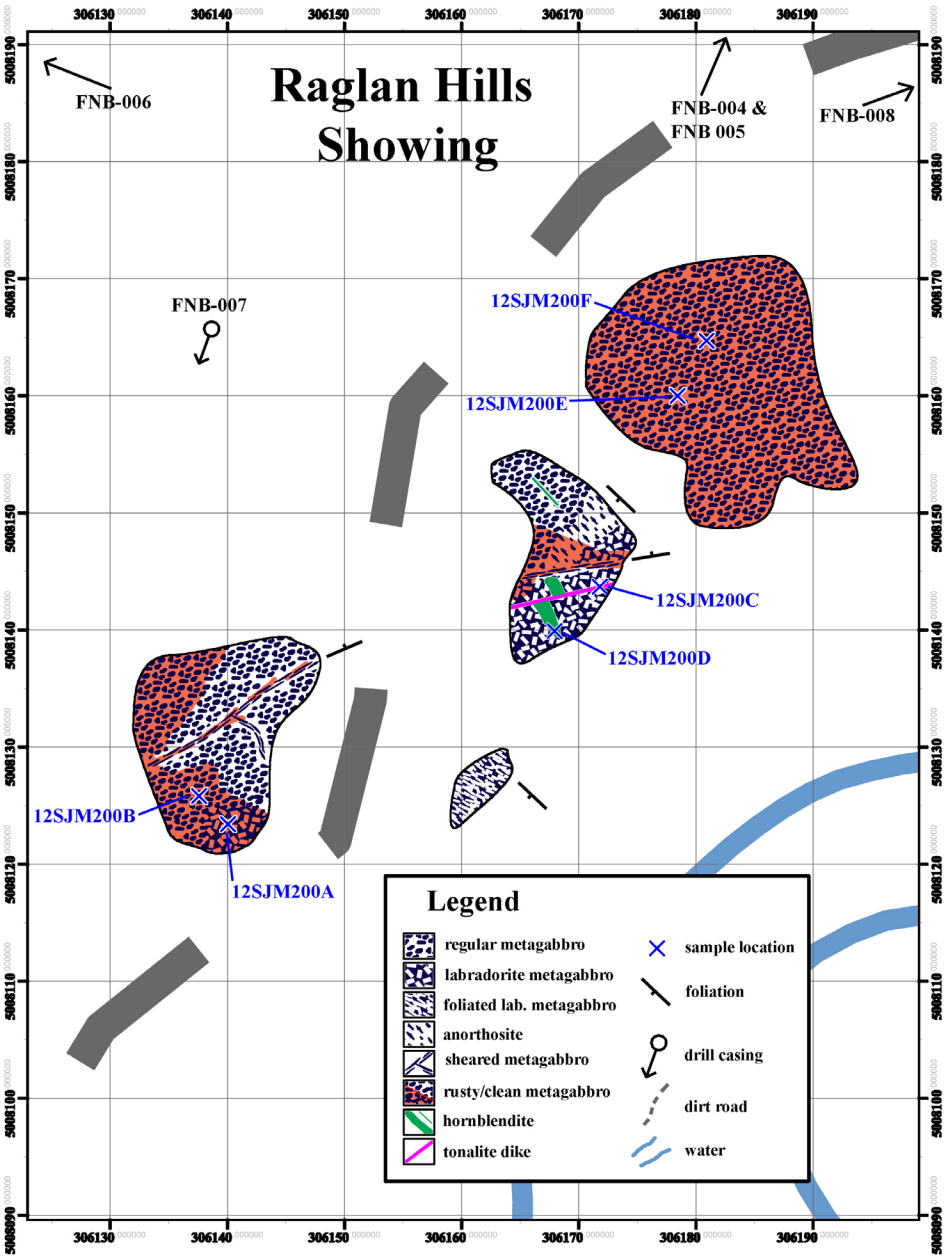

Figure 7.28 – sketch outcrop map of the Raglan Hills showing, from Magnus (2013b). UTM coordinate system = NAD 83, zone 18.

Despite the lack of sulphide mineralization associated with the olivine metagabbro, in a hypothetical situation which included a source of sulphur external to the magma, sulphur saturation could have been reached, and a Ni-rich monosulphide solution (mss) would have formed. Assuming the partition coefficients of Ni and Cu between silicate melt and sulphide melt (mss) are roughly equal (Ni is only slightly larger than Cu), considering the concentrations of Ni and Cu in the olivine gabbro, the concentration of Ni in the mss would be at least one order of magnitude (up to 2 orders, considering the slight difference in partition coefficients) greater than that of Cu. However, in the samples of mineralized labradorite metagabbro, the concentration of Cu is consistently higher than the concentration of Ni.

Considering the magma composition and its concentration of metals, two genetic models for the formation of the Raglan Hills showing are plausible.

Magmatic Model

- A pulse of magma begins to crystallize, as described in chapter 7.11, with regular to calcic leucogabbro (labradorite float-cumulates) forming near the roof of the chamber. Naturally, these felsic melts are deficient in Ni and Cu, as those metals would have fractionated into the more mafic phases.

- As a new pulse of magma breaks through the roof of the chamber, mafic magma is again capable of interacting with a sulphur source (likely sulphur-rich siliciclastic rocks, since no evidence of an evaporitic environment or anhydrite have been observed), causing a monosulphide solution to form, which would siphon Ni and Cu from magma flowing through the new conduit.

- The dense monosulphide solution would sink, and interfere with the buoyant plagioclase feldspars present in the previous pulse of magma, forming the net-textured sulphide mineralization observed in the current labradorite metagabbro.

- Excess Cu may have been derived from assimilated host rocks, possibly even from the same source as the extra sulphur.

This model requires that the interpreted layered nature if the intrusion is true, but it does explain the extremely localized nature of the occurrence, provided there was a significant volume of mafic to ultramafic magma passing through the conduit, which is observable as the positive aeromagnetic anomaly present near the occurrence. This model also requires no structural control, and would mean that the veins of pyrrhotite-marcasite-chlorite-white mica purely represent metamorphic remobilization of the metals on a small scale.

Structural Model

Despite the wonderful magmatic story told above, there is an obvious coincidence between the Raglan Hills showing and the structural features observed on a map scale through geophysical analysis combined with parallel structural features observed on an outcrop scale.

As seen in figure 7.26, the showing lies almost directly above an intersection between two major structures: one northeast striking feature which is observed disrupting the magnetic signatures of rocks within and surrounding the Raglan Hills metagabbro and one northwest-striking feature which is observed dextrally-offsetting positive aeromagnetic anomalies (olivine gabbro) in the core of the intrusion. As described above, parallel structural features are present in the Raglan Hills showing: northwest-striking shear zones, and a penetrative southeast-striking protomylonitic foliation.

Since the northeast-striking feature disrupts the positive aeromagnetic anomalies, which might require fluids with dynamic oxygen and/or sulphur fugacities, it is conceivable that these fluids could have dissolved, transported and deposited the Ni-Cu as sulphide mineralization. The

nearby olivine gabbro (positive aeromagnetic anomaly) may have served as a source for the remobilized metals. However, a physical or geochemical trap is required to cause the saturation and exsolution of sulphide minerals (the conduit cutting through sulphur-rich material provides both in the previous model). The pre-existing northwest-striking protomylonitic foliation may have contained appropriate metamorphic fluids for the precipitation of sulphide minerals, which would naturally occur at the intersection between these features.

As seen in chapter 7.3, the Fe^{2+}/Fe^{3+} ratios of rocks proximal to the northeast-trending feature are more oxidized than the bulk of the Raglan Hills metagabbro, indicating that this feature did indeed host metamorphic fluids with at least dynamic oxygen fugacity. However, occurrences of retrograde chlorite are also coincident with this feature, similar to the development of chlorite, white mica and marcasite, a low-temperature alteration mineral after pyrrhotite, in the Raglan Hills showing. If this entire feature is associated with late, low-temperature alteration, then the coincidence between these structures and the sulphide mineralization is purely coincidental.

7.16.2 - Raglan West Showing

The second occurrence is the Raglan West showing, located at 300942E, 5004474N, proximal to several small positive aeromagnetic anomalies interpreted to represent pieces of Fe-tholeiitic amphibolite dikes (figure 7.27).

Locally, regular metagabbro and pyroxenite (altered to hornblendite) are the dominant rock-types, with several occurrence of highly deformed Fe-tholeiitic amphibolite. One local outcrop of regular metagabbro is also cut by a 15cm shear zone, with associated alteration. The outcrop at the showing is composed of regular metagabbro, metapyroxenite and highly altered metagabbro.

Several small (<5cm) shear zones are observed cutting through the metapyroxenite, which contains minor disseminated sulphides (pyrrhotite with minor pyrite and chalcopyrite), and contains Ni and Cu concentrations similar to those of the olivine metagabbro at the Raglan Hills showing, with 423.8 ppm Ni and 73.4 ppm Cu. The pyroxenite is composed of roughly 70% pyroxene, partially altered to green hornblende, with trace plagioclase and titanite.

One larger shear zone (10 cm thick) which is located along the contact between the metapyroxenite and regular metagabbro, oriented at roughly 100/48, is composed of fine-grained granoblastic hornblende and plagioclase with alternating bands rich in biotite and diopside. Samples from this shear zone contain up to 1704 ppm Ni and 1216 ppm Cu hosted in sulphide minerals present in the diopside-rich bands in the shear zone. There is also abundant sericite and marcasite alteration associated with the shear zone, along with hematite mineralization parallel to the foliations.

Applying the SCSS formula to the sample of pyroxenite, it would have reached sulphide saturation at roughly 530 ppm S, similar to the samples of olivine metagabbro tested earlier. This rock, however, contains 1019 ppm S, and assuming the bulk rock composition has not changed significantly during metamorphism (which it likely has not, considering that primary pyroxene

crystals are still present), it would appear that the sulphides present in this sample are indeed magmatic in nature. This was likely caused by assimilation of a sulphur-rich host-rock, similar to that proposed for the Raglan Hills showing.

The remobilized sulphide minerals in this outcrop, present within the shear zone and associated with low temperature alteration minerals (white mica, marcasite, hematite), are reminiscent of the remobilized sulphide minerals at the Raglan Hills showing, and suggest that the fluids which remobilized the sulphides were present throughout the intrusion during metamorphism, and were only capable of transporting nickel and copper to a limited lateral extent.

7.16.3 - Ore-forming Process

Evidence from the two occurrences described here suggests that both magmatic and metamorphic processes have contributed to sulphide mineralization in the Raglan Hills metagabbro. The sulphide minerals were likely originally precipitated from the regular gabbroic magma which was brought to SCSS by assimilation of S-rich country rocks (pyritic paragneiss), which are locally sparsely intercalated with the carbonate metasedimentary rocks of the Bancroft terrane, hence the localization of mineralization. Slightly oxidizing (hematite precipitation, sulphide dissolution), slightly acidic (marcasite and sericite alteration) metamorphic fluids then locally remobilized the Ni-Cu mineralization, upgrading the concentration of metals by depositing them in veins.

Radiogenic (Re-Os, Pt-Os) and stable (O, S) isotopic studies on the mineralized samples combined with fluid inclusions studies on the metamorphic rocks of the Raglan Hills metagabbro might help in determining the true source of the metals and sulphur in these deposits, as well as the nature and source of the metamorphic fluids which were capable of remobilizing these metals.

7.16.4 - Mineralization Potential and Recommendation for Exploration

Apart from the known occurrences, it is important to assess the mineralization potential for the Raglan Hills metagabbro as a whole, in order to help determine whether this intrusion and others like it are capable of containing significant, economic mineral deposits.

To begin, the simplest task is to review the elemental concentrations in the different rock-types described within the intrusion. Box plots for Ni and Cu contents for each rock type are displayed in figure 7.29, and shows that samples of olivine metagabbro and hornblendite tend to contain the highest concentrations of nickel, whereas the samples of calcic metagabbro and clinopyroxenite tend to have the highest concentrations of copper (apart from samples from the mineralized occurrences). So, if one were to explore for nickel and copper in this intrusion, the first step would be to locate these rock-types.

As described earlier, metamorphism of the olivine metagabbro tends to produce magnetic hornblendite, which is recognisable on an aeromagnetic map. In fact, a large area of interpreted olivine metagabbro/hornblendite is located in the center of the intrusion. However, as shown by the studies on the known occurrences, this olivine metagabbro would not precipitate sulphide

minerals by itself, and requires an external source of sulphur. Not only this, but to produce significant amounts of sulphide mineralization, a large volume of magma would need to interact with this sulphur source in order to maximize the amount of metals available to form the deposit. Hence one must look for perturbations in the olivine gabbro; any irregularities which might indicate that the magma has interacted with wall-rocks or that there was a significant flux of magma.

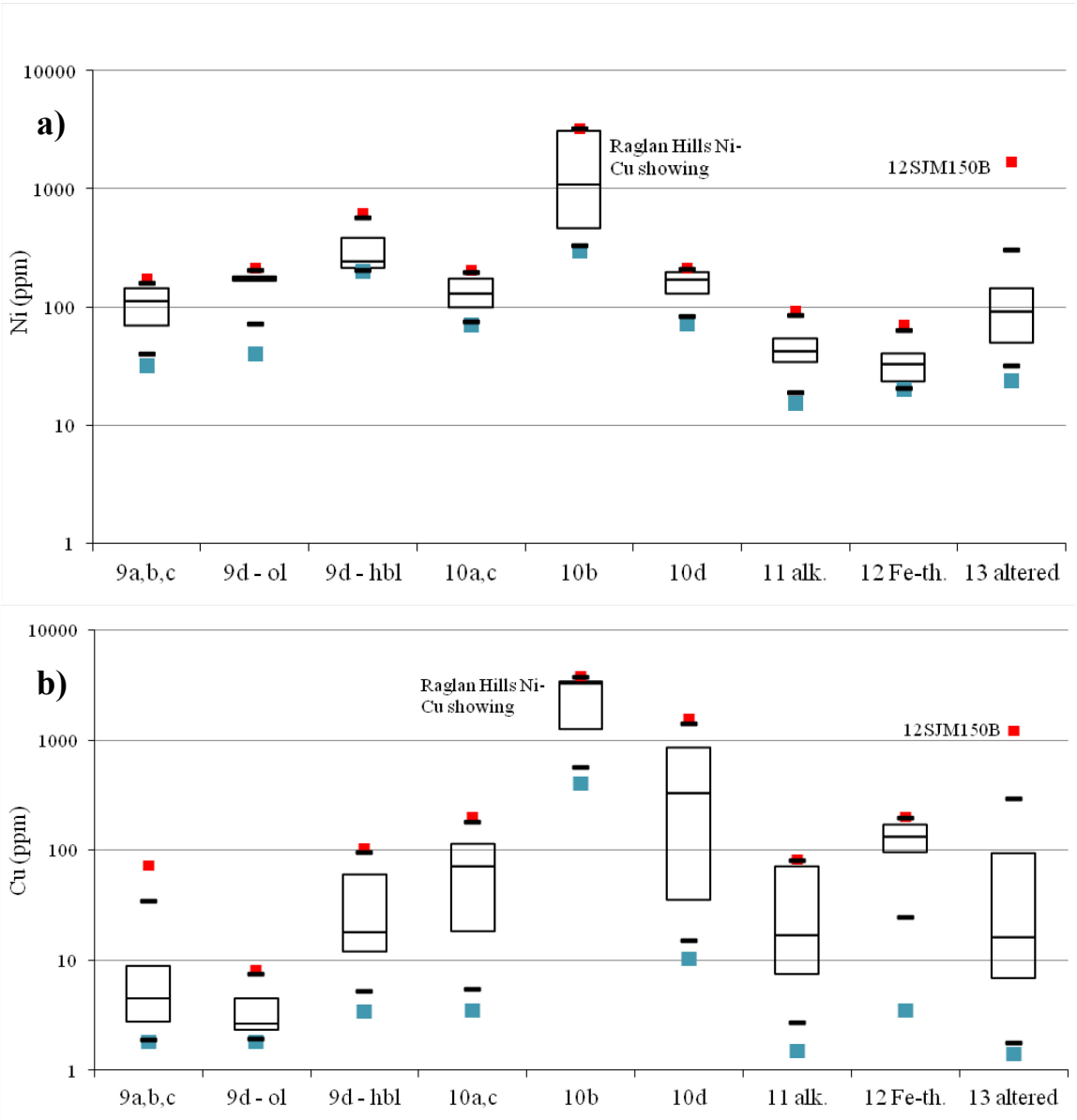

Figure 7.29 – logarithmic box plots for a) nickel and b) copper contents for all samples collected from the Raglan Hills metagabbro, grouped into their specific rock types. Note that the samples of labradorite metagabbro (calcic leucogabbro) from the Raglan Hills showing and sample 12SJM150B from the Raglan West showing are rich in both metals. For each plot, the boxes contain 50% of the data surrounding the median value (middle line), the black ticks contain 90% of the data, and the blue and orange squares represent the minimum and maximum values.

It is recommended to map the center of the intrusion in detail, in combination with rigorous geochemical sampling with a focus on the olivine metagabbro and hornblendite. By mapping and analyzing the igneous and metamorphic textures throughout these rocks and comparing those to the metal and sulphur concentrations in each sample may help identify ideal sites for sulphide mineralization. Proximity to large-scale structures may also help to upgrade the metal concentrations, raising the potential for economic mineralization. A detailed soil survey focussed around the positive magnetic anomalies (figure 7.26) could be a relatively inexpensive method to help identify potential sulphide mineralization occurrences within the intrusion, especially in areas where bedrock outcrops are scarce.

8 - Conclusions

The Raglan Hills metagabbro is a complicated mafic intrusion which was likely emplaced at around 1229 Ma into an extensional back-arc setting from a depleted mantle source (heterogeneous on a small scale). It experienced little to no crustal assimilation during ascent, and subsequently underwent two major thrusting and thrust-folding deformation events and one major dextral shearing event while being subjected to amphibolite-facies metamorphism.

The intrusion is primarily composed of arc-related mafic gabbroic rocks that underwent significant fractional crystallization of plagioclase during cooling, producing localized layered fabrics. Interaction between this magma and the calcium-metacarbonate rocks which host the intrusion likely caused the formation of a similar calcium-rich magma which underwent fractional crystallization of diopside during cooling. Arc-related iron tholeiitic dikes cross-cut the original gabbroic rocks, followed by a pulse of alkalic gabbro, both likely derived from the same mantle source as the original gabbro, although generated under different melting conditions.

Interaction between mafic phases of the original magma with sparse sulphur-rich wall-rocks, both along the margins of the intrusion and around xenoliths within the magma chamber, produced localized and variably fertile Ni-Cu sulphide occurrences.

Northwest-vergent thrusting and folding during the Shawinigan and Ottawan orogenies transposed the intrusion northwestward toward the Central Metasedimentary Belt Boundary Thrust Zone, causing the formation of the basal thrust sheet and its abundant and highly varied metasomatic alteration patterns, and possibly involved localized partial melting. Dextral ductile shearing along the McArthurs Mills Shear Zone, located along the southwest margin of the intrusion caused locally intense mylonitic deformation and metasomatism, and is likely the cause of the remobilization and concentration of Ni-Cu sulphides in the core of the intrusion.

Slightly oxidized, slightly acidic fluids in the core of the intrusion caused varied degrees of mobilization of chalcophile, large ion lithophile and high field strength elements during regional metamorphism, and likely took advantage of pathways through plagioclase early on, until the large-scale development of amphiboles facilitated more efficient fluid transport. Poor interconnectivity of plagioclase laths and deficiency of hydrous components in the olivine metagabbro retarded metamorphism and caused the formation of coronitic textures. Fluid inclusion analysis and more in-depth petrographic analysis of these rocks may provide a better, more accurate understanding of the processes of metamorphism which affected the intrusion.

Nd-Sm isotopic analyses suggest that the parental magmas were derived from a depleted mantle source, supported by Rb-Sr analysis of samples using an acid-leaching technique. Nd-Sm isochron analysis supports the 1229 Ma U-Pb zircon crystallization age obtained by Pehrsson et al. (1996), whereas Rb-Sr isochron analysis produces an age of 955 Ma, coincident with the Ottawan Orogeny, and may provide an estimate of the time of closure of the Rb-Sr isotopic system during metamorphic cooling. High positive εNd values (+6.4) belonging to samples of Fe-tholeiitic amphibolite suggest the presence of a non-metasomatized mantle component in the melt source, which is only sampled during exceptionally high degrees of partial melting.

Whole rock geochemical variability between the Raglan Hills metagabbro and its contemporary gabbroic intrusions of the Lavant intrusive suite, but similar Nd-Sm isotopic ratios, suggest that the Lavant gabbroic intrusions were melted and crystallized under a variety of conditions, but were all derived from a similar mantle source beneath a locally thin crust.

The existence of additional Ni-Cu sulphide occurrences in the Raglan Hills intrusion is likely; however the probability that they are economic is low, given the scarcity of S-rich country rocks and the low volume of nickel-rich magma (olivine gabbro) relative to the remainder of the intrusion. Detailed mapping, geophysical and geochemical sampling programs are needed for the majority of the mafic intrusions present in the Central Metasedimentary Belt, in order to determine if any other intrusions represent new prospective areas for Ni-Cu sulphide mineralization.

9 - References

Allègre, C.J., Brévart, O., Dupré, B. And Minster, J.F. 1980. Isotopic and chemical effects produced by a continuously differentiating convecting Earth mantle; Philosophical Transactions of the Royal Society of London, Series A, v.297, p.447-477.

Allmendinger, R.W., Cardozo, N.C. and Fisher, D. 2013. Structural Geology Algorithms; Vectors and Tensors, Cambridge University Press, Cambridge, 289p.

Bowen, N.L, and Andersen, O. 1914. The Binary System MgO-SiO2; American Journal of Science, v.37, p.487-500.

Brownlow, A.H. 1996. Geochemistry, Prentice-Hall, New Jersey, 580p.

Cardozo, N., and Allmendinger, R.W. 2013. Spherical projections with OSXStereonet; Computers and Geosciences, v.51, p.193-205.

Carr, S.D., Easton, R.M., Jamieson, R.A., and Culshaw, N.G. 2000. Geologic transect across the Grenville orogen of Ontario and New York; Canadian Journal of Earth Sciences, v.37, p.193-216.

Carter, T.R., Colvine, A.C. and Meyn, H.D. 1980. Geology of base metal, precious metal, iron and molybdenum deposits in the Pembroke–Renfrew area; Ontario Geological Survey, Mineral Deposits Circular 20, 186p.

Corfu, F. And Easton, R.M. 1997. Sharbot Lake terrane and its relationships to Frontenac terrane, Central Metasedimentary Belt, Grenville Province: new insights from U-Pb geochronology; Canadian Journal of Earth Sciences, v.34, p.1239-1257.

Cousens, B.L., Spera, F.J., and Dobson, P.F. 1993. Post-eruptive alteration of silicic ignimbrites and lavas, Gran Canaria, Canary Islands: strontium, neodymium, lead and oxygen isotopic evidence; Geochimica et Cosmochimica Acta, v.57, p.631-640.

DePaolo, D.J. 1981. Neodymium isotopes in the Colorado Front Range and crust-mantle evolution in the Proterozoic; Nature, v.291, p.193-196.

DePaolo, D.J. and Wasserburg, G.J. 1976. Inferences about magma sources and mantle structure from variations of $^{143}Nd/^{144}Nd$; Geophysical Research Letters, v.3, p.743-746.

Easton, R.M. 1992. The Grenville Province and the Proterozoic history of central and southern Ontario; Geology of Ontario, Ontario Geological Survey, Special Volume 4, Part 2, p.714-904.

Easton, R.M. 2012. Geology and mineral potential of the Brudenell area, northeastern Central Metasedimentary Belt, Grenville Province, with an emphasis on the syenitic rocks; Ontario Geological Survey, Open File Report 6280, p.12-1 to 12-17.

Easton, R.M., Duguet, M. and Magnus, S.J. 2011. Geology and mineral potential of the northeastern central metasedimentary belt, Grenville Province; Ontario Geological Survey, Open File Report 6270, p.5-1 to 5-23.

Frost, B.R., Barnes, C.G., Collins, W.J., Arculus, R.J., Ellis, D.J., and Frost, C.D. 2001. A Geochemical Classification for Granitic Rocks; Journal of Petrology, v.42, p.2033-2048.

Gemmell, T. 2009. Geochemical, petrographic and isotope analysis of the Lavant Gabbroic Complex within the Sharbot Lake domain; unpublished BSc thesis, Carleton University, Ottawa, Ontario, 36p.

Geospec Consultants 2013 – tonalite age Geospec Consultants 2013. LA-MC-ICP-MS and U–Pb isotopic analyses age dating of zircon and baddeleyite for Northern Development and Mines; Ontario Geological Survey, internal report, 39p.

Grant, J.A. 2005. Isocon analysis: a brief review of the method and applications; physics and chemistry of the earth, v.30, p.997-1004.

Hanmer, S. and McEachern, S. 1992. Kinematical and rheological evolution of a crustal-scale ductile thrust zone, Central Metasedimentary Belt, Grenville orogen, Ontario; Canadian Journal of Earth Sciences, v.29, p1729-1790.

Hatcher, R.D. Jr. 1995. Structural Geology, principles, concepts and problems, 2nd ed.; Prentice Hall, New Jersey, 525p.

Hewitt, D.F. 1954. Geology of the Brudenell–Raglan area; Ontario Department of Mines, Annual Report, 1953, v.62, pt.5, 123p.

Irvine, T.N. and Baragar, W.R.A. 1971. A guide to the chemical classification of the common volcanic rocks; Canadian Journal of Earth Sciences, v.8, p.523-548.

Jensen, L.S. 1976. A new cation plot for classifying subalkalic volcanic rocks; Ontario Division of Mines, Miscellaneous Paper 66, 22p.

Jessett, K. 2010. The petrology and geochemistry of the Glamorgan Gabbro, Ontario; unpublished BSc thesis, Carleton University, Ottawa, Ontario, 59p.

LeMaitre, R.W. 1976. The Chemical Variability of some Common Igneous Rocks; Journal of Petrology, v.17, p.589-637.

Lesher, C.M., Goodwin, A.M., Campbell, I.H., and Gorton, M.P. 1986. Trace-element geochemistry of ore-associated and barren felsic metavolcanic rocks in the Superior province, Canada; Canadian Journal of Earth Sciences, v.23, p.222-237.

Li, C. And Ripley, E.M. 2005. Empirical equations to predict the sulfur content of mafic magmas at sulfide saturation and applications to magmatic sulfide deposits; Mineralium Deposita, v.40, p.218-230.

Lindsley, D.H. 1983. Pyroxene thermometry; American Mineralogist, v.68, p.477-493.

Lumbers, S.B. 1982. Renfrew; Ontario Geological Survey, Map 2462, scale 1:100 000.

Lumbers, S.B. and Vertolli, V.M. 2001. Precambrian Geology, Denbigh Area; Ontario Geological Survey, Preliminary Map P3437, scale 1:50,000.

Magnus, S.J., Cousens, B. And Easton, R.M. 2012. Geology and Mineral Potential of the Raglan Hills metagabbro, northeastern central metasedimentary belt, Grenville Province; Ontario Geological Survey, Open File Report 6280, p.14-1 to 14-9.

Magnus, S.J. 2013a. Raglan Hills metagabbro and environs, Grenville Province; Ontario Geological Survey, Preliminary Map P3774, scale 1:20,000.

Magnus, S.J. 2013b. Geological, geochemical, geophysical and petrographic data from the Raglan Hills area, Central Metasedimentary Belt, Grenville Province, Ontario; Ontario Geological Survey, Miscellaneous Release – Data 309.

McDonough, W.F. and Sun, S.S. 1995. The composition of the earth; Chemical Geology, v.120, p.223-253.

Morimoto, N. 1988. Nomenclature of pyroxenes; American Mineralogist, v.73, p.1123-1133.

Norry, M.J., and Fitton, J.G. 1983. Compositional differences between oceanic and continental basic lavas and their significance; p.5-19 in Hawkesworth, C.J. and Norry, M.J. (Editors), Continental Basalts and Mantle Xenoliths; Shiva, University of California, 272p.

Ontario Geological Survey 2010a. Airborne magnetic and electromagnetic surveys, colour-filled contours of the residual magnetic field and electromagnetic anomalies, Bancroft area—Purchased data; Ontario Geological Survey, Map 60 149, scale 1:20 000.

——— 2010b. Airborne magnetic and electromagnetic surveys, shaded colour image of the second vertical derivative of the residual magnetic field and Keating coefficients, Bancroft area—Purchased data; Ontario Geological Survey, Map 60 164, scale 1:20 000.

Pearce, J.A., Harris, N.B.W. and Tindle, A.G. 1984. Trace element discrimination diagrams for the tectonic interpretation of granitic rocks; Journal of Petrology, v.25, p.956-983.

Pehrsson, S., Hanmer, S. and van Breemen, O. 1996. U-Pb geochronology of the Raglan gabbro belt, Central Metasedimentary Belt, Ontario: implications for an ensialic marginal basin in the Grenville orogen; Canadian Journal of Earth Sciences, v.33, p.691-702.

Shimizu, R.P.N. and Allègre C. J. 1976. $^{143}Nd/^{146}Nd$, a natural tracer: an application to oceanic basalts; Earth Planetary Science Letters, v.31, p.269-278.

Rivers, T. 1997. Lithotectonic elements of the Grenville Province: review and tectonic implications; Precambrian Research, v.86, p.117-154.

Smith, T.E., Harris, M.J., Huang, C.H., and Holm, P.E. 2001. The geochemical nature of the igneous rocks of the Sharbot Lake domain, Central Metasedimentary Belt, Ontario; Canadian Journal of Earth Science, v.38, p.1037-1057

Spear, F.S. 1993. Metamorphic Phase Equilibria and Pressure-Temperature-Time Paths; Mineralogical Society of America, Washington, 799 pages.

Sun, S.S. and McDonough, W.F. 1989. Magmatism in the Ocean Basins; Special Publications, Geological Society of London, v.42, p.313-345.

Terrasoft 2012 – Igpet for Windows. Used for plotting spider diagrams.

Appendix A

P3774 Raglan Hills metagabbro and environs, Grenville Province

http://www.geologyontario.mndmf.gov.on.ca/mndmaccess/mndm_dir.asp?type=pub&id=P3774

Magnus, S.J. 2013a. Raglan Hills metagabbro and environs, Grenville Province; Ontario Geological Survey, Preliminary Map P3774, scale 1:20,000.

Appendix B

MRD-309 Geological, geochemical, geophysical and petrographic data from the Raglan Hills area, Central Metasedimentary Belt, Grenville Province

http://www.geologyontario.mndmf.gov.on.ca/mndmaccess/mndm_dir.asp?type=pub&id=MRD309

Magnus, S.J. 2013b. Geological, geochemical, geophysical and petrographic data from the Raglan Hills area, Central Metasedimentary Belt, Grenville Province, Ontario; Ontario Geological Survey, Miscellaneous Release – Data 309.